

# The low-mass stellar population in the young cluster Tr 37

## Disk evolution, accretion, and environment<sup>\*\*\*</sup>

Aurora Sicilia-Aguilar<sup>1</sup>, Jinyoung Serena Kim<sup>2</sup>, Andrej Sobolev<sup>3</sup>, Konstantin Getman<sup>4</sup>, Thomas Henning<sup>5</sup>, Min Fang<sup>1</sup>

<sup>1</sup>Departamento de Física Teórica, Facultad de Ciencias, Universidad Autónoma de Madrid, 28049 Cantoblanco, Madrid, Spain  
e-mail: aurora.sicilia@uam.es

<sup>2</sup>Steward Observatory, University of Arizona, 933 North Cherry Avenue, Tucson, AZ 85721-0065

<sup>3</sup>Astronomical Observatory, Ural Federal University, Lenin Avenue 51, 620000 Ekaterinburg, Russia

<sup>4</sup>Department of Astronomy & Astrophysics, 525 Davey Laboratory, Pennsylvania State University, University Park PA 16802

<sup>5</sup>Max-Planck-Institut für Astronomie, Königstuhl 17, 69117 Heidelberg, Germany

Submitted 9 May 2013, accepted 30 July 2013

### ABSTRACT

**Aims.** We present a study of accretion and protoplanetary disks around M-type stars in the 4 Myr-old cluster Tr 37. With a well-studied solar-type population, Tr 37 is a benchmark for disk evolution.

**Methods.** We used low-resolution spectroscopy to identify and classify 141 members (78 new ones) and 64 probable members, mostly M-type stars. H $\alpha$  emission provides information about accretion. Optical, 2MASS, Spitzer, and WISE data are used to trace the SEDs and search for disks. We construct radiative transfer models to explore the structures of full-disks, pre-transition, transition, and dust-depleted disks.

**Results.** Including the new members and the known solar-type stars, we confirm that a substantial fraction ( $\sim 2/5$ ) of disks show signs of evolution, either as radial dust evolution (transition/pre-transition disks) or as a more global evolution (with low small-dust masses, dust settling, and weak/absent accretion signatures). Accretion is strongly dependent on the SED type. About half of the transition objects are consistent with no accretion, and dust-depleted disks have weak (or undetectable) accretion signatures, especially among M-type stars.

**Conclusions.** The analysis of accretion and disk structure suggests a parallel evolution of dust and gas. We find several distinct classes of evolved disks, based on SED type and accretion status, pointing to different disk dispersal mechanisms and probably different evolutionary paths. Dust depletion and opening of inner holes appear to be independent processes: most transition disks are not dust-depleted, and most dust-depleted disks do not require inner holes. The differences in disk structure between M-type and solar-type stars in Tr 37 (4 Myr old) are not as remarkable as in the young, sparse, Coronet cluster (1-2 Myr old), suggesting that other factors, like the environment/interactions in each cluster, are likely to play an important role in the disk evolution and dispersal. Finally, we also find some evidence of clumpy star formation or mini-clusters within Tr 37.

**Key words.** stars: pre-main sequence – protoplanetary disks – stars: late-type — open clusters and associations: individual: Tr 37

## 1. Introduction

The evolution of accretion disks around low-mass stars, and the way protoplanetary disks cease to accrete and disappear, presumably after forming planets, is since long matter of discussion. Protoplanetary disks around solar-type stars have typical lifetimes of few Myr (Haisch et al. 2001; Sicilia-Aguilar et al. 2006a; Hernandez et al. 2007; Fedele et al. 2010), but the high variety of disk morphologies at a given age suggests that disk evolution is controlled by several mechanisms. Various physical processes can be invoked for disk removal, including grain growth, photoevaporation, and planet formation. In addition, other external parameters may also contribute to define the path followed by a dispersing disk, such as age, stellar mass,

\* Observations reported here were obtained at the MMT Observatory, a joint facility of the Smithsonian Institution and the University of Arizona.

\*\* Based on observations collected at the German-Spanish Astronomical Center, Calar Alto, jointly operated by the Max-Planck-Institut für Astronomie Heidelberg and the Instituto de Astrofísica de Andalucía (CSIC).

stellar and planetary companions, initial conditions, cluster environment, crowdedness in the star-forming region, and angular momentum of the collapsing core (Hartmann et al. 2006; Bouwman et al. 2006; Alexander & Armitage 2009; Fang et al. 2013a; Sicilia-Aguilar et al. 2013; Dullemond et al. 2006). Further processes (ejection in multiple systems, photo-erosion of cores by massive nearby stars; Bate et al. 2005, 2012; Whitworth & Zinnecker 2004) may also play a role in the formation of low-mass systems. The unexpected and not yet understood relation between stellar mass and accretion rate ( $dM/dt \sim M^{-3}$ ; Natta et al. 2004; Hartmann et al. 2006; Fang et al. 2009; but also  $dM/dt \sim M^{-1.2}$ ; Barentsen et al. 2011) is consistent with these multiple parameters affecting disk evolution (Clarke & Pringle 2006; Gatti et al. 2008; Herczeg & Hillenbrand 2008).

Multiwavelength observations of disks around faint objects are a challenge for current instrumentation. There is a lack of combined optical photometry, spectroscopy, and complete IR data for large samples of very low-mass objects. The first observations of disks around very low-mass stars and brown dwarfs (BD) suggested that they are lower-mass analogs of the typical

T Tauri disks. Their disks are flared, show active accretion with strong  $H\alpha$  emission, silicate emission from small grains in the disk atmosphere, processed and crystalline silicates, and dust continuum emission down to the far-IR and millimeter wavelengths (Muench et al. 2001; Klein et al. 2003; Mohanty et al. 2004; Jayawardhana et al. 2005; Apai et al. 2005; Scholz et al. 2007; Scholz & Jayawardhana 2008; Harvey et al. 2010, 2012a,b). Many of these observations were biased towards the most luminous disks and stronger accretors. Spitzer data suggested that there is an important fraction of harder-to-detect, settled, low-mass, and transitional disks with inner gaps around the very low-mass objects (masses  $<0.2 M_{\odot}$  down to the BD regime; Morrow et al. 2008). IR silicate spectroscopy of M-type stars also suggested differences in innermost disk evolution (Kessler-Silacci et al. 2007; Sicilia-Aguilar et al. 2007, 2008; Pascucci et al. 2009). Differences in the disk structure, dead zones, and accretion mechanisms for the lower-mass objects could also change the evolution of the disk and the formation of planets around very low-mass stars (Hartmann et al. 2006).

More recent observations suggest that the stellar mass is not the only parameter that controls the disk structure and subsequent evolution. Studies of stars in sparse clusters vs. more populous star-forming regions point to differences in the disk fraction vs. age trend. Sparse clusters would have relatively lower disk fractions at an early age, but these disks may survive for longer timescales compared to more massive regions (Fang et al. 2013a). The Herschel Space Telescope has traced the typical sizes and structures where young stars are formed (Arzoumanian et al. 2011; Hacar et al. 2013), revealing the details of star-forming filaments. Surprisingly, some sparse associations, instead of being quiet low-mass star-forming regions, appear to be very crowded, active, and interactive already at a very early stage (Sicilia-Aguilar et al. 2013). The cluster dynamics, interactions, and angular momentum in the collapsing cloud could also affect the initial mass function (IMF) and the disk properties and subsequent evolution (Hsu et al. 2012, 2013; Becker et al. 2013; Dullemond et al. 2006).

With this work we want to address disk evolution and its dependency on stellar mass/spectral type and environment by studying the low-mass members in the Tr 37 cluster. Tr 37 is located at 870 pc distance (Contreras et al. 2002) and part of the Cep OB2 complex (Platais et al. 1998; Patel et al. 1995, 1998). The cluster is a key region for disk evolutionary studies due to its intermediate age ( $\sim 4$  Myr; Sicilia-Aguilar et al. 2005) compared to the typical disk lifetimes (3-10 Myr; Sicilia-Aguilar et al. 2006a; Hernández et al. 2007; Fedele et al. 2010). Multi-wavelength studies (Sicilia-Aguilar et al. 2004, 2005, 2006a,b; from now on SA04, SA05, SA06a, and SA06b) have targeted the solar-type population in the region, finding evidence of substantial disk evolution and dust processing (SA06a; Sicilia-Aguilar et al. 2007, 2011b, from now on SA11). Detailed  $H\alpha$  photometry surveys (Barentsen et al. 2011) revealed an extended population of accreting stars, some of which could be younger than the main cluster (SA05, Getman et al. 2012).

The disk structure for the solar-type population has been already extensively discussed in SA06a and SA11. Using a combination of optical (photometry and spectroscopy), Spitzer (IRAC, MIPS, and IRS), and millimeter-wave (IRAM) data, together with simple radiative transfer models (RADMC; Dullemond & Dominik 2004), we constrained disk parameters and deviations from typical, uniform, flared disks. Here we present a detailed multiwavelength study of the low-mass population in Tr 37. By using optical spectroscopy, we were able to classify more than 200 objects among cluster members and probable

members, including 78 newly identified members, most of them M-type stars. Combining this information with our previous optical photometry and Spitzer IRAC/MIPS data, we analyze the disk characteristics of the objects and put them in context comparing them to our previous study of the solar-type stars. All observations are presented in Section 2. In Section 3 we examine the membership of the candidates and derive their fundamental stellar properties. In Section 4 we explore the implications of the newly discovered objects for disk dispersal and evolution. Finally, Section 5 summarizes our results.

## 2. Observations and data reduction

### 2.1. Optical and IR data and candidate selection for spectroscopy

This study aimed to complete the previous work of SA05/SA06a/SA11 on the disks around solar-type stars in the Tr 37 cluster, which was approximately complete for stars with spectral types K4-M2, by addressing the M-type population in the cloud. Optical photometry and spectroscopy are required to confirm the cluster membership, to obtain spectral types, to detect accretion, and to estimate extinction, age, and stellar mass. The starting point of the target selection was the deep optical photometry obtained at Calar Alto Observatory with the LAICA camera on the 3.5m telescope, consisting of deep observations with the standard UVRI Johnsons filters (see Sicilia-Aguilar et al. 2010 for a detailed description of the observations and data reduction). The data had a large dynamical range, being complete in the range  $U \sim 15-21$ ,  $V \sim 13-21$ ,  $R_J \sim 12-21$ , and  $I_J \sim 11-20$  mag. The low-mass candidates relevant for our survey were in general too faint to be detected with the U band filter. The requirement for the objects to be preferably candidate M-type members resulted in a selection of objects with  $R_J = 17-20.5$  mag, considering that the extinction over Tr 37 is moderate and relatively uniform ( $A_V = 1.56 \pm 0.55$  mag). Examining the 2MASS (Cutri et al. 2003) counterparts of our optical targets allowed to refine the selection of objects consistent with diskless late-type stars and the locus of classical T Tauri stars (CTTS) in the J-H vs H-K diagram (Bessell & Brett 1988; Meyer et al. 1997), although for M-type stars with evolved disks, the excesses in H and K bands are usually very small or negligible. The 2MASS coordinates were also used for the later spectroscopy, given the strong requirements of multiobject spectrographs.

To complete the spectral energy distributions (SEDs) of the candidates, we re-reduced the Spitzer IRAC and MIPS observations (from both our previous datasets in SA06a, and Spitzer archival data), following the method described in SA11. These new photometry is not significantly different from that of SA06a, although the use of a more recent pipeline with improved flat fielding, and smaller apertures result in more accurate magnitudes for the in-cloud sources and a better detection of very faint objects in the MIPS  $24\mu\text{m}$  maps. To ensure that contamination by cloud emission or ghosts remains minimal, we visually inspected all the candidates. In particular, detailed inspection of the  $24\mu\text{m}$  data was necessary to remove objects suffering from nebular emission.

For the spectroscopic followup, we selected the sources with ages under 100 Myr that were consistent with solar- and M-type stars at 870 pc distance according to the V vs V-I and V-R diagrams and the Siess et al. (2000) isochrones. This produced a list of about 400 targets, of which approximately 100 had IR excesses consistent with circumstellar disks and that lacked spec-

troscopic characterization. We assigned priority to allocating the fibers and slits to objects with IR excess, followed by those with isochrone ages  $<10$  Myr, and finally those between 10-100 Myr. All the observed targets are listed in the Appendix A, Table A.1, together with the relevant information about  $H\alpha$ , Li I emission, presence of disks, spectral type, extinction, and membership (see Section 3 for details). A few remaining fibers were assigned to previously known objects, or to objects with strong IR excesses but lacking optical data. This study is thus biased towards objects with disks, so we cannot estimate the disk fraction. The main advantage is that we covered more than 90% of the candidate M-type stars with IR excesses, obtaining a superb dataset to explore the various disk structures. The photometry data (optical, 2MASS, and Spitzer) are listed only for the members and probable members in the Appendix A, Tables A.2 and A.3.

For completeness, after the survey we also checked the WISE database for counterparts to our objects. The Spitzer data are preferred because the larger WISE beam often suffers from strong contamination due to cloud emission, resulting in overestimated fluxes, especially in bands 3 and 4. Nevertheless, band 3 ( $12\mu\text{m}$ ), together with IRAC  $8\mu\text{m}$ , offers valuable information regarding the silicate emission. Whenever there was a good agreement between IRAC and WISE bands 1 and 2, MIPS  $24\mu\text{m}$  and WISE band 4 ( $22\mu\text{m}$ ), we assume there is no significant contamination and thus use the  $12\mu\text{m}$  WISE data. The WISE fluxes were obtained applying the Wright et al. (2010) color corrections depending on the Spitzer SED shape. The WISE data used in this project are also listed in the Appendix A, Table A.4.

The spectroscopic properties of the observed objects and membership criteria are described in Section 3. Thanks to the strong candidate selection criteria, the efficiency of the survey was very high, with about 90% of candidates with isochronal ages younger than 10 Myr and IR excesses being confirmed as cluster members. The success rate fell down to  $\sim 5$ -20% among the objects without excess. A number of objects with very low S/N could not be ruled out nor confirmed as members (see Table A.1). A few examples of SEDs of members with IR excesses are shown in Figure 1. The SEDs of all members and probable members with IR excesses are displayed in the Appendix B, Figures B.1-B.6, and the SEDs classification criteria are discussed in Section 4.1.

## 2.2. SCORPIO multislit/6m Russian SAO RAS Telescope

One observational campaign took place with the SCORPIO (Spectral Camera with Optical Reducer for Photometric and Interferometric Observations) multislit spectrograph (Afanasiev & Moiseev 2005) at the 6m telescope of the Special Astrophysical Observatory of the Russian Academy of Sciences, in the Northern Caucasus. The observations were obtained during 2008 October 4, 5, and 6. SCORPIO is a multislit spectrograph with 16 movable long slits (each of  $18''$ ) that can be placed over a  $2.9\times 5.9$  arcmin<sup>2</sup> field. We observed 3 configurations, with slits allocated to cover between 12 and 16 candidate objects. We used the grism VPHG1200r, with a spectral coverage 5700-7500 Å and a  $5$  Å/pix resolution. Due to the poor weather conditions, we had to reduce the exposure time to  $3\times 15$ -10 min per field.

The observations were reduced following standard IRAF<sup>1</sup> procedures within the *specred* package, in particular, routines

within the *twodspec.apextract* package. The spectra were bias-corrected, flat fielded, and extracted. The wavelength calibration was performed with a Ne lamp, observed with the same slit configuration as the datasets. The sky subtraction was done by using the sky spectra adjacent to the star in the slit. A total of 18 new member candidates were identified among the observed objects. The main limitation of these observations was the poor S/N of the data, due to the poor weather conditions, that did not allow us to clearly detect the Li I absorption in most of the candidates. We therefore re-observed many of these objects in our subsequent spectroscopic program with the MMT. The advantage of using SCORPIO is that the long slit data allow unambiguous subtraction of the nebular emission around the sources.

## 2.3. Hectospec/MMT Spectroscopy

The candidate objects were observed during two campaigns with the multifiber spectrograph Hectospec on the 6.5m MMT telescope in Mount Hopkins, AZ. The first set of observations were taken on 2009 July 14 and 19, and the second one on 2010 May 17 and 19. The weather conditions were fair during both campaigns. Hectospec is a multifiber spectrograph with 300 fibers that can be allocated to individual objects or sky over a 1 degree field of view. We took at total of 3 configurations, each one including between 180 and 220 candidate objects, plus numerous sky positions. We used the 270 gpm grating, with a spectral coverage from  $\sim 3650$ - $9200$  Å and a typical resolution of  $5$  Å. This is the same setup we used for the observations of the solar-type stars (SA05). For each field, we took  $3\times 30$  min exposures, followed by sky observations obtained by shifting the whole configuration by  $5''$  and exposing  $3\times 10$  min. These sky observations are particularly useful to attain a good sky subtraction in the cases of faint targets or objects in regions with complicated background, since they provided the sky spectrum in a region very close to the objects, and obtained with the same fiber.

The bias, flat fielding, and wavelength calibration were done with standard IRAF tasks within the *dofibers* package. For the wavelength calibration, we used a HeNeAr calibration lamp. Due to the offsets between the even- and odd-numbered fibers, the wavelength calibration was done separately for the even and odd fibers. The one-dimensional spectra were extracted and combined before the sky subtraction. The sky subtraction can be a problem in regions like Tr 37, where substantial, spatially-variable emission from the H II region can affect the  $H\alpha$  line, one of our main membership diagnostics. For each night, we classified all the sky spectra in "bright", "medium", and "faint", according to the intensities of the nebular emission lines (especially,  $H\alpha$ , [N II], and [O I]), combining the three sets to create bright, medium, and faint sky templates. Each template resulted from a minimum of 20 spectra. The three templates were subtracted from all the objects, and we then examined the success of each sky subtraction by checking the night sky and nebular emission lines. We then selected the best-subtracted spectrum. For about a fourth of the objects, none of the three sky subtractions provided a good result (either by excess or by defect). In those cases, we used the wavelength-calibrated individual sky spectra taken in the proximity of the star, which improved the subtraction of the nebular and night sky lines, although the difference in exposure time resulted in a higher noise than in the cases where the sky template spectra were applied. Some examples of spectra are shown in Figure 2.

<sup>1</sup> IRAF is distributed by the National Optical Astronomy Observatories, which are operated by the Association of Universities for Research in Astronomy, Inc., under cooperative agreement with the National Science Foundation.

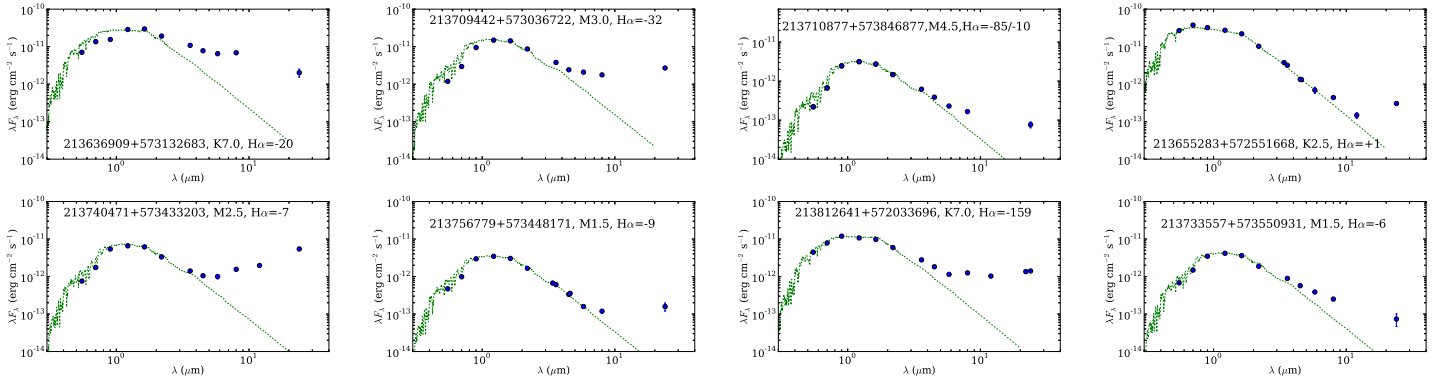


Fig. 1: Examples of SEDs of some of the members with IR excess. For comparison, the photosphere of a star with the same spectral type from the MARCS models (Gustafsson et al. 2008) is displayed. All datapoints have been extinction-corrected according to their individual values of  $A_V$  and assuming a standard extinction law (see Table A.1. Information about the  $H\alpha$  EW (in  $\text{\AA}$ ) is also displayed. The rest of SEDs of objects with IR excesses are displayed in the online material.

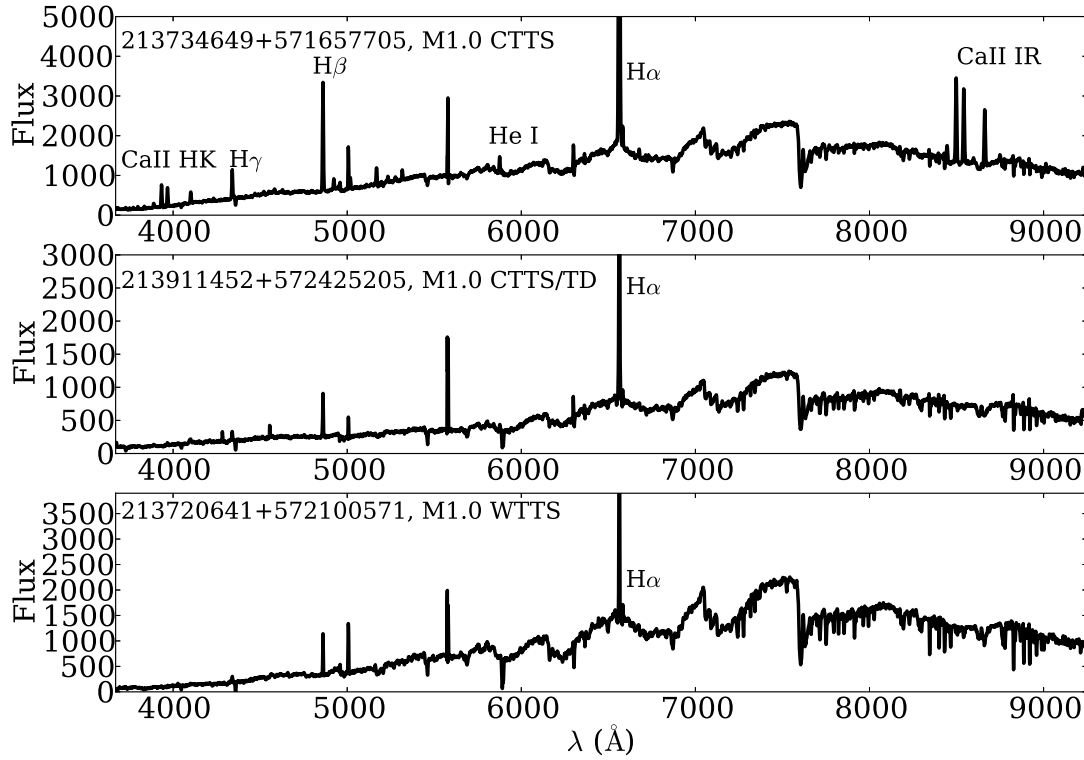


Fig. 2: Some examples of spectra taken with the MMT/Hectospec. The  $H\alpha$  features are cut to reveal more details of the whole spectra. Note that the spectra still show some telluric lines in emission (mostly at  $5577$  and  $5004\text{\AA}$ ). The flux is in arbitrary instrumental units.

#### 2.4. CAFOS/2.2m Calar Alto narrow band imaging

Since our previous spectroscopic surveys had revealed substantial forbidden line emission in the Tr 37 globule, we also performed a narrow band imaging in the [S II] lines using the Fabry-Pérot interferometer with the CAFOS wide-field imager mounted on the 2.2m telescope in Calar Alto. The data were obtained as part of a Director Discretionary Time program on 28 August 2009.

We obtained images centered in the Tr 37 globule, around the CTTS 14-141, RA(2000) DEC(2000) 21:36:49.41 +57:31:22.0, which showed remarkable variable forbidden line emission in our previous spectroscopic surveys. We obtained 3 dithered 600s exposures with the Fabry-Pérot interferometer at  $6716$ ,  $6730$ , and  $6750\text{\AA}$ , resulting in narrow-band images centered on the two [S II] lines and a continuum observation with the same width in the line-free region around  $6750\text{\AA}$ . An additional  $3\times 10s$  Johnsons R band image was also obtained for comparison. The data were reduced (bias, flat field) and combined according to the

standard procedures using IRAF packages. Finally, a line-only image was obtained by subtracting the continuum 6750 Å image from the [S II] ones. To improve the S/N, we combined both [S II] lines for the final result. We did not attempt any flux calibration, which is difficult due to the properties of the filter and to the fact that there is a wavelength drift over the CAFOS field. The resulting data clearly reveals several shocks in the field, not only associated to 14-141, but also to several of the protostars and embedded objects in the cloud (see Figure 3).

### 3. Analysis

#### 3.1. Spectral types and extinction

As a preliminary step to determine the membership and properties, we obtained spectral types for all the observed objects, which are listed in the Appendix A, Table A.1. The spectral types of the objects with good S/N were derived using the combinations of indices employed for the classification of K-M3 stars in Cep OB2 by Sicilia-Aguilar et al. (2004), and a similar scheme for M3-M8 stars as it was used for classification of the Coronet cluster members (Sicilia-Aguilar et al. 2008). The classification of M3-M8 stars was based on the indices defined by Kirkpatrick et al. (1995), Martín et al. (1996), and Riddick et al. (2007). From the indices therein, we selected the best ones that did not suffer from strong problems due to atmospheric features, extinction, or lack of S/N in the blue (see Table 1). The calibration in Sicilia-Aguilar et al. (2004) is done in effective temperature (see Table 2). The effective temperatures ( $T_{eff}$ , in units of  $10^3$  K) are derived as  $T_{eff}=T_0 + b \times (I-I_0)$ , where  $I$  is the measured index, and  $T_0$ ,  $I_0$ , and  $b$  are the zero-point values of effective temperature and index, and the slope of the relation resulting from the fit of several standard stars (Sicilia-Aguilar et al. 2004). The index  $I$  is obtained as a function of the flux in different wavelength ranges ( $F_{\lambda_1-\lambda_2}$  is the flux between the wavelengths  $\lambda_1$  and  $\lambda_2$  in Å). The values of  $T_{eff}$  are transformed to spectral types using the calibration by Kenyon & Hartmann (1995). The spectral types of objects observed with SCORPIO were derived by direct comparison to standard stars, given their reduced wavelength coverage. We also note that since the SCORPIO spectra do not include the main features for classification of G/K stars, stars other than M-type observed by SCORPIO have very uncertain spectral types.

The indices are not applicable out of a given spectral range. Therefore, we did a preliminary visual classification of the stars as "earlier than G", "GK-type", and "M-type" before computing the spectral types. Due to our selection criteria, most of the stars found to be earlier than G are unlikely members, and they are simply listed in Table A.1 as "early type" (E). For the objects classified as "GK-type", we used the MgI and CaI indices. The number of indices applicable to G-type and early-K stars is also very low, so the spectral types of objects earlier than K5 were refined by comparison to standard stars. For the objects classified as "M-type", we used first the TiO 6185 index to determine whether the object was earlier or later than M3. For objects earlier than M3, we then used the CaI and TiO71 indices to refine the spectral type. For M3 or later types, we used the PC1, R1, and R3 indices to derive a preliminary spectral type, which was refined by using the TiO 8465, VOa, VOb, and PC2 indices, if within their applicable range. For each star, the final spectral type is calculated as the average of the types obtained with the applicable indices. In all cases, we performed a visual comparison with standard stars to check that the estimated spectral type is in agreement with the appearance of the spectrum.

Table 1: Indices used to derive the spectral type for stars later than M2.5.

Name	$\lambda$ Numerator	$\lambda$ Denominator	Range	Calibration	Reference
PC1	7030-7050	7525-7550	M3-M9	$-0.06+2.95 X$	1,2,4
PC2	7540-7580	7030-7050	M4-M8	$-0.63+3.89 X$	1,2,4
R1	8025-8130	8015-8025	M2.5-M8	$2.8078+21.085(X-1.044)-53.025(X-1.044)^2+60.755(X-1.044)$	3
R2	8415-8460	8460-8470	M3-M8	$2.9091+10.503(X-1.035)-14.105(X-1.035)^2+8.5121(X-1.035)$	3
R3	(8125-8130)+(8415-8460)	(8015-8025)+(8460-8470)	M2.5-M8	$2.8379+19.708(X-1.035)-47.679(X-1.035)^2+52.531(X-1.035)$	3
TiO 8465	8405-8425	8455-8475	M3-M8	$3.2147+8.7311(X-1.085)-10.142(X-1.085)^2+5.6765(X-1.085)$	3
VOa	(7350-7370)+(7550-7570)	7430-7470	M5-M9	$5.0705 + 11.226(x-0.982)+6.7099(x-0.982)^2$	3
VOb	(7860-7880)+(8080-8100)	7960-8000	M4-M9	$3.4875 + 29.469(x-1.017)-156.53(x-1.017)^2+394.28(x-1.017)+325.44(x-1.017)^4$	3

**Notes.** Indices used for spectral typing of mid- and late-M type stars. The wavelengths are given in Å. In the calibration, X represents the index obtained by dividing the numerator and denominator, and the resulting number indicates the M subtype. References: 1= Kirkpatrick et al. (1995); 2= Martín et al. (1996); 3= Riddick et al. (2007); 4= Sicilia-Aguilar et al. (2008)

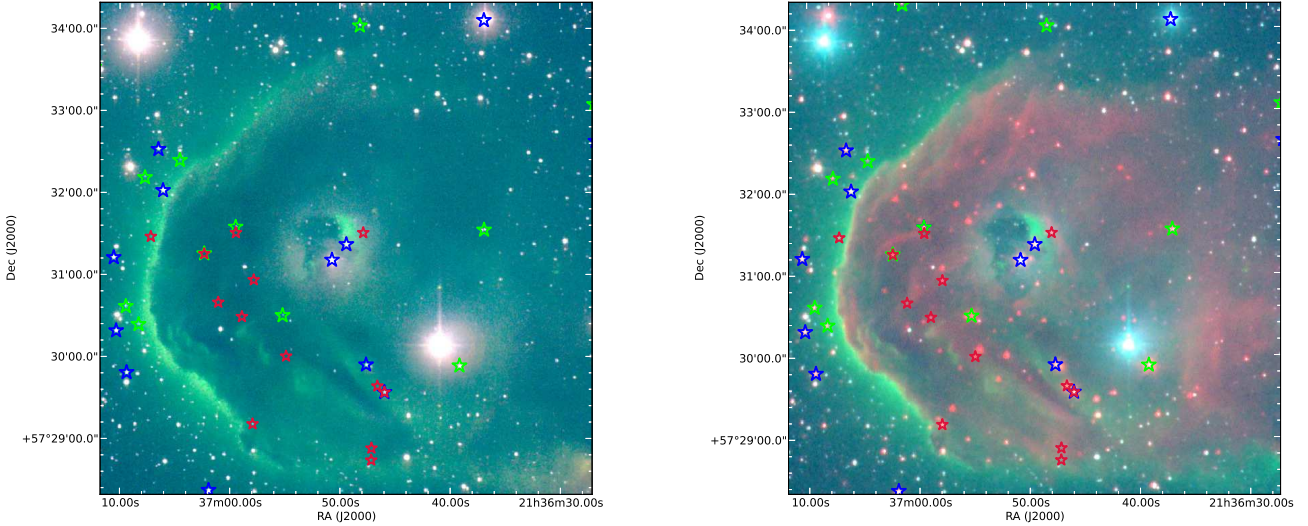


Fig. 3: Two 3-color images of the IC 1396 A globule. Left: narrow band at 6750Å, [S II] combined at 6716 and 6730Å, and R band as red, green, and blue, respectively. Right: IRAC1, [S II] combined at 6716 and 6730Å, and R band as red, green, and blue, respectively. Known members detected via optical spectroscopy are marked as blue stars, new members are marked as green stars. Spitzer embedded candidates (SA06a) are marked by red stars.

Table 2: Indices used to derive the spectral type for G,K,M-type stars.

Name	$T_0$ (10 K)	$I_0$	b (10 K)	Range ( $T_{eff}/10^3$ K, Spec. Type)	Index (I)
TiO 6185	3.40	$1.58 \pm 0.03$	$-0.94 \pm 0.11$	3-3.9, M5-M0	$F_{6165-6210}/F_{6100-6150}$
TiO 7140	3.40	$1.99 \pm 0.02$	$-0.40 \pm 0.03$	3-3.7, M5-M2	$F_{7125-7155}/F_{7020-7050}$
MgI	5.35	$0.84 \pm 0.02$	$5.50 \pm 0.28$	4.8-6, K2-G0	$(2 \times F_{5160-5180}) / (F_{5005-5025} + F_{5225-5245})$
CaI	3.22	$1.43 \pm 0.01$	$-1.18 \pm 0.05$	3-3.6, M5-M3	$(F_{6000-6200} + F_{6300-6320}) / (2 \times F_{6155-6175})$
CaI	4.10	$1.16 \pm 0.03$	$-8.74 \pm 0.80$	3.6-5.1, M3-K1	$(F_{6000-6200} + F_{6300-6320}) / (2 \times F_{6155-6175})$

**Notes.** Indices used for spectral typing of G, K, and early-M star (Sicilia-Aguilar et al. 2004).

The few cases where there was a discrepancy between the derived type and the visual inspection could be tracked to different problems (presence of stellar or sky emission lines, lack of S/N in part of the spectrum, contamination by scattered light) that were addressed by removing the discrepant indices, and using the non-contaminated ones to derive the final spectral type.

In case of the objects with more than one spectra, we derived the spectral type for each one and consider the result of the best S/N spectrum (if the quality of both was very different). There is a very good agreement between all estimates (within 1-2 subtypes, depending on spectral type and data quality). Spectral types had been previously derived for 14 among the 17 objects in common with our previous campaigns. Among these, we recover the previous spectral type ( $\pm 1$  subtype) in 9 cases, 2 cases are off by up to 2 subtypes, and 3 are off by up to 3 subtypes (corresponding mostly to faint M-type stars with low S/N in this or in previous surveys and/or limited spectral coverage). This confirms our typical estimated error of 1-2 subtypes, strongly depending on the S/N. In some cases, real spectroscopic variations were observed between 2009 and 2010, probably due to variations in the accretion activity and in the stellar spots. Two examples of this behavior are 213701319+573418289 (M3.0/M1.0, 2009 spectrum later than the 2010 one) and 213710877+573846877 (M4.5/M2.0, later in 2009).

We obtained the extinction of each object by comparing the observed optical data at VRI with the theoretical colors for young Taurus stars with the same spectral type (Kenyon & Hartmann 1995), and applying the relations of Cardelli et al. (1989) to derive  $A_V$  from  $E(V-I)$  and  $E(V-R)$  for the Johnsons filters. Whenever VRI photometry was available, we used both  $E(V-I)=0.521 A_V$  and  $E(V-R)=0.249 A_V$ , estimating  $A_V$  as the average, with an error corresponding to the standard deviation. In the cases where one optical band was missing, we used the available data (V-I, V-R, or R-I) to compute the extinction, and estimated the error considering the typical spectral typing error. In the cases where no optical data (or only one optical band) were available, the extinction was derived from the 2MASS photometry, considering the theoretical colors from Bessell & Brett (1988) and the corresponding relations for  $E(J-H)=0.092 A_V$  and  $E(H-K)=0.076 A_V$ . For the few objects that are confirmed to be members but have no reliable spectral types, we take the average cluster extinction ( $A_V=1.6$  mag; SA05). The final extinctions are listed in the Appendix A, Table A.1.

### 3.2. Membership

The membership of the stars was established by a combination of several indicators. Typical youth indicators are the Li I absorption at 6708Å and the  $H\alpha$  equivalent width (EW). The EW

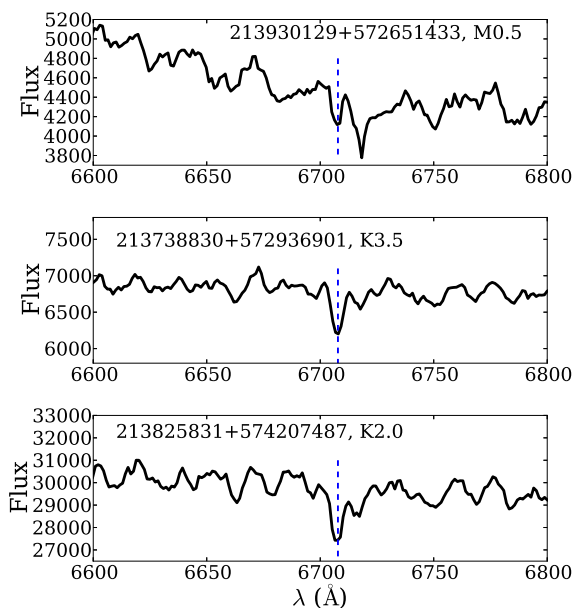


Fig. 4: Some examples of Li I detections with the MMT/Hectospec. The flux is in arbitrary instrumental units. The broad photospheric lines in 213825831+574207487 are also typical of a relatively fast rotator.

of both  $H\alpha$  and Li I are listed in Table A.1. Table A.5 lists other lines that have been observed in some members, mostly strongly accreting CTTS where the whole Balmer series is visible, together with the Ca II IR triplet, He I lines, Ca II H and K lines, and some Fe I and O I emission (Hamann & Persson 1992; Appenzeller et al. 1986), plus a few objects with forbidden [S II] and [O I] lines related to shocks (Hamann 1994). The most reliable indicator of youth for late-type stars is the Li I absorption at 6708Å (Figure 4). Objects with clear Li I detection are labelled as sure members, and objects with good S/N at 6708Å and no evidence of Li I absorption as labeled as non-members. Unfortunately, the Li I line is not always detectable in these faint objects, so we need additional membership criteria.

The  $H\alpha$  line in emission is the main characteristic of T Tauri stars. In general, we followed the criteria of White & Basri (2003) regarding accretion and the distinction between classical and weak-line T Tauri stars (CTTS/WTTS). For the objects observed with the multifiber spectrograph Hectospec, sky subtraction is complicated due to the strong nebular emission in Tr 37, so low  $H\alpha$  EW values are uncertain. Young, non-accreting M-type stars can be hard to classify based on their  $H\alpha$  emission since one of the main sources of contamination are older dMe stars in the field. Therefore, late-type stars with strong  $H\alpha$  emission ( $>10\text{\AA}$ ) were classified as members, especially if the Spitzer data show an excess consistent with a disk. Stars with weak  $H\alpha$  emission ( $<10\text{\AA}$ ) and no disk were considered as potential members, requiring additional information to confirm membership. Stars with  $H\alpha$  absorption, especially those with late K or M spectral types<sup>2</sup>, were rejected as non-members.

Our previous study of the solar-type stars revealed that the extinction towards Tr 37 is moderate, relatively constant over the cluster (except in the globules), and mostly due to foreground

<sup>2</sup> Some early K and late G WTTS may have nearly zero emission, despite their youth, with the White & Basri (2003) criterion for CTTS being as low as  $H\alpha$  EW  $>3\text{\AA}$ .

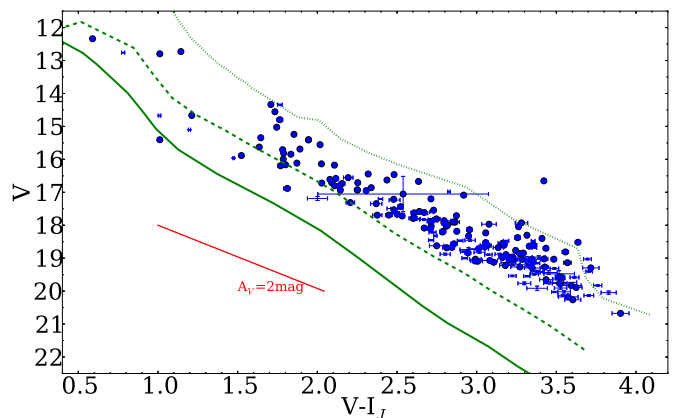


Fig. 5: A V vs V-I (Johnson system) diagram of the members (large filled circles) and probable members (small points) found in this survey. For comparison, the Siess et al. (2000) isochrones for 1, 10, and 100 Myr are displayed, transformed into the Johnsons system according to Fernie (1983) and Getman et al. (2012). An extinction vector (Cardelli et al. 1989) is also displayed. Errorbars (considering the photometric and  $A_V$  errors) are also displayed, although they are often smaller than the symbols.

material. The distance of the cluster (870 pc, Contreras et al. 2002) imposes a minimum extinction around  $A_V=1$  mag, and the study of the solar-type population revealed an average extinction of  $A_V=1.56\pm0.55$  mag, with nearly all the bona-fide members outside the globule having  $A_V <3.5$  mag (SA05). This allows us to use the extinction as a further membership criterion, by defining the extinction ranges expected for the cluster members. Since this survey targeted fainter and thus potentially more extinguished members, we explored the extinction distribution of our newly found objects with Li I absorption (42 in total). The average extinction and standard deviation is  $A_V=1.94\pm0.69$  mag. There are no Li I-detected members with  $A_V >4$  mag, and only 7% have extinctions  $\geq 3.5$  mag. There are also no Li I members with extinctions lower than 0.8 mag, and only 5% of the members have extinctions below 1 mag, while 29% have  $A_V \geq 1.5$  mag. Therefore, we consider as candidate members all the objects with extinctions in the range 1-4 mags. Objects in this range with additional membership indicators (strong  $H\alpha$  emission, IR emission from a disk) are considered as sure members, while objects with no additional indicators of youth (no Li I absorption, no disk, weak  $H\alpha$ , but extinction consistent with the cluster values) are considered as probable members. Objects with extinctions out of the cluster range but strong indicators of membership (strong accretion-related lines and disk emission) are considered as members.

Finally, since this survey was fully independent of the X-ray observations of the IC 1396A globule by Getman et al. (2012), we also checked the objects in common with X-ray observations. A total of 23 of the X-ray YSO candidates and 16 of the non-Xray YSO with disks were found in common with our member selection, all labeled as sure and probable members. Four probable members with X-ray detections were thus upgraded to sure members. Three further objects (one probable member, two probably non-members) were listed among uncertain X-ray detections, and we are keeping their original membership classification.

Placing the new members and probable members in the V vs. V-I diagram (Figure 5), we find that their ages are consistent

with the mean age of 4 Myr derived previously (SA05). Since the Siess et al. isochrones are given in the Cousins system, we transformed them into the Johnsons system following the prescriptions of Fernie (1983, for blue stars,  $V-I_c < 1.5$  mag), and Getman et al. (2012, for red stars,  $V-I_c > 1.5$  mag). A few of the objects appear below the 10 Myr isochrone, but in most cases they are stars with flared disks and high (or even anomalous) extinction being thus probably UXor candidates (all labeled in Table A.1). In addition, early K and G stars tend to deviate from typical isochrone models, probably due birthline uncertainties (Hartmann 2003). Some of the probable members that have anomalous positions in the V vs. V-I diagram may be contaminants, giving us an idea of the uncertainty in the membership of the objects marked with 'P'.

Taking into account the five different criteria (Li I absorption,  $H\alpha$  emission, disk excess, extinction, and X-ray), from the initial collection of 565 objects observed, we arrive to a collection of 141 sure members, plus 64 probable members and 33 probable non-members. The rest of the 308 observed stars are rejected as non-members or marked as uncertain cases on the basis of low S/N (19 in total). A total of 28 identified members are in common with the  $H\alpha$  survey of Barentsen et al. (2011), and 17 objects corresponded to re-observations of previously identified members in SA05 and SA06b<sup>3</sup>. One further object was suggested to be a YSO by Morales-Calderón et al. (2009). Excluding the objects that had been previously suggested to be members by the different authors, we arrive to 78 newly identified members and 64 probable members (to be confirmed with future followup observations), mostly M-type stars and GK members with extinctions higher than the cluster average and with protoplanetary disks.

## 4. Discussion

### 4.1. Disk structure and the accretion/disk connection

As we had found in our previous papers (SA06a; Sicilia-Aguilar et al. 2007), there is a large variety of disk morphologies in Tr 37. We have classified the new disks following the scheme developed in our Spitzer IRS-based study (SA11). The main criteria for defining the disk evolutionary state are the presence of inside-out evolution, as in transitional and pre-transitional disks, and the evidence of generalized small-dust depletion, as in homologously depleted disks (Currie et al. 2009). A comparison of the disk slope at short and long wavelengths is fundamental to distinguish disks with evidence of inside-out evolution, although the silicate feature at  $10\mu\text{m}$  also plays an important role. Objects with inner gaps or partially cleared disks, such as pre-transitional disks (Espaillat et al. 2010), have weak near-IR fluxes, strong silicate features, and strong mid-IR excesses, are especially hard to identify without spectroscopic information. Low fluxes at  $24\mu\text{m}$  and longer wavelengths are a key to identify small-dust-depleted disks.

To quantify inner disk evolution, we consider  $\alpha(\lambda_1 - \lambda_2)$ , defined as the SED slope between two wavelengths:

$$\alpha(\lambda_1 - \lambda_2) = \frac{\log(\lambda_1 F_{\lambda_1}) - \log(\lambda_2 F_{\lambda_2})}{\log \lambda_1 - \log \lambda_2}. \quad (1)$$

<sup>3</sup> These include 11-1499, which was labeled as probably non-member following the criteria in this study, but had Li I absorption in our better S/N spectra from SA05 and X-ray emission according to Getman et al. (2012), so we consider it as member, and the previously identified probable member 21-851, now rejected as cluster member.

Objects with nearly photospheric colors ( $[3.6]-[4.5] < 0.2$  mag,  $\alpha(3.6-4.5) \sim -3.0$  to  $-2.13$ ) but significant excess at longer wavelengths are classified as transition disks (TD). Disks with moderate to low near-IR excess ( $[3.6]-[4.5] \sim 0.2$  to  $0.4$  mag,  $\alpha(3.6-4.5) \sim -2.13$  to  $-1.30$ ) and a change in the sign of the slope between 8-12 and  $24\mu\text{m}$  are labelled as “kink” disks (according to SA06a terminology) and are good candidates for pre-transitional disks (PTD).

Regarding the small-dust mass, and based on our previous results (SA11), we consider objects with low IR fluxes at all wavelengths and reduced  $24\mu\text{m}$  fluxes as globally dust-depleted disks. Dust-depleted disks have near-IR in the PTD range or lower, but with similarly steep slopes at all other wavelengths and thus very low  $24\mu\text{m}$  fluxes (for K- and M-type stars,  $\lambda F_{\lambda} \leq 2 \cdot 3 \times 10^{-13}$  erg  $\text{cm}^{-2} \text{s}^{-1}$ ). We labelled the objects in Table A.3 according to the disk classification. Figure 6 is color-coded to show the different disk types vs. the SED slopes at different wavelengths. The final classification also requires visual inspection of all the SEDs to detect the few cases that satisfy the mentioned criteria but display SEDs that evidently do not correspond to the presumed disk class. Objects with uncertain photometry/excesses are also excluded from the following analysis and discussion.

Several studies have suggested a strong connection between the IR excesses typical of protoplanetary disks and active accretion (e.g. Sicilia-Aguilar et al. 2006b, 2010; Fedele et al. 2010) while some others suggested that the differences between non-accreting, WTTS and CTTS in terms of disks are minimal (e.g. Cieza et al. 2007; Oliveira et al. 2013). Differences in accretion between transitional and non-transitional disks have also been matter of debate (Najita et al. 2007; Muzerolle et al. 2010; Sicilia-Aguilar et al. 2010; Fang et al. 2009, 2013b; Merín et al. 2010). Tr 37 is an interesting region, having a large number of disks with signs of evolution and a disk fraction slightly below 50% (SA06a). A first approach including all known low-mass stars with spectral types G, K, M, suggests a high correlation between the  $H\alpha$  EW, the SED slopes, and our disk classification (Figure 7; the disk classification is shown in the color-code). Figure 8 displays the  $H\alpha$  EW vs. the effective temperatures ( $T_{\text{eff}}$ ) for the whole sample of low-mass members, also color-coded according to their disk types. Instead of separating the objects in CTTS/WTTS according to their  $H\alpha$  EW, we directly considered the measured  $H\alpha$  EW within each disk class, and performed a double-side Kolmogorov-Smirnov (KS) test to find out the probability that the  $H\alpha$  EW of different types of objects are drawn from the same sample.

Table 3 summarizes the results of the KS test. We find unmistakable evidence of a different distribution of  $H\alpha$  EW between objects with disks (including all types of disks) and without disks (no evidence of excess emission at any wavelength), with probabilities nominally 0 that both distributions are drawn from the same sample. We also find significant differences between the  $H\alpha$  EW of TD and full-disks, mostly related to the fact that between 40 and 60% of the TD have  $H\alpha$  values consistent with non-accreting stars<sup>4</sup>, while this is extremely rare among full-disks. Fang et al. (2009, 2013b) found that the fraction of strong accretors ( $H\alpha \text{ EW} > 2 \times H\alpha_{\text{threshold}}$  for a given spectral type) in the Orion Lynds 1641 and 1630N clouds is around 60% among full disks, while only 21-26% of the TD have comparable high accretion. Fang et al. (2013b) inventoried a sample of  $\sim 1390$  YSOs in Lynds 1641. Their sample includes more than 60

<sup>4</sup> Note that although  $H\alpha$  EW is a good indicator of accretion, further data like high-resolution  $H\alpha$  spectroscopy or U band photometry is needed to rule out cases with very low accretion rates



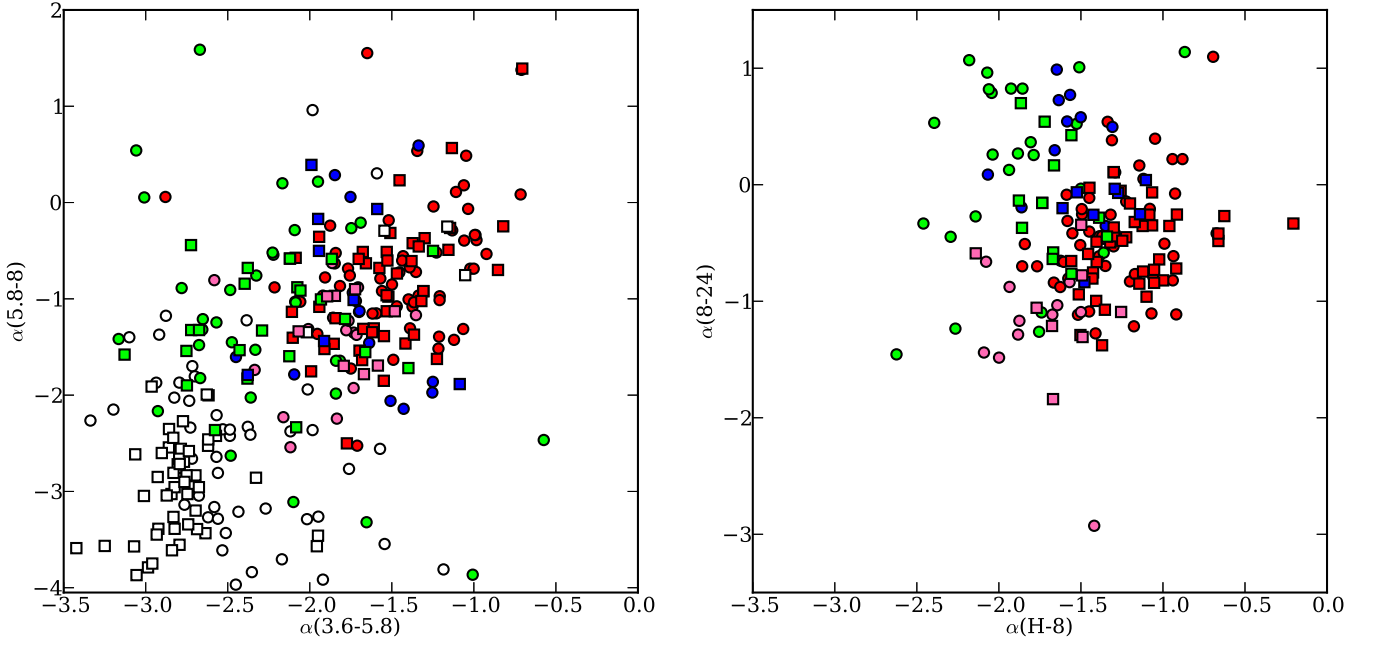


Fig. 6: Different disk slopes for the objects with different spectral types. Circles mark the newly identified members, squares denote the previously known ones. Diskless objects are open symbols (none of the diskless objects is detected at  $24\mu\text{m}$ , and in general diskless objects with apparent excesses are due to contamination and/or uncertain photometry). Red symbols are the typical full-disks. Green symbols mark the TD. Blue symbols mark the PTD. Pink symbols mark the dust-depleted disks.

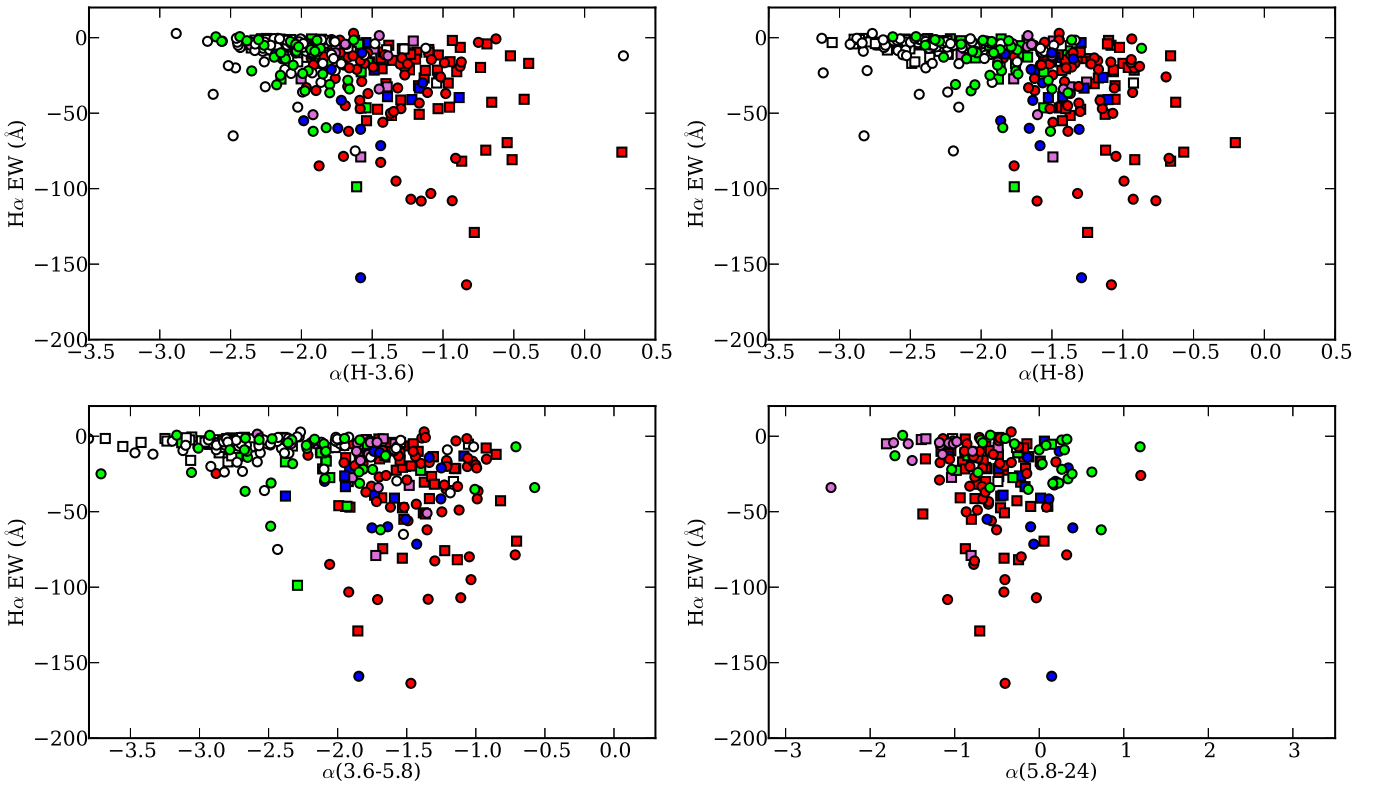


Fig. 7:  $\text{H}\alpha$  EW vs. disk slope for the members of Tr 37. Known members from previous work are marked as squares (SA05, SA06a,b). New sure members from this work are displayed as circles. Diskless stars are open symbols, typical full-disks are colored in red, PTD are marked in blue, TD are colored in green, and dust-depleted objects appear in pink.

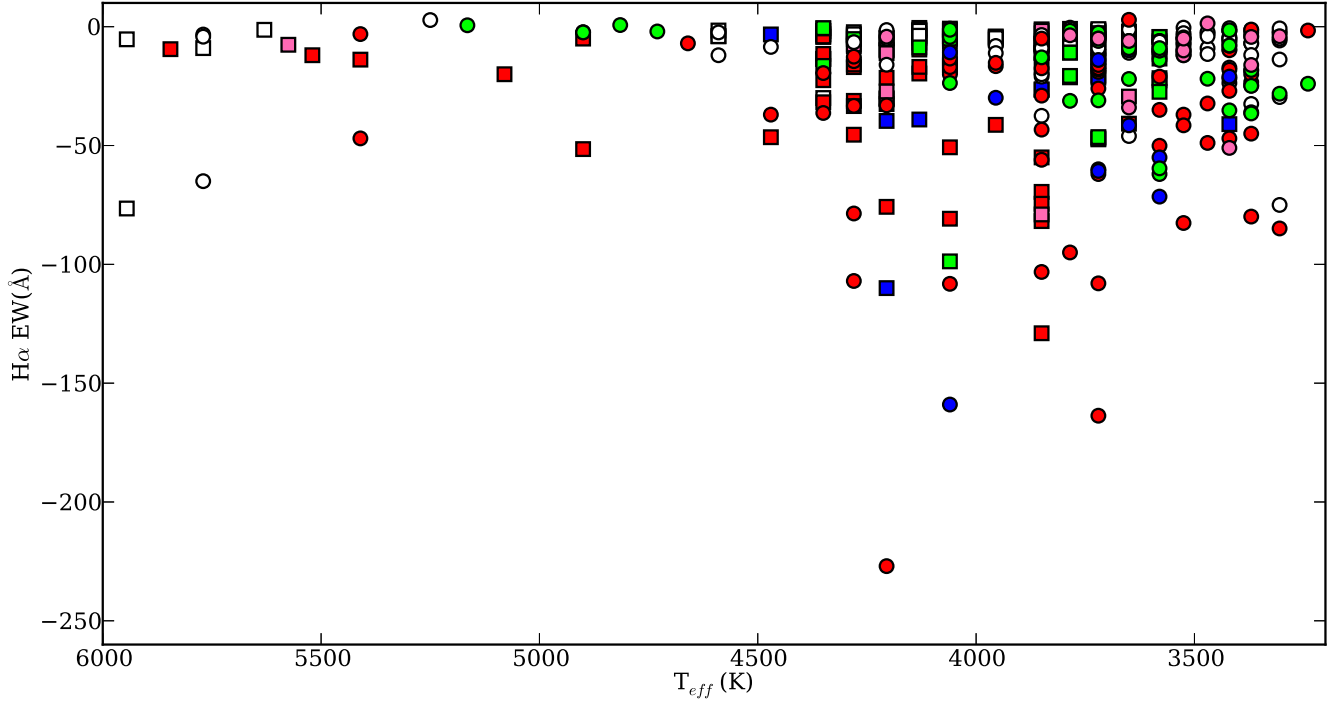


Fig. 8:  $H\alpha$  EW vs. effective temperature for the objects with different types of disks. Squares denote the stars observed in our previous programs, while new members from this work are marked by circles. Diskless stars are open symbols, full-disks are colored in red, PTD are marked in blue, TD are colored in green, and dust-depleted objects appear in pink.

Table 3: Results of the double-sided KS probability test for the  $H\alpha$  EW for objects with different types of disks.

Disk types	2006 Sample	2013 Sample	All Objects	M-type	G/K-type	Comments
Full-disks/Diskless	1E-17	6E-8	1E-22	7E-12	2E-11	Strong difference
Full-disks/PTD	0.47	0.63	0.28	0.62	0.57	No significant difference
Full-disks/TD	0.0001	0.02	5E-6	0.009	5E-5	Significant difference
Full-disks/Depleted	0.07	0.004	3E-4	0.001	0.24 <sup>a</sup>	Significant difference (only M-type stars)
Diskless/PTD	1E-5	4E-4	1E-8	1E-5	5E-4	Strong difference
Diskless/TD	0.007	0.07	0.001	0.0001	0.28	Significant difference (only M-type stars)
Diskless/Depleted	0.006	0.61	0.16	0.82	0.005 <sup>a</sup>	Potential difference (only GK stars)
Diskless/Diskless	1E-14	4E-6	4E-18	2E-10	1E-8	Strong difference

**Notes.** The 2006 sample corresponds to the members identified in our previous work, the 2013 sample includes the newly detected objects in this work. <sup>a</sup> Small number statistics, only 6 depleted disks among G/K stars.

PTD/TD objects which have observed with spectroscopy measuring  $H\alpha$  EW. Among their PTD/TD sample, 36 objects can be classified as TD, and 25 sources as PTDs according to our criteria. The fractions of accretors in both samples are  $42\pm 11\%$  and  $52\pm 14\%$ , respectively. Therefore, the results in the Orion Lynds clouds are consistent with Tr 37.

Dust-depleted disks have also significantly lower  $H\alpha$  EW, and thus significantly lower accretion rates (sometimes consistent with no accretion) than normal full-disks. This supports the idea of a strong connection between gas and dust evolution, where both signs of inside-out evolution (in TD) and global dust depletion appear to be related to lower accretion rates. Observations of evolved disks and accretion signatures in older clusters, like  $\gamma$  Velorum (Hernández et al. 2008; Jeffries et al. 2009) and  $\eta$  Cha (Lawson et al. 2004; Bouwman et al. 2006; Sicilia-Aguilar et al. 2009) show that, despite the differences in environment and disk classes, there is a clear trend for evolved disks to display reduced or even zero accretion rates, consistent with parallel dust

and gas evolution. On the other hand, the  $H\alpha$  EW and thus the accretion rates of PTD and full-disks are not significantly different. This is remarkable, since PTD are good candidates to host clean gaps in their disks, maybe related to planet formation (Espaillat et al. 2010). It could be due to difficulties to identify disks with gaps from unresolved observations and lacking spectra of the  $10\mu\text{m}$  region, or be a direct consequence of most of the full-disks in Tr 37 having moderate accretion rates, compared to younger regions like Taurus (SA06b; Sicilia-Aguilar et al. 2010). Although half of the TD have  $H\alpha$  EW consistent with no accretion, and most of the dust-depleted disks also show relatively low  $H\alpha$  EW, the difference between diskless and diskless objects is still remarkable even if TD and dust-depleted disks are included.

We also explored whether the differences in accretion vs. disk type depend on the spectral type. Table 3 reveals that the differences are subtle. Non-accreting TD seem to be more frequent around G/K-type stars. One explanation could be that for

a given excess, the holes in a G/K-type star will be much larger than in M-type objects, although it could also indicate that accretion can survive for longer time in the disks around M-type objects, once the inner disk starts dispersing. The data also suggests that M-type dust depleted disks are consistent with no accretion, which is in agreement with our observations of M-type stars in the Coronet cluster (Sicilia-Aguilar et al. 2008, 2011a). Nevertheless, a remarkable difference is that while most of the disks around M-type stars in the Coronet cluster are dust-depleted or have very low disk mass compared to their stellar mass ( $M_d/M_* < 10^{-4}$ ; Sicilia-Aguilar et al. 2013), strongly dust-depleted disks are a minority among M-type stars in Tr 37, at least considering our detection limits at  $24\mu\text{m}$ . In general, the differences in accretion and disk structure between G-K type and M-type stars are smaller in Tr 37 than observed in the Coronet cluster (Currie & Sicilia-Aguilar 2011).

#### 4.2. Radiative transfer models of the disks

To extract quantitative information from our previous disk structure classification, we followed the scheme in SA11, using the RADMC radiative transfer code (Dullemond & Dominik 2004) to model a subset of the disks within each class (normal full-disks, PTD, TD, and dust depleted disks). The basic parameters in the RADMC code are the inner disk radius, the outer disk radius ( $R_{disk}$ ), the disk vertical scale height, and the dust distribution. The inner disk radius is set to the place where the temperature is 1500 K, approximately the dust sublimation radius, and the outer disk radius is taken to be 100 AU, although our data offers a poor constrain on this parameter and there is substantial degeneration between disk radius and total disk mass. The disk vertical scale height is given as  $H/R \propto R^{1/7}$ , although we also computed the scale given by hydrostatic equilibrium. Finally, the dust distribution is taken to be a collisional power law with exponent -3.5, between a typical minimum size of  $0.1\mu\text{m}$  and a typical maximum size of  $100\text{--}10000\mu\text{m}$ . The gas to dust ratio is 100, and gas and dust are always assumed to be well-mixed, with all dust grains having the same temperature distribution. The stellar parameters (mass, radius) are derived from the optical data and spectral types, using the transformations in Siess et al. (2000) and Kenyon & Hartmann (1995). The dust is considered as amorphous silicate dust with equal amount of magnesium and iron (Jäger et al. 1994; Dorschner et al. 1995<sup>5</sup>). We also include 25% of carbon grains with the same size distribution than the silicate dust. The SEDs are calculated for an intermediate disk inclination (45 degrees), although for these relatively flat disks, there is little difference unless the disk is viewed edge-on.

As in our previous papers, our models are not aimed at a perfect reconstruction of the SED, but at exploring the parameter space. Starting with the most simplified model possible, we check whether any structural differences are required to obtain SEDs similar to the ones we observe by varying only the disk mass and the vertical scale height (with values not far from hydrostatic equilibrium). Only if no reasonable fit is attained in this way, we proceed to change the inner disk radius, the dust grain distribution (reducing the content of small dust grains or increasing the maximum grain size), and also to introduce radial variations in the vertical structure and/or the dust composition. There is a very strong degeneration between the flaring of the outer disk, the total disk mass, the grain distributions in the inner and outer disk, and the radius (or disk temperature) at which the disk properties (flaring, density, grain size distribution) change.

Constraining the precise properties of individual disks with unresolved observations is highly degenerated, so our purpose is to prove that a simple disk structure cannot reproduce the observed SEDs for TD and PTD, unless some radial changes are included, even if the precise values of the varying parameters cannot be determined. Table 4 summarizes the model disk parameters within each disk class. A brief discussion on each class and the most appropriate models follows.

##### 4.2.1. The typical full-disks

The full-disks (Figure 9) are easy to reproduce by regulating the disk mass to fit the  $24\mu\text{m}$  point, and changing the vertical scale height, either assuming a global power law for the disk flaring at all radii or hydrostatic equilibrium. The required vertical scale heights do not depart much from hydrostatic equilibrium, although we find disks that appear higher than predicted by hydrostatic equilibrium (especially, among the higher mass disks) while other disks tend to be flatter, as expected from dust settling. We modeled three objects, with different spectral types and different disk masses, 213659108+573905636, 213751210+572436151, and 213823950+572736175, in representation of this broad and numerous class.

Disks with large excesses, like 213659108+573905636, require a very large amount of mass in small dust grains. Although the maximum grain size is unconstrained, if we assume a collisional distribution with maximum grain sizes over  $100\mu\text{m}$  and a gas to dust fraction of 100, we would require disk masses about 10% of the estimated stellar mass. This would be on the upper limit according to submillimeter and millimeter observations (Andrews & Williams 2005, 2007). On the other hand, disks like that around 213823950+572736175, with a low-to-moderate mass, probably require large grains to account for mass enough to sustain the accretion rates we expect from their strong  $H\alpha$  emission.

Other disks have very strong near-IR excesses but a lower  $24\mu\text{m}$  than expected, suggestive of strong flaring but a very low dust mass, even if we consider substantial grain growth (e.g. 213751210+572436151, 213809997+572352782). This is similar to other disks in the Coronet cluster (CrA-159 and HBC 677; Sicilia-Aguilar et al. 2013). Further observations at longer wavelengths are needed to clarify the total dust content and other special structures that could affect their morphology, like truncation or gaps at larger radii. As a first approach, we consider these disks within the full-disk class.

##### 4.2.2. The pre-transitional disks

The pre-transitional disks (Figure 10) are the hardest class to identify with our available data. The lack of a mid-IR spectrum and information on the silicate feature are a strong constraint to identify disks with partially optically thin regions in their inner disks (Espaillat et al. 2010; SA11). Nevertheless, the high  $8\text{--}12\mu\text{m}$  fluxes and sharp kinks in the mid-IR suggest disks where the properties in the innermost and outer disk change. Our models do not include gaps, although a gap created by a companion or by photoevaporation can offer a natural barrier to explain the radial changes in properties. Since this class is the most problematic, we selected 6 objects as examples (213658737+573848181, 213734649+571657705, 213929250+572530299, 213929408+570630605, 213945201+574912946, 213954058+572933454) and ran different models to show the degeneration of the various pa-

<sup>5</sup> See <http://www.astro.uni-jena.de/Laboratory/OCDB/newsilicates.html>

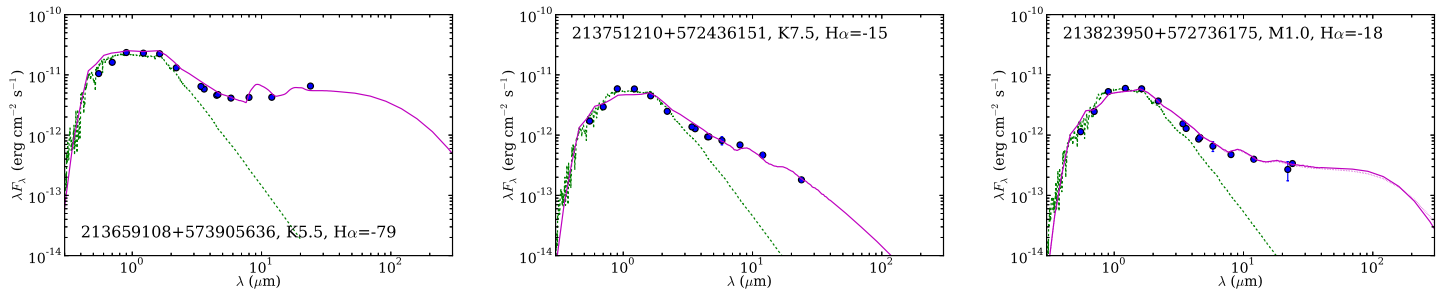


Fig. 9: Disk models for selected SEDs of typical full-disks (magenta lines). See Table 4 for information on the individual models. For comparison, the photosphere of a star with the same spectral type from the MARCS models (Gustafsson et al. 2008) is displayed. All datapoints have been extinction-corrected according to their individual values of  $A_V$  and assuming a standard extinction law (see Table A.1. Information about the  $H\alpha$  EW (in  $\text{\AA}$ ) is also displayed.

rameters. Our list of models is far from complete, but it shows that, despite the degeneracy, the SEDs reveal that some radial variations in disk properties are needed. The radial changes, reflected in Table 4, are a signature of a distinct inner and outer disk, with different flaring, inner radius, grain sizes, and mass.

The case of 213734649+571657705 shows that a simple full-disk model fails to both reproduce the inner and outer disk properties (dashed line in Figure 10), while a change in grain size distribution and flaring offers a good compromise to reproduce the SED (bold line). 213945201+574912946 offers a practical example of the impossibility to fit a pre-transitional SED with a simple full-disk model (dashed line), that would require extreme flattening far beyond hydrostatic equilibrium and a very large mass to account for the turn up at  $24\mu\text{m}$ , but would still overestimate the fluxes at  $8\text{--}12\mu\text{m}$ . A model with a differentiated inner disk and hydrostatic equilibrium comes close to the result (dotted line), but we note that the best fit is attained by assuming the inner disk has a larger vertical scale height than predicted by hydrostatic equilibrium (bold line).

#### 4.2.3. The transitional disks

For transitional disks (Figure 11), we have evidence for an inner hole that is most likely devoid of small dust. We constructed models for objects with different spectral types and different size holes, parameterized by the temperature of the inner disk rim. As for pre-transitional disks, there is a great degeneracy between disk scale height, dust composition, and size of the hole, although the low near-IR fluxes cannot be explained without cutting the dust distribution at a temperature significantly lower than the dust destruction temperature (see for instance the large grain model for 213756779+573448171, which fails to reproduce the low near-IR fluxes).

Without information on silicate emission it is hard to constrain the minimum grain size. Dust distributions with larger minimum size grains produce lower near-IR emission. The total disk mass is also highly dependent on the outer disk radius and on the vertical scale height. Some of the disks could be close to hydrostatic equilibrium, with only minimal differences in some cases (e.g. 213633647+573517477). In others, the strong excesses require a vertical scale height over the hydrostatic equilibrium (e.g. 213735713+573258349), or the weak emission asks for a reduced vertical scale height (e.g. 213756779+573448171). The mass of certain TD, even assuming a significant grain growth, is well below  $10^{-4}M_*$ , which means that they also appear to be substantially dust-depleted (e.g. 213914837+573756779). Nevertheless, the main differ-

ence with this class, as we explain in 4.2.4, is that not all dust-depleted disks need to have an inner hole, and not all TD need to have very low small-dust-grain masses.

#### 4.2.4. The dust depleted disks

Dust-depleted disks (Figure 12) are also relatively simple. They can be reproduced with model without radial variations, but require a very low small dust mass (at least, with very low mass in the submicron to  $20\text{--}30\mu\text{m}$  range) and/or very strong settling. There is a strong degeneracy between mass and vertical scale height. In general, if we assume that the dust-depleted disks are in hydrostatic equilibrium, we require a total mass several orders of magnitude below the typical values of normal full-disks. If we impose strong settling and disk flattening, the small dust grain depletion does not need to be so dramatic, although in general an increase of mass over one order of magnitude (for the same grain size distribution) cannot be compensated by flattening the disk, since the  $24\mu\text{m}$  fluxes would increase far beyond what is observed (e.g. 213030129+572651433). Some of the depleted disks may also have inner holes; 213854760+572450268 is one example where the failure of various models to reproduce simultaneously the  $24$  and  $8\mu\text{m}$  flux may indicate the presence of a small hole. However, this is not always necessary and most of them do not satisfy the criteria for TD.

The mass of the disk also depends strongly on the disk radius and on the maximum grain size, but even assuming millimeter-sized maximum grain sizes requires a very low mass for the disk, compared to typical full-disk values (see for instance 213733557+573550931). This implies that even if our data does not allow us to fully rule out a total higher disk mass in the disks classified as dust-depleted, the mass content in grains smaller than  $20\text{--}30\mu\text{m}$  needs to be very low, which is in any case a strong sign of evolution. From the analysis in Section 4.1, the dust depleted disks clearly show accretion differences with respect to full disks. Therefore, despite the degeneration between disk mass and disk flaring/settling, which has also been discussed in the literature (e.g. Espaillat et al. 2012), our study suggests that these disks are in a different evolutionary stage from typical full disks. Even if we cannot constrain the mass of the disks, and even if the case is particularly hard for M-type stars that have naturally lower near-IR excesses, the low probabilities that M-type dust depleted disks and M-type full disks are drawn from the same collection of objects, and the fact that M-type dust depleted disks and M-type diskless stars are consistent with the same  $H\alpha$  values (see Table 3) strongly point to a different evolutionary status compared to full disks. Accretion

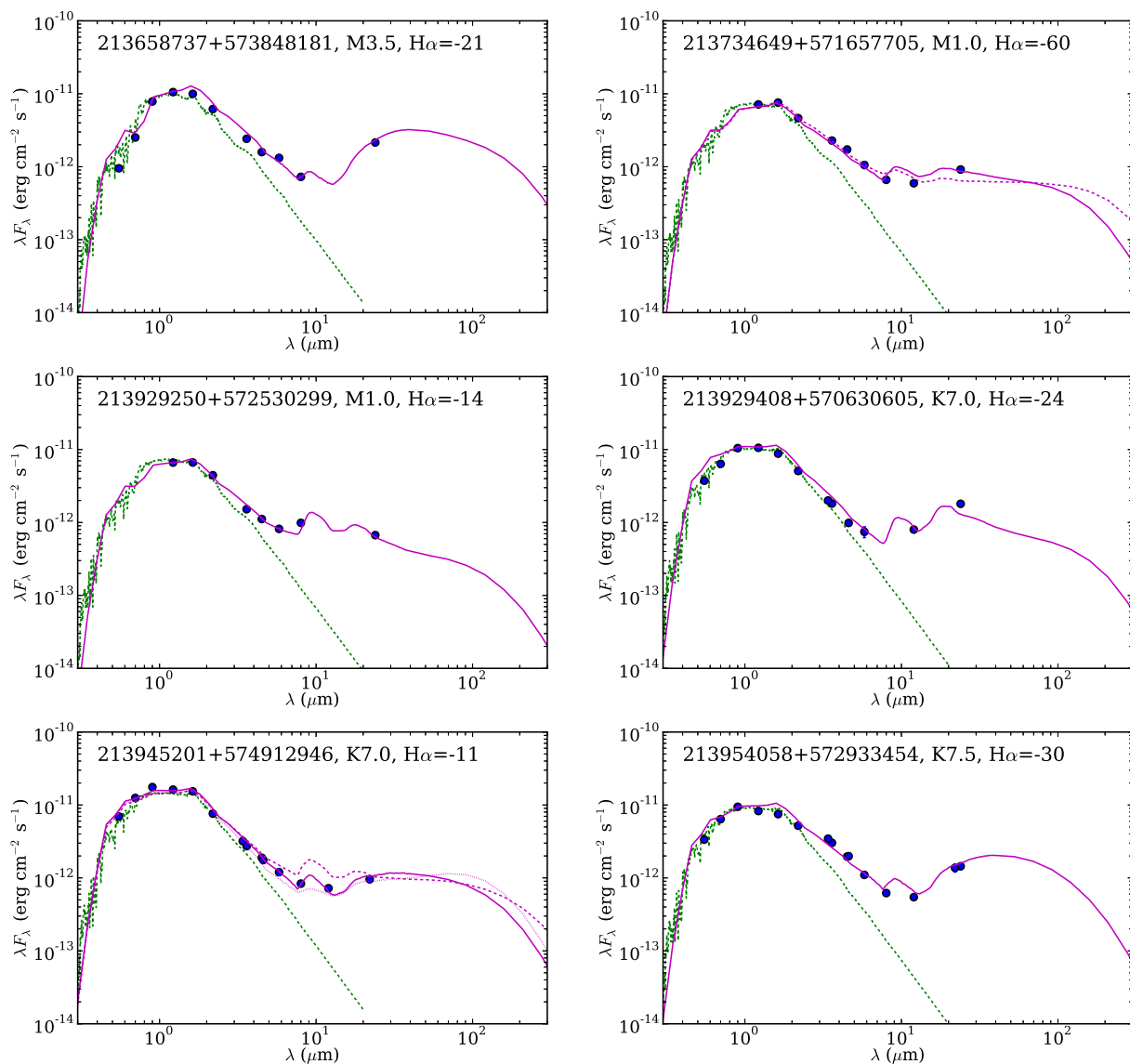


Fig. 10: Disk models for selected SEDs of pre-transitional disks (magenta lines). See Table 4 for information on the individual models. For comparison, the photosphere of a star with the same spectral type from the MARCS models (Gustafsson et al. 2008) is displayed. All datapoints have been extinction-corrected according to their individual values of  $A_V$  and assuming a standard extinction law (see Table A.1. Information about the  $H\alpha$  EW (in  $\text{\AA}$ ) is also displayed.

termination/gas depletion may be a sign of parallel dust and gas evolution, and also favor stronger dust settling within the disk. The study of silicate features (as in the case of 01-580; Sicilia-Aguilar et al. 2011a), and far-IR/submillimeter observations are a key to better constrain the disk mass of these objects, their structure, and the presence of settling (see for instance the models for 213930129+572651433 and 213944898+573537212).

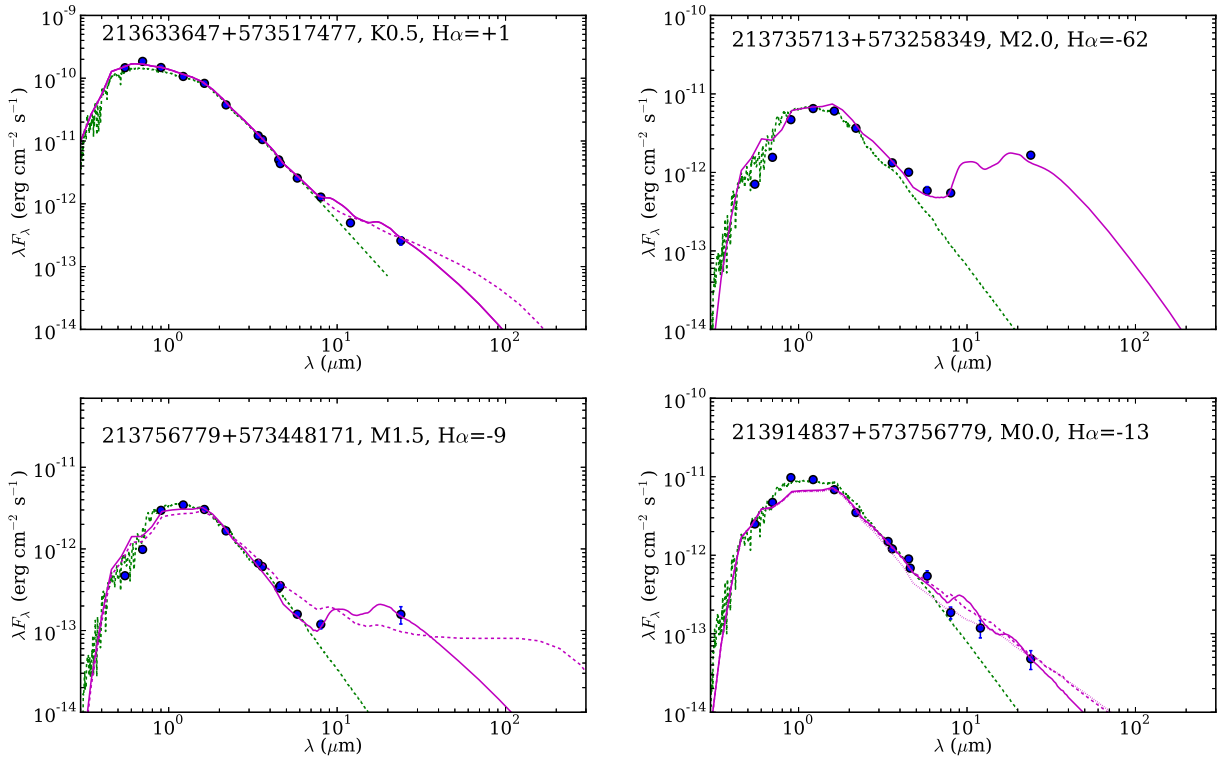


Fig. 11: Disk models for selected SEDs of transitional disks (magenta lines). See Table 4 for information on the individual models. For comparison, the photosphere of a star with the same spectral type from the MARCS models (Gustafsson et al. 2008) is displayed. All datapoints have been extinction-corrected according to their individual values of  $A_V$  and assuming a standard extinction law (see Table A.1. Information about the  $H\alpha$  EW (in  $\text{\AA}$ ) is also displayed.

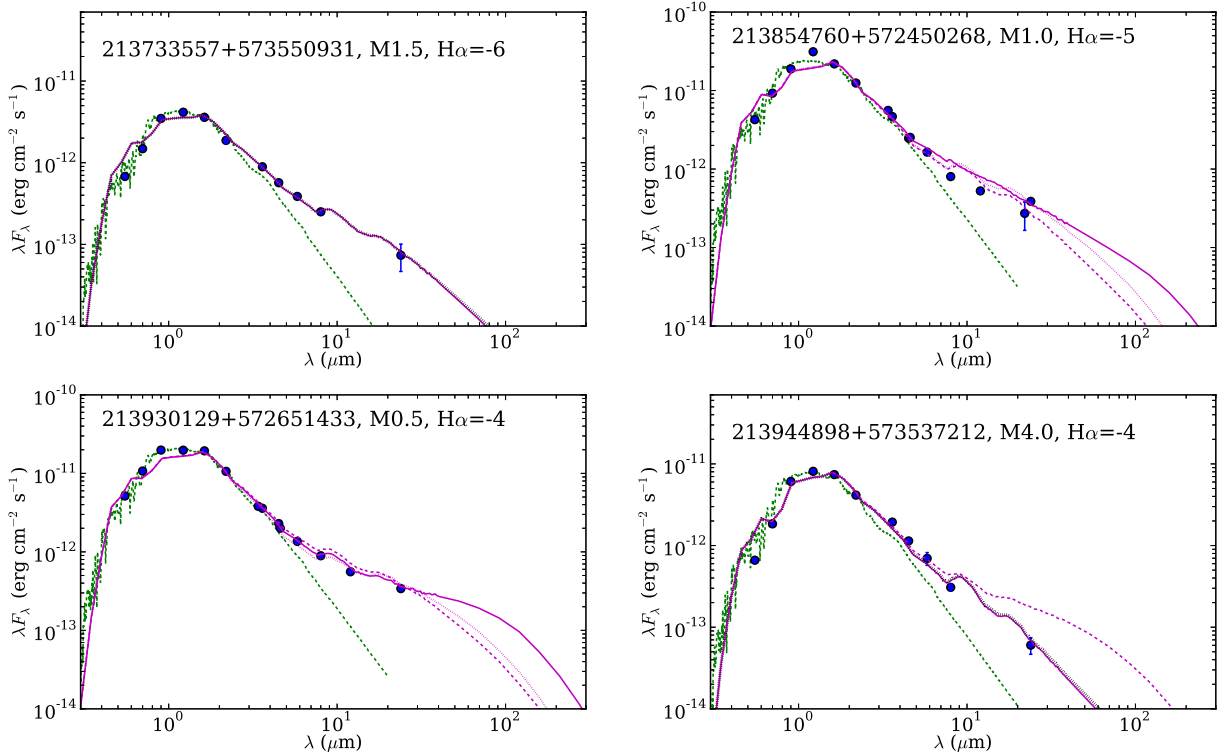


Fig. 12: Disk models for selected SEDs of dust-depleted disks (magenta lines). See Table 4 for information on the individual models. For comparison, the photosphere of a star with the same spectral type from the MARCS models (Gustafsson et al. 2008) is displayed. All datapoints have been extinction-corrected according to their individual values of  $A_V$  and assuming a standard extinction law (see Table A.1. Information about the  $H\alpha$  EW (in  $\text{\AA}$ ) is also displayed.

Table 4: Disk models for selected members, according to their disk structure. The comments also include a reference to the models plotted in the figures.

Object	$T_{eff}$ (K)	$R_*$ ( $R_\odot$ )	$M_*$ ( $M_\odot$ )	$M_{disk}$ ( $M_\odot$ )	$a_{min}$ - $a_{max}$ ( $\mu m$ )	$H_{Rdisk}/R_{disk}$	$T(R_{in})$ (K)	Comments/Model reference in plots
<b>Full-disks</b>								
213659108	4330	1.49	1.0	0.08	0.1-100	0.12	1500	Very massive, rich in small dust (bold line)
213751210	3955	0.80	0.7	2.4E-5	0.1-10000	0.25	1500	Very low-mass, maybe smaller radius? (bold line)
213823950	3729	0.92	0.6	2.9E-4	0.1-100	0.15	1500	Normal-to-low disk mass, mass depends on grain size (bold line)
"	3729	0.92	0.6	2.4E-3	0.1-10000	0.15	1500	Normal-to-low disk mass, mass depends on grain size (dashed line)
<b>PTD</b>								
213658737	3500	1.40	0.3	3.0E-3	0.1-100	0.13/0.22	1500/120	Less flared, less dense inner disk (bold line)
213734649	3720	1.00	0.45	4.5E-4	0.1-2/0.1-100	0.15/0.20	1500/300	Change in grain distribution inner/outer disk (bold line)
"	3720	1.00	0.45	4.5E-4	0.1-100	0.16	1500	Cannot fit mid-IR and near-IR properly (dashed line)
213929250	3720	1.00	0.40	2.0E-4	0.1-2/0.1-100	0.16/0.18	1500/400	Radial change in grain size and vertical scale height (bold line)
213929408	4060	1.15	0.80	8.0E-4	0.1-2/0.1-100	0.13/0.12	1500/200	Optically thin, small-grain inner disk (bold line)
213945201	4060	1.40	0.80	0.04	0.1-100	0.07	1500	An extreme attempt to fit with a uniform disk model (dashed line)
"	4060	1.40	0.80	6.4E-4	0.1-100	hydro	1500/200	Needs more flaring in inner part (dotted line)
"	4060	1.40	0.80	4.8E-4	0.1-100	0.13/0.11	1500/200	Best with puffed inner disk (bold line)
213954058	3960	1.10	0.80	4.0E-4	0.1-100	0.14/0.23	1500/150	Needs a thin inner disk and a thick, flared outer disk (bold line)
<b>TD</b>								
213633647	5165	2.90	2.00	4.0E-6	20-1000	0.32/hydro	500	No small dust, inner hole (dashed line)
"	5165	2.90	2.00	9.6E-8	0.1-100	0.32	500	Small grains, lower mass, silicate feature (bold line)
213735713	3580	1.10	0.35	7.0E-5	0.1-10000	0.20	250	Low mass, low $T(R_{in})$ , high vertical scale height (bold line)
213756779	3650	0.75	0.40	1.6E-5	0.1-10000	0.15	350	Low mass, inner hole (bold line)
"	3650	0.75	0.40	1.2E-4	20-10000	0.08	1500	Low scale height, large grains, no hole, too much near-IR excess (dashed line)
213914837	3850	1.05	0.50	2.5E-7	0.1-100	0.06	1500	Small grains, very low mass, overpredicts 8-12 $\mu m$ excess (bold line)
"	3850	1.05	0.50	4.0E-6	20-1000	0.06	1500	No small grains, better fit to 8-12 $\mu m$ but still high (dashed line)
"	3850	1.05	0.50	3.0E-6	20-1000	0.06	800	Best fit includes small hole (dotted line)
<b>Depleted</b>								
213733557	3700	0.80	0.50	1.5E-6	0.1-100	0.12	1500	Without strong grain growth, very low mass (bold line)
"	3700	0.80	0.50	1.5E-5	0.1-10000	0.12	1500	Larger grain size, higher mass, but still depleted (dotted line)
213854760	3720	1.90	0.40	8.0E-5	20-1000	0.06	1500	Too much 8-12 $\mu m$ excess (bold line)
"	3720	1.90	0.40	2.0E-6	0.1-100	0.05	1500	Extremely low vertical scale height underpredicts 24 $\mu m$ (dashed line)
"	3720	1.90	0.40	8.0E-5	20-1000	hydro	1500	Hydrostatic equilibrium overpredicts 8-12 $\mu m$ excess (dotted line)
213930129	3785	1.69	0.70	7.0E-4	0.1-100	0.05	1500	Very settled disk with small grains (bold line)
"	3785	1.69	0.70	5.6E-6	0.1-100	0.08	1500	Lower mass disk, close to hydrostatic equilibrium (dashed line)
"	3785	1.69	0.70	4.9E-6	0.1-100	hydro	1500	Hydrostatic equilibrium, lower disk mass (dotted line)
213944898	3500	1.21	0.26	1.3E-5	0.1-100	0.08	1500	Very settled disk with low mass still has too much mid-IR excess (dashed line)
"	3500	1.21	0.26	3.9E-6	0.1-100	0.10	1500	Lower mass, higher vertical scale height (bold line)
"	3500	1.21	0.26	3.9E-5	0.1-10000	0.10	1500	If strong grain growth is assumed, the mass may be higher (black dotted line)

**Notes.** RADMC disk models for selected members with different disk structures (normal full-disks, pre-transitional disks [PTD], transitional disks [TD], and dust-depleted disks [Depleted]). The names of the objects have been shortened to fit the table. The stellar parameters ( $T_{eff}$ ,  $R_*$ ) are determined from the optical observations and spectroscopy. The disk parameters are modified to reproduce the observed SED in the whole wavelength range, starting with the simplest possible model (see Section 4.2). The disk masses are estimated assuming a gas-to-dust ratio of 100 and a collisional distribution for the dust with grain sizes  $a_{min}$ - $a_{max}$ . The outer disk radius is taken to be 100 in all cases. A larger radius would also result in a larger dust mass. For pre-transitional disks with physically different inner and outer disks, we give the grain distributions, vertical scale height, and inner rim temperature for both the inner and the outer disk. In case of different models, the comments include a reference to the appropriate figure.

### 4.3. What drives disk evolution and dispersal in Tr 37? Clues from accretion, dust, and environment

Putting together the members found in our previous papers and the newly found ones, we sum up to 361 low-mass (spectral types G, K, M) members in Tr 37. The current results are consistent with our previous estimates of the disk frequency ( $48 \pm 5\%$ , including all objects with excesses down to  $24\mu\text{m}$ , SA06a), although since this survey was strongly biased towards objects with disks, we cannot re-estimate the disk fraction.

Among the 218 stars with disks (excluding Class I and uncertain objects), the full-disk objects are the most numerous, with a total of 111 stars (about 51% of the total). The least numerous are the pre-transitional disks (21 disks or nearly 10% of the total) and depleted disks (25 objects, about 11% of the total). The detection rate of PTD is low probably because of the lack of silicate feature observations. Our study of IRS spectra (SA11) suggests that the group of PTD is likely more numerous than estimated here from photometry alone. The group of dust-depleted objects has to be also regarded as a lower limit, since detection of low  $24\mu\text{m}$  excesses among the latest-type stars are also compromised. Finally, transitional disks sum up to 61 objects, or about 28% of the sample. In total, objects with evidence for inside-out evolution (considering as such both transitional and pre-transitional disks) conform nearly 38% of the total sample, being a substantial fraction of the total population of disked objects. An important degree of dust evolution has thus occurred in Tr 37, also in agreement with the significantly low accretion rates observed among cluster members (SA06b; Sicilia-Aguilar et al. 2010), suggestive of parallel dust and gas evolution in the disks.

Our current spectra do not allow us to estimate the accretion rates of the observed objects due to the uncertainty in the sky subtraction. However, considering as a typical value that of  $3 \times 10^{-9} M_{\odot}/\text{yr}$  (Sicilia-Aguilar et al. 2010), and an age of 4 Myr, one would expect that the disks would have had a minimum disk mass of  $0.012 M_{\odot}$ . To reconcile this value with the typical disk masses observed, in general lower by at least a factor of few to one order of magnitude, strong grain growth needs to be taken into account. This is particularly important in case of the disks with very low dust masses and relatively strong  $H\alpha$  emission (like 213751210+572436151), that would be about to lose their disks within less than  $10^4$  yr. If we do not include strong grain evolution or an anomalous gas to dust fraction, we would need to assume that are witnessing a very special moment of disk evolution in Tr 37, where a large fraction of disks is expected to disperse within the next  $\sim 10^5$  years, which is highly unlikely from the statistical point of view and considering the age spread among Tr 37 members. Dust evolution (and thus a higher disk mass than expected) would be the only way to ensure that formation of giant planets is still possible among Tr 37 disks, if it has not occurred yet.

We also find evidence that not all disks evolve along the same path. Some TD have very large  $24\mu\text{m}$  excesses, while others appear to be also dust-depleted, a sign that inner holes can appear both in massive, small-grain-rich, disks and in disks that are substantially depleted of small dust grains. Other disks are depleted of small dust grains but still have near-IR excesses, suggesting that small-dust depletion alone does not trigger the immediate opening of a hole in the disk. Moreover, although dust-depleted disks will also probably suffer inside-out evolution later on and enter the class of dust-depleted TD, they will not go through the "classical" TD phase (with no near-IR excess followed by a sharp increase at mid-IR wavelengths and a strong  $24\mu\text{m}$  ex-

cess), given that they do not have enough mass nor vertical scale height. This would need to be considered when estimating the lifetime of "classical" TD. The diversity of objects is a sign of the different disk dispersal processes at work in a cluster as old as Tr 37 ( $\sim 4$  Myr for the central population). The differences observed between the accretion behavior of full-disks and TD/dust-depleted objects discussed in Section 4.1 suggests that gas accretion and dust evolution evolve in a parallel way. However, the fact that about 50% of TD are consistent with no accretion, while this is exceptionally rare among normal full-disks, is also a sign that not all disks with similar SEDs correspond to physically similar objects, confirming our previous results (Sicilia-Aguilar et al. 2010, SA11).

The stars in Tr 37 reveal several paths of disk evolution (see a sketch of disk types in Figure 13). In general, evolution occurs from the inside-out, but the time scale when an inner hole develops in a disk appears to be different: in some cases, substantial dust depletion, settling, or both, occur without the disk developing an inner hole, while in some other cases, disks develop an inner hole while still being massive and very flared. To open a hole by photoevaporation (e.g. Clarke et al. 2001; Alexander et al. 2006; Gorti et al. 2009), the accretion rate or viscous transport through the disk needs to drop below a certain level first. Therefore, in general objects with no significant accretion, low dust mass, and inner holes are good candidates to photoevaporation-related holes or to very massive companions that can block accretion. Nevertheless, very massive disks would also be less likely to disperse via photoevaporation until their mass and accretion rate have decreased sufficiently to prevent refilling of the inner hole by viscous evolution. This would make it more likely that their holes are related to other processes, like stellar companions or planet formation. Objects with transitional and dust-depleted disks that still have significant accretion are good candidates to suffer strong grain growth (maybe combined with settling), which would affect the IR excess but not the accretion rate, or very low-mass companions, that would not block the flow of gas through the gap. In the case of PTD, the differences in dust properties (especially, grain size) observed between the inner and the outer disk could be due to dust filtering in a planet-formation scenario (Rice et al. 2006), as we had also previously suggested in SA11. Recent spatially resolved observations show that the possibility of dust filtering/dust trapping in certain parts of the disk is a real one, and that gas flow across gaps appears to occur (Van der Marel et al. 2013; Casassus et al. 2013). More data, in particular, silicate feature observations, and ideally also spatially resolved observations, would be needed to better define the class of PTD.

We also explored the dependency of SED shape and disk structure with the spectral type/stellar mass. Figure 14 shows a plot of the median SED for the K-type and M-type objects with disks, scaled in both cases to the flux in band H and corrected by the individual extinction values of the objects. The plot includes the results of all the known members with well-defined IR excesses, excluding those with anomalous SEDs and/or photometric problems. This sums up to 76 K-type stars and 109 M-type stars. Although M-type stars have systematically lower IR excesses over the photosphere and the upper quartile for M-type stars hardly reaches the mean values for the K-type objects, the difference is not as dramatic as observed in the Coronet cluster (Currie & Sicilia-Aguilar 2011). The  $24\mu\text{m}$  data in Tr 37 are not complete, so we expect to miss a substantial part of the objects with low  $24\mu\text{m}$  excesses, especially among the fainter M-type stars. Nevertheless, the most striking result in the young (1-2 Myr) Coronet cluster is not the presence of disks with very



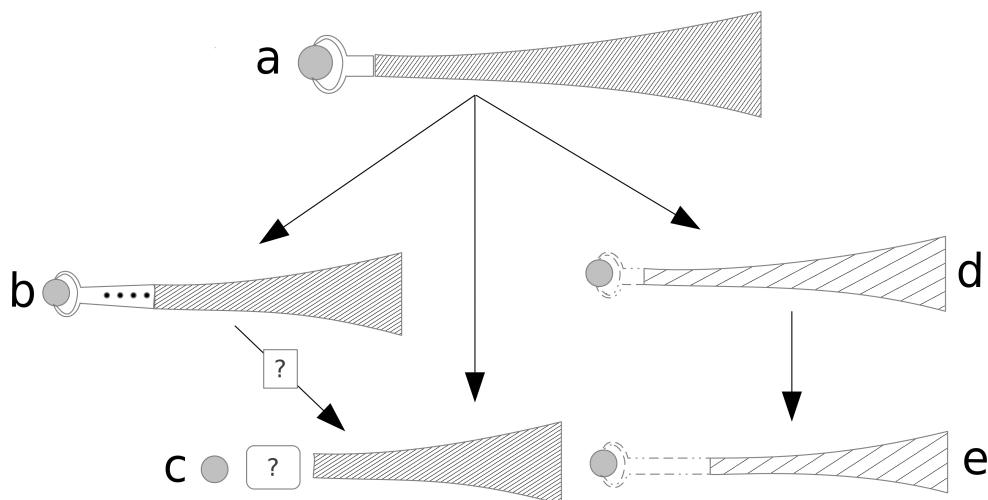


Fig. 13: A sketch of the different evolutionary paths discussed in the text. The full, accreting disk is represented by the sketch 'a'. Such a disk can evolve in (at least) 3 different ways: suffering strong grain growth and ending up as an accreting TD (b), suffering other inner-disk removal processes (e.g. photoevaporation, removal by massive companions of stellar or planetary origin) to result in a non-accreting TD (c), or experiencing small-dust removal at all radii (due for instance to generalized grain growth) and resulting in a small-dust depleted disk, typically with reduced accretion (d). While accreting TD may later on transform into non-accreting TD or even dust-depleted TD (e), dust-depleted disks would not go through a typical TD stage (b,c) even if they later on also disperse from the inside-out (e). The list of evolved structures is not supposed to be complete, and the final outcome of each evolutionary path (e.g. star with planetary system) is not constrained with our present data.

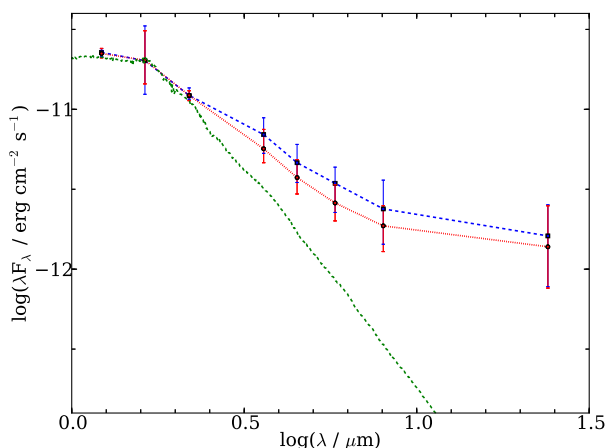


Fig. 14: Median SED for the objects with disks for spectral type K (blue dashed line) and M (red dotted line), with quartiles at each wavelength.

low masses, but the absence of massive disks among the M-type stars, which is not the case in Tr 37. The analysis of the  $H\alpha$  EW in the different spectral type classes in Tr 37 also suggest that K- and M-type stars in Tr 37 are more similar in terms of accretion and disk properties than their counterparts in the Coronet cluster. Disks around M-type stars in Tr 37 are apparently *less evolved* than in the Coronet cluster, although we would expect the opposite from their ages, a signature that time evolution alone cannot explain the observed disk properties in Tr 37 and the Coronet cluster.

Besides age, the main differences between the Coronet cluster and Tr 37 are the number of members and the stellar density. In the Coronet cluster, we find about 50 stars (including resolved multiple systems) within a radius of about 0.15pc (Sicilia-Aguilar et al. 2013). The membership count is probably close

to complete for spectral types between B9 and M6, considering that the cluster has been observed in the optical, X ray, IR, and submillimeter (e.g. López-Martí et al. 2005, 2010; Groppi et al. 2004 2007; Peterson et al. 2011; Sicilia-Aguilar et al. 2008, 2011a). Taking into account only the number of stars and not their mass, we arrive to a stellar density of about 3000 stars/pc<sup>3</sup>. In Tr 37, if we take a cluster radius of 5 pc, we count about 360 stars with spectral types O6 to M6, including both disked and diskless objects. If we account for a similar number of stars without disks that we may have missed in our surveys, and allow for a binarity rate of 50%, we arrive to about 1000 stars in total, resulting in a density of 2 stars/pc<sup>3</sup>. Even if our member number estimates are wrong by a factor of few, the density difference between both regions would still be close to 3 orders of magnitude.

The outskirts of the cluster may be less dense than the cluster center (e.g. Barentsen et al. 2011), but the difference in stellar density between the Coronet and Tr 37 would still be very large. Even if we consider that Tr 37 has suffered substantial expansion to arrive to its current stage (at a typical rate of 1pc/Myr), an initial cluster size of 2 pc would only produce a density of 30 stars/pc<sup>3</sup>. Moreover, Spitzer observations (SA06a) and isochrone considerations (SA05; Getman et al. 2012) suggest that the population in the outskirts is most likely younger and formed in-situ, not by expansion of the original cluster. According to Section §7 of Getman et al. (2012) there are 235 (>60) stars down to 0.1M<sub>⊙</sub> near (inside) the IC 1396A globule, within the volume of roughly 75 pc<sup>3</sup> (7 pc<sup>3</sup>). Assuming a binary rate of 50%, this gives 5 stars/pc<sup>3</sup> (10 stars/pc<sup>3</sup>) near (inside) the globule. This source density is still much lower than that of the Coronet cluster. The immediate result is that, while the early formation phases of stars in a compact, dense cluster like the Coronet would be heavily compromised by star-star interactions that could affect envelopes and disks, the environment in Tr 37 would have been much less interactive, allowing for larger envelopes and also larger disks masses. The initial disk struc-

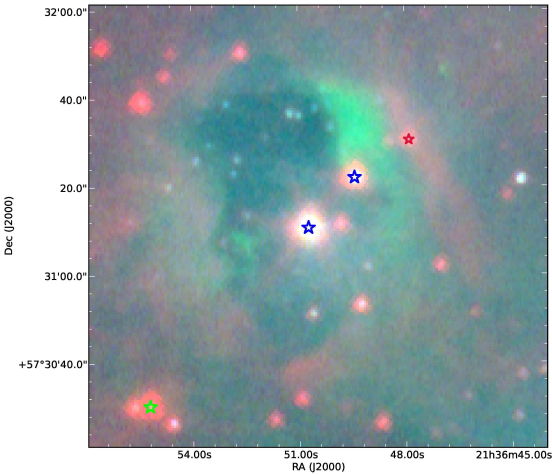


Fig. 15: Detail of the 3-color (IRAC1, [S II] combined at 6716 and 6730Å, and R band as red, green, and blue, respectively) image of the IC 1396 A globule, zooming around V390 Cep (in the center of the clearing) and 14-141 (marked in blue). Embedded Spitzer-detected objects are marked as red stars.

ture may also pre-determine the evolutionary path that the disk will follow. Later on, other phenomena like the effect of the central O6 star may also contribute to disk dispersal in Tr 37 (e.g. Mercer et al. 2009).

#### 4.4. The star-cloud interactions in Tr 37: Mini-clusters and sequential star formation

Besides the fact that the O6 star HD 206267 shapes the large IC 1396A globule and other structures in the outskirts of Tr 37, our forbidden line images also reveal a smaller-scale interaction between some of the low-mass members and the remaining cloud. Figure 15 reveals a complex shocked structure in the surroundings of V390 Cep (21:36:50.72 +57:31:10.7, also known as MVA-60; Marschall & Van Altena 1987) and the K6 star 14-141 (Sicilia-Aguilar et al. 2004). The star 14-141 is known to show variable accretion and to be associated to variable forbidden line emission suggestive of time-variable shocks in the proximities of the star (Sicilia-Aguilar et al. 2010). In addition, the [S II] images reveal a large area emitting in forbidden lines, associated to the rim of the cloud in the proximity of 14-141. It is not possible to distinguish whether the shock is due to 14-141 or associated to more embedded objects within the cloud. There is a very embedded, reddened object that can be seen in the Spitzer images, although due to the variable background it is not possible to extract accurate photometric information from it.

There is also evidence of a small jet or shock on the other side of the bubble surrounding 14-141, with no object related to it. From its location, it could be related to V390 Cep, which is classified as a variable Ae star (despite its lack of IR excess at any of the Spitzer wavelengths). The shock emission would be located at about 13000 AU projected distance from V390 Cep. In addition, our Hectospec spectra reveal forbidden emission towards a few other stars (213744131+573331130, 213810759+574013683, 213942378+573348653, and 214059633+572210994; see Table A.5). All this suggest that even the low-mass stars in the cluster

contribute to shaping the surrounding cloud, which could have an effect on local star formation.

We had already mentioned the age difference between the solar-type stars in the cluster center compared to the most embedded objects to the west of Tr 37, located within the IC 1396A globule (SA05; SA06a; Barentsen et al. 2011; Getman et al. 2012). In this spectroscopic survey, we took advantage of our previous knowledge of the cloud structure to obtain spectra of the objects associated with some smaller globules (of the order of 20"-40", or approximately 0.1-0.2 pc at a distance of 870 pc; Contreras et al. 2002). The most remarkable structures contain 6 and 2 stars clearly associated with the extended IR emission, respectively, plus other surrounding objects that could be either associated or projected onto the nebula, forming what we call here "mini-clusters" (Figure 16).

The larger globule or mini-cluster (Figure 16, left) is remarkable because of the very strong H $\alpha$  emission of all its associated stars, which have very strong IR excesses as well. This small stellar group had been already noticed in the H $\alpha$  survey by Barentsen et al. (2011) and in the X-ray/IR study of Getman et al. (2012), Section 8.3.2. The region also host the binary B3+B5 star CCDM+5734, which was found to have a transitional disk with a large hole and evidence of small silicate dust (Sicilia-Aguilar et al. 2007). The second structure (Figure 16, right) contains the star 213911452+572425205. This object appears as emerging from the cloud tip and shows a large IR excess and a large number of accretion-related emission lines in its spectrum. The globule also contains 213905519+572349596, a star without evidence of disk nor accretion. Although obtaining ages of these embedded objects is problematic, the extreme H $\alpha$  values and IR excesses of all of them (except 213905519+572349596) could indicate that the stars are younger than the general Tr 37 population, either related to triggered or sequential star formation within small surviving globules in the cluster, or maybe to structures in the younger outskirts of the cluster, seen in projection, or clumpy star formation.

## 5. Summary and conclusions

We performed a spectroscopic survey targeting the low-mass members of the 4 Myr-old cluster Tr 37. The spectra allowed us to identify a large number of new members and, together with our already available data (optical photometry, 2MASS, and IR Spitzer IRAC/MIPS data), to study the connection between accretion indicators and IR excesses from protoplanetary disks. From our study, Tr 37 emerges as a relatively evolved young cluster where its surviving disks display a variety of evolutionary signs. The results of this work are summarized below:

- The survey provided data on spectral types, accretion, and extinction for 205 cluster members and probable members, leading to the discovery of 78 new cluster members, and 64 probable members. Most of these members are M-type (M0-M5) stars with IR excesses typical of protoplanetary disks and accretion indicators.
- Gas accretion, detected via the H $\alpha$  EW, is strongly correlated with the presence of disks. A KS test including the new and the previously known members reveals a nominally 0 probability that both disked (with all types of disks) and diskless objects are drawn from the same distribution. We also find significant differences between the accretion behavior of full-disks and disks with strong evidence of evolution (TD and dust-depleted disks). About half of the TD are consistent with no accretion (being similar to diskless stars), while

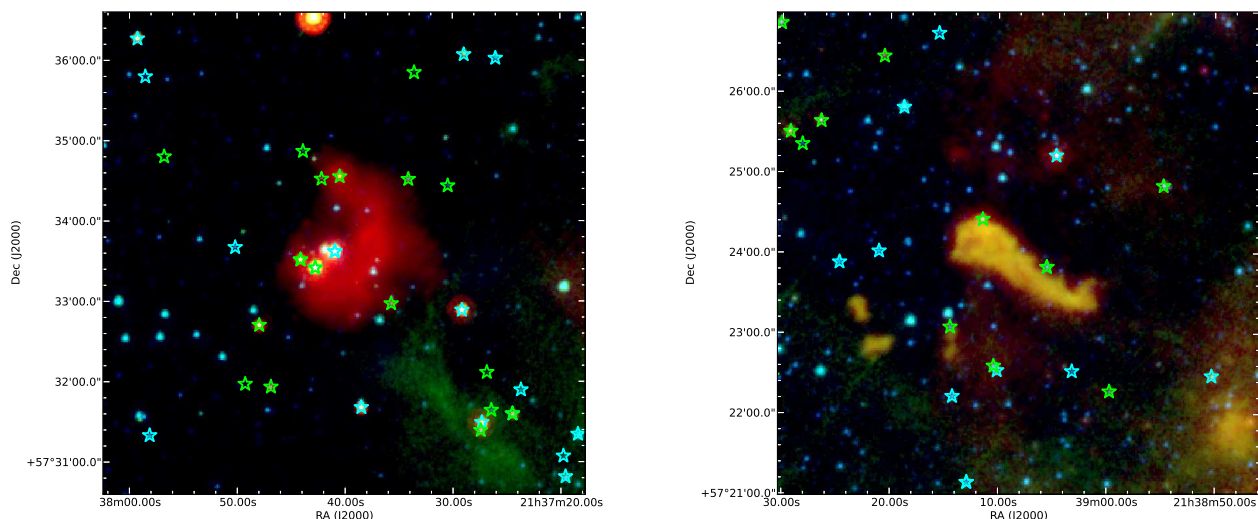


Fig. 16: Two 3-color (3.6, 8, 24  $\mu\text{m}$ ) image of the small globules or mini-clusters in Tr 37. Previously known members are marked as cyan stars, new members (from this work) are marked as green stars.

the other half have  $H\alpha$  values similar to full-disks. Dust-depleted disks, in particular those around M-type stars, also show significantly lower  $H\alpha$  EW. This suggests that dust and gas evolve in a parallel way: Objects with no evidence of dust evolution are very unlikely to have suffered accretion termination, while accretion termination (or very strong suppression of accretion) is common among transitional and dust-depleted disks. The difference in accretion behavior between dust depleted and full disks also suggests that objects with very low 24 $\mu\text{m}$  excesses are in a different evolutionary stage, although it is not possible to tell if this is caused by parallel dust and gas evolution, by strong dust settling after partial gas depletion, or by both.

- We find a tentative trend (limited by low number statistics) that accreting TD are more frequent among M-type stars than among GK-type stars, which could be either related to the larger holes in the disks around GK-type stars for the same IR excess, or indicate that accretion last longer in the TD around M-type stars. GK-type dust-depleted disks are generally accreting, in contrast with M-type dust-depleted disks, pointing to a faster termination of accretion in M-type stars after global dust evolution. Further observations of similar objects are required to confirm or reject these points.
- We used the RADMC radiative transfer code to model a sample of disks with different types of SEDs. Full-disks can be reproduced with simple models with different degrees of grain growth, vertical scale height, and disk masses. Transitional disks require an inner hole to account for the lack of near-IR excess, although the hole size (or the temperature of the inner disk rim) is highly dependent on the dust properties and vertical scale height. Pre-transitional disks models require a change in disk properties between the innermost and outer disk, although there is a high degree of degeneracy between location of the radius at which the properties change, dust distributions on both sides, and vertical scale heights. Dust-depleted disks with very low 8-24 $\mu\text{m}$  fluxes and reduced near-IR excesses require substantial mass depletion, if we assume the disk is in hydrostatic equilibrium. Strong settling may contribute to low near-IR excess, but a

dust mass in small ( $<20\mu\text{m}$ ) grains significantly lower than in full disks is still needed to account for the low mid-IR fluxes and the steep shape of the SED.

- Including all the Tr 37 population identified in this and in the previous study (over 200 objects with spectral types G,K, and M), we studied the prevalence of signs of inside-out evolution and dust depletion in the disks. More than 1/3 of the disks show signs of inside-out evolution (inner holes, or changes in disk properties between the inner and outermost disk). About 10% of the disks have significant dust depletion, resulting in very low mid-IR fluxes and typically low accretion rates. Nearly 20% of the disks with inner holes (TD) have also very low mid-IR excesses and are most likely dust depleted as well. Among full-disks, substantial evolution in the form of grain growth needs also to be assumed to obtain disk masses in the appropriate range for the accretion rates observed.
- The diversity of disks in Tr 37 suggests that not all disks follow the same evolutionary path: while inside-out evolution seems to be the rule, we find that some disks develop inner holes while keeping a relatively massive outer disk, while others lose a significant fraction of their small dust grains before their inner parts are cleared. This points to several effects contributing to disk dispersal.
- Our study of Tr 37 does not reveal the striking differences observed the young Coronet cluster, among K-type and M-type stars (Currie & Sicilia-Aguilar 2011). Non-accreting and depleted disks among M-type stars are not as frequent as in the Coronet, even though Tr 37 is substantially older. A possible explanation is the very different environment and, in particular, the stellar density in both regions. While recent studies suggest a density of the order of 3000 stars/ $\text{pc}^3$  in the sparse Coronet cluster, the density in Tr 37 is about 2-3 orders of magnitude lower. This suggests that the differences in disk properties observed between both regions could be related to very different environment and initial conditions, like early interactions. Frequent close interactions at a protostellar level could result in lower initial disk masses and a

lack of massive disks among low-mass stars, which is what we observe in the Coronet cluster.

- Finally, we also studied the stellar content of several small globules in Tr 37, finding that some of them harbor mini-clusters with a few members. The stars within these mini-clusters show preferentially full-disks with strong IR excesses and strong emission lines. This suggests that the objects could be younger than the extended Tr 37 population, which could be indicative of very small-scale sequential (or clumpy) star formation in the region.

**Acknowledgments:** The authors are grateful to V.L. Afanasiev for conducting the SCORPIO observations, and V.V. Krushinsky and P.A. Boley for their help in the preparation of the observations with the 6m Telescope of SAO RAS, and also to P. Berlind, N. Caldwell, and M. Calkins at the MMT observatory. We also thank C. Dullemond for his help with the RADMC code, and the anonymous referee for his/her careful comments that helped to clarify and organize this paper.

Based on observations collected at the German-Spanish Astronomical Center, Calar Alto, jointly operated by the Max-Planck-Institut für Astronomie Heidelberg and the Instituto de Astrofísica de Andalucía (CSIC). We also thank Calar Alto Observatory for allocation of director's discretionary time to this program.

This work is based on observations made with the Spitzer Space Telescope, which is operated by the Jet Propulsion Laboratory, California Institute of Technology under a contract with NASA. This publication makes use of data products from the Wide-field Infrared Survey Explorer, which is a joint project of the University of California, Los Angeles, and the Jet Propulsion Laboratory/California Institute of Technology, funded by the National Aeronautics and Space Administration. It also makes use of data products from the Two Micron All Sky Survey, which is a joint project of the University of Massachusetts and the Infrared Processing and Analysis Center/California Institute of Technology, funded by the National Aeronautics and Space Administration and the National Science Foundation.

ASA acknowledges support of the Spanish MICINN/MINECO "Ramón y Cajal" program, grant number RYC-2010-06164, and the action "Proyectos de Investigación fundamental no orientada", grant number AYA2012-35008. MF is also supported by AYA2012-35008.

## References

Afanasiev V.L. & Moiseev A.V., 2005, *PaZh*, 31, 214  
Alexander, R., Clarke, C., Pringle, J., 2006 *MNRAS*, 369, 229  
Alexander, R. D., & Armitage, P. J. 2009, *ApJ*, 704, 989  
Apai, D.; Pascucci, I.; Bouwman, J.; Natta, A.; Henning, Th.; Dullemond, C. P., 2005, *Sci*, 310, 834  
Appenzeller, I., Jankovics, I., Jetter, R., 1986, *A&ASS* 64, 65  
Arzoumanian, D., André, P., Didelon, P., et al. 2011, *A&A*, 529, L6  
Barentsen, G., Vink, J. S., Drew, J. E., et al. 2011, *MNRAS*, 415, 103  
Bate, M., et al. 2005, *MNRAS*, 356, 1201  
Bate, M. R. 2012, *MNRAS*, 419, 3115  
Bessell, M.S. & Brett, J.M., 1988, *PASP*, 100, 113  
Bouwman, J.; Lawson, W. A.; Dominik, C.; Feigelson, E. D.; Henning, Th.; Tielens, A. G. G. M.; Waters, L. B. F. M., 2006, *ApJ*, 653, 57  
Cardelli, J., Clayton, G., Mathis, J., 1989, *ApJ*, 345, 245  
Casassus, S., van der Plas, G., M. S. P., et al. 2013, *Nature*, 493, 191  
Clarke, C., Gendrin, A., & Sotomayor, M., 2001, *MNRAS* 328, 485  
Clarke, C., & Pringle, J., 2006, *MNRAS*, 370, L10  
Cieza, L., Padgett, D. L., Stapelfeldt, K. R., et al. 2007, *ApJ*, 667, 308  
Contreras, M.E., Sicilia-Aguilar, A., Muzerolle, J., Calvet, N., Berlind, P., Hartmann, L. 2002, *AJ*, 124, 1585  
Currie, T., Lada, C. J., Plavchan, P., Robitaille, T. P., Irwin, J., & Kenyon, S. J. 2009, *ApJ*, 698, 1

Currie, T., & Sicilia-Aguilar, A. 2011, *ApJ*, 732, 24  
Cutri R.M., Skrutskie, M.F., van Dyk, S. & 25 more coauthors, 2003yCat.2246, 0C, *VizieR On-line Data Catalog: II/246*  
Dorschner, J., Begemann, B., Henning, T., Jäger, C., & Mutschke, H., 1995, *A&A*, 300, 503  
Dullemond, C., & Dominik, C., 2004, *A&A*, 417, 159  
Dullemond, C., Natta, A., Testi, L., 2006, *ApJL* 645, 69  
Espaillat, C., et al. 2010, *ApJ*, 717, 441  
Espaillat, C., Ingleby, L., Hernández, J., et al. 2012, *ApJ*, 747, 103  
Fang, M., van Boekel, R., Wang, W., Carmona, A., Sicilia-Aguilar, A., & Henning, T. 2009, *A&A*, 504, 461  
Fang, M., van Boekel, R., Bouwman, J., et al. 2013a, *A&A*, 549, A15  
Fang, M., Kim, J. S., van Boekel, R., et al. 2013b [arXiv:1304.7777]  
Fedele, D., van den Ancker, M. E., Henning, T., Jayawardhana, R., & Oliveira, J. M. 2010, *A&A*, 510, A72  
Fernie, J., 1983, *PASP*, 95, 782  
Gatti, T., Natta, A., Randich, S., Testi, L., & Sacco, G., 2008 *A&A* 481, 423  
Getman, K. V., Feigelson, E. D., Sicilia-Aguilar, A., et al. 2012, *MNRAS*, 426, 2917  
Groppi et al., 2004, *ApJ*, 612, 946;  
Groppi, C. E., Hunter, T. R., Blundell, R., & Sandell, G. 2007, *ApJ*, 670, 489  
Gullbring, E., Hartmann, L., Briceño, C., Calvet, N., 1998, *ApJ* 492, 323  
Gustafsson, B., et al. 2008, *A&A* 486, 951  
Hacar, A., Tafalla, M., Kauffmann, J., & Kovács, A. 2013, *A&A*, 554, A55  
Haisch, K., Lada, E., & Lada, C., 2001, *ApJ*, 553, 153  
Hammann, F., & Persson, S.E., 1992a, *ApJS* 82, 247  
Hamann, F., 1994, *ApJS*, 93, 485  
Hartmann, L., 2003, *ApJ*, 585, 398  
Hartmann, L., D'Alessio, P., Calvet, N., & Muzerolle, J., 2006, *ApJ*, 648, 484  
Harvey, P. M., Jaffe, D. T., Allers, K., & Liu, M. 2010, *ApJ*, 720, 1374  
Harvey, P. M., Henning, T., Ménard, F., et al. 2012a, *ApJ*, 744, L1  
Harvey, P. M., Henning, T., Liu, Y., et al. 2012b, *ApJ*, 755, 67  
Herczeg, G. J., & Hillenbrand, L. A. 2008, *ApJ*, 681, 594  
Hernández, J., Hartmann, L., Megeath, S.T., et al., 2007, *ApJ*, 662, 1067  
Hernández, J., Hartmann, L., Calvet, N., et al. 2008, *ApJ* 686, 1195  
Jäger, C., Mutschke, H., Begeman, B., Dorschner, J., Henning, Th., 1994, *AA*, 292, 641  
Jayawardhana, R., Mohanty, S., Basri, G., 2005, *Mem.S.A.It.* 76, 295  
Jeffries, R. D., Naylor, T., Walter, F. M., Pozzo, M. P., & Devey, C. R. 2009, *MNRAS*, 393, 538  
Kenyon, S.J. & Hartmann, L., 1995, *ApJS*, 101, 117  
Kessler-Silacci, J., et al., 2007, *ApJ*, 659, 680  
Kirkpatrick, J. D.; Henry, T. J.; Simons, D. A. 1995, *AJ*, 109, 797  
Klein, R., Apai, D., Pascucci, I., Henning, Th., Waters, L., 2003, *ApJ*, 593, 57  
Lawson, W., Lyo, A., Muzerolle, J., 2004, *MNRAS*, 329, 29  
López-Martí, B., Eislöffel, J., Mundt, R., 2005, *AA*, 444, 175  
López Martí, B., Spezzi, L., Merín, B., Morales-Calderón, M., Bouy, H., Barrado Y Navascués, D., & Eislöffel, J. 2010, *A&A*, 515, A31  
Martín, E., Rebolo, R., Zapatero-Osorio, M.R., 1996, *ApJ*, 469, 706  
Marschall, L.A. & van Altena, W.F., 1987, *AJ*, 94, 71  
Mercer, E. P., Miller, J. M., Calvet, N., Hartmann, L., Hernandez, J., Sicilia-Aguilar, A., & Gutermuth, R. 2009, *AJ*, 138, 7  
Merín, B., Brown, J. M., Oliveira, I., et al. 2010, *ApJ*, 718, 1200  
Meyer, M. R., Calvet, N., & Hillenbrand, L. A. 1997, *AJ*, 114, 288  
Mohanty, S., Jayawardhana, R., Natta, A., Fujiyoshi, T., Tamura, M., Barrado y Navascués, D., 2004, *ApJ* 609, L33  
Morrow, A. L.; Luhman, K. L.; Espaillat, C.; D'Alessio, P.; Adame, L.; Calvet, N.; Forrest, W. J.; Sargent, B.; Hartmann, L.; Watson, D. M.; Bohac, C. J., 2008, *ApJ* 676, 143  
Muench, A., Alves, J., Lada, Ch., Lada, E., 2001, *ApJ* 558, 51  
Muzerolle, J., Allen, L. E., Megeath, S. T., Hernández, J., & Gutermuth, R. A. 2010, *ApJ*, 708, 1107  
Najita, J., Strom, S., Muzerolle, J., 2007, *MNRAS* 368, 379  
Natta, A., Testi, L., Neri, R., Schepherd, D., Wilner, D., 2004, *A&A*, 416, 179  
Natta, A., Testi, L., Randich, S., Muzerolle, J., 2005, *Mem. S.A.It.*, 76, 343  
Oliveira, I., Merín, B., Pontoppidan, K. M., & van Dishoeck, E. F. 2013, *ApJ*, 762, 128  
Pascucci, I., Apai, D., Luhman, K., Henning, Th., Bouwman, J., Lahuis, F., Natta, A., 2009, *ApJ* 696, 143  
Patel, N.A., Goldsmith, P.F., Snell, R.L., Hezel, T. & Xie, T., 1995, *ApJ*, 447, 721  
Patel, N.A., Goldsmith, P.F., Heyer, M.H. & Snell, R.L., 1998, *ApJ*, 507, 241  
Peterson, D.E., et al. 2011, *ApJSS* 194, 43  
Platais, I., Kozhurina-Platais, V., van Leeuwen, F., 1998, *AJ*, 116, 2423  
Rice, W., Armitage, P., Wood, K., Lodato, G., 2006, *MNRAS* 373, 1619  
Riddick, F. C.; Roche, P. F.; Lucas, P. W., 2007, *MNRAS*, 381, 1067  
Scholz, A., Jayawardhana, R., Wood, K., et al. 2007, *ApJ*, 660, 1517  
Scholz, A., & Jayawardhana, R., 2008, *ApJ* 672, 49  
Sicilia-Aguilar, A., Hartmann, L., Briceño, C., Muzerolle, J., Calvet, N., 2004, *AJ* 128, 805 (SA04)

- Sicilia-Aguilar, A., Hartmann, L., Hernández, J., Briceño, C., Calvet, N., 2005, AJ 130, 188 (SA05)
- Sicilia-Aguilar, A., Hartmann, L., Calvet, N., Megeath, S.T., Muzerolle, J., Allen, L., D'Alessio, P., Merín, B., Stauffer, J., Young, E., Lada, C., 2006a, ApJ 638, 897, SA06a
- Sicilia-Aguilar, A., Hartmann, L., Fürész, G., Henning, Th., Dullemond, C., Brandner, W., 2006b, AJ 132, 2135 (SA06b)
- Sicilia-Aguilar, A., Hartmann, L., Watson, D., Bohac, C., Henning, Th., et al., 2007, ApJ 659, 1637
- Sicilia-Aguilar, A.; Henning, Th.; Juhász, A.; Bouwman, J.; Garmire, G.; Garmire, A., 2008, ApJ, 687, 1145
- Sicilia-Aguilar, A., Bouwman, J., Juhász, A., et al., 2009, ApJ, 701, 1188
- Sicilia-Aguilar, A., Henning, Th., Hartmann, L., 2010, ApJ, 710, 597
- Sicilia-Aguilar, A., Henning, T., Kainulainen, J., & Roccatagliata, V. 2011a, ApJ, 736, 137
- Sicilia-Aguilar, A., Henning, T., Dullemond, C. P., et al. 2011b, ApJ, 742, 39 (SA11)
- Sicilia-Aguilar, A., Henning, T., Linz, H., et al. 2013, A&A, 551, A34
- Siess, L., Dufour, E. & Forestini, M. 2000 A&A , 358, 593
- van der Marel, N., van Dishoeck, E. F., Bruderer, S., et al. 2013, Science, 340, 1199
- White, R., & Basri, G., 2003, ApJ, 582, 1109
- Whitworth, A., Zinnecker, H., 2004, A&A 427, 299
- Wright, E.L., et al. 2010, AJ 140, 1868

## Appendix A: Complete data tables of observed objects, their classification, and the photometry of members and probable members

The following tables contain the full information (object type and membership) of the objects observed with Hectospec/MMT (Table A.1), followed by the photometry data on members and probable members (Tables A.2 and A.3).

Table A.1: Observations and spectroscopic information. This table lists all observed objects, their Li and H $\alpha$  EW, and membership criteria. The objects IDs are based on the spectrograph (optical) coordinates. If H $\alpha$  appears in absorption, we label it as "Abs." in the corresponding column. If Lithium absorption can be excluded for EW larger than 0.1, we label it as 'N' in the corresponding column. Membership and presence of disks are marked as 'Y' (yes), 'N' (no), 'P' (probable), and 'pN' (probably not). In case the disk excess was observed only at one wavelength, we label it (e.g. P(24) indicates that the object has probably an excess, but only at 24 $\mu$ m). Undetermined values of the spectral type, uncertain membership, and uncertain IR fluxes are marked with 'X', objects with spectral types earlier than G are marked with 'E'. The errors in the spectral type are of 0.5 subtypes for objects K5 or later, 1 subtype for early K stars, and 2-3 subtypes for G-type objects. The best spectral types (in case of multiple values due to different observations with different S/N) are marked with <sup>b</sup>. Objects previously identified by Sicilia-Aguilar et al. (2005, 2006a,b) are marked with <sup>1</sup> (and their previous names are given in the comments), those identified by Barentsen et al. (2011) are marked with <sup>2</sup>, those in common with Morales-Calderón et al.(2009) are marked with <sup>3</sup>, objects with X-ray counterparts in Getman et al.(2012) are marked with <sup>4</sup>, and further IR-excess sources in the same paper are marked with <sup>5</sup>. In the comments field, we mention if there is any problem due to IR nebular emission (Neb.), nearby objects (Nobj.), if the SED suggest that the object is variable (Var.), if the object appears older than 10 Myr in the V vs V-I diagram (oVVI), or any other observation regarding the star/disk.

Spect. ID	H $\alpha$ EW (Å)	Li EW (Å)	Sp. Type	A <sub>V</sub> (mag)	Disk?	Campaign	Member?	Comments
213539203+573021561	Abs.	—	X	—	X	2009-MMT	N	
213541592+573127753	Abs.	—	X	—	X	2010-MMT	N	
213542993+573337049	-16	—	M4.0	1.1±0.6	Y	2009-MMT	Y <sup>4</sup>	
213554323+573443434	-8	—	Late	—	N	2009-MMT	N	
213555607+573003406	Abs.	N	G9.0	6.4±1.9	N	2010-MMT	N	
213601910+573430689	-1	—	K3.0	3.1±0.0	Y	2009-MMT	X	
213602343+573326502	Abs.	—	G9.0	2.8±0.2	Y	2009-MMT	N	
213602762+572834046	Abs.	—	X	—	N	2009-MMT	N	
213603888+572712198	Abs.	—	X	—	pN	2010-MMT	N	
213606037+573139138	-0.1	—	K1.5	3.6±0.1	Y	2009-MMT	N	
213607980+572637096	-11:	—	E-ClassI	—	Y	2010-MMT	Y	
213610280+573249821	Abs.	—	K1.5	4.1±0.0	P	2009-MMT	N	
213611098+572801471	Abs.	—	K0.0	4.6±0.0	P	2009-MMT	N	
213615231+572958174	Abs.	N	K0.0	4.6±0.0	pN	2010-MMT	N	
213617003+572639925	-23	—	M3.5	0.8±0.5	N	2009-MMT	N	
213617593+572510785	Abs.	—	X	—	N	2009-MMT	N	
213617600+572353249	Abs.	—	K1.5	2.7±0.2	N	2009-MMT	N	
213618699+573626870	-4	0.3	M3.5	0.9±0.3	N	2009-MMT	Y	
213618850+572649552	-1	—	K1.0	2.8±0.2	P	2009-MMT	N	
213619969+573527805	-6	—	M4.5	1.3±0.8	N	2009-MMT	Y	
213620628+572839896	Abs.	—	X	—	pN	2010-MMT	X	
213622159+572327898	-12	—	M3.5	1.1±0.6	N(24)	2009-MMT	pN <sup>4</sup>	Neb.
213622379+573141225	-9	0.1:	M3.0	3.3±0.9	pN	2010-MMT	Y	
213624769+572244914	Abs.	—	K1.0	3.4±0.1	N	2009-MMT	N	
213625078+572750265	-80	—	M4.0	1.2±0.6	Y	2009-MMT	Y <sup>1, 2</sup>	21362507.5727502
213626039+573327463	Abs.	—	K1.0	3.7±0.1	N	2009-MMT	N	
213626897+573304351	-21	—	M0.0	3.6±0.5	pN	2010-MMT	Y <sup>4</sup>	Neb., Nobj.
213627742+573202223	Abs.	N	K3.0	5.9±1.8	pN	2010-MMT	N	
213633647+573517477	Abs.	—	K0.5	3.0±0.2	Y(24)	2009-MMT	Y	Var.?, oVVI
213634910+572612281	-5	pN	M1.0	1.7±0.6	pN(8)	2010-MMT	pN	
213635322+572622430	Abs.	—	K2.5	3.9±1.0	N	2009-MMT	N	
213636558+573559377	Abs.	—	K1.0	3.0±0.2	N	2009-MMT	N	
213636909+573132683	-20	—	K7.0	3.3±0.2	Y	2009-MMT	Y <sup>4</sup>	
213637760+572458219	0	—	K1.0	3.5±0.2	N	2009-MMT	N	
213638543+573641056	-2	—	M3.0	0.4±0.5	N	2009-MMT	N	
213639147+572953326	-3	0.2	G9.0	5.3±0.4	Y	2009-MMT	Y <sup>4</sup>	oVVI, Earlier?
213641152+573702713	-7	0.3	M1.5	2.0±0.7	N	2010-MMT	Y <sup>4</sup>	
213641358+572204113	-11	0.1:	M2.0	2.0±1.0	N	2010-MMT	P	
213642470+572523186	-27	—	M3.5	1.4±0.7	Y	2009-MMT	Y <sup>3</sup>	
213643679+572331935	Abs.	N	K1.5	5.5±1.7	pN	2010-MMT	N	
"	Abs.	N	K1.5	5.5±1.7	pN	2010-MMT	N	
213643940+571838724	0	—	G7.0	6.6±0.6	P	2009-MMT	N	
213647421+571942074	Abs.	—	K0.0	3.0±0.2	N	2009-MMT	N	
213648190+573402084	-2	—	M1.5	1.4±0.2	N	2009-MMT	Y <sup>4</sup>	
213649612+572309317	-2	—	K0.0	5.8±1.9	N	2009-MMT	N	

Table A.1: Continued.

Spect. ID	H $\alpha$ EW (Å)	Li EW (Å)	Sp. Type	A $_V$ (mag)	Disk?	Campaign	Member?	Comments
213649639+573212770	-1	—	K0.0	5.3±0.2	N	2009-MMT	N	
213649653+572125909	Abs.	—	K0.0	2.8±0.2	N	2009-MMT	N	
213650683+572303728	Abs.	—	K2.5	2.7±0.1	N	2009-MMT	N	
213651349+573810594	Abs.	—	G9.0	5.6±2.2	N	2009-MMT	N	
213653210+572052112	-9	—	M1.0	1.6±0.7	pN	2010-MMT	P	
213655201+573030103	-45:	—	ClassI?	—	Y	2010-MMT	Y	Neb.,lowSN
213655283+572551668	Abs.	—	K2.5	2.6±0.2	Y	2009-MMT	Y	oVVI
213657982+574058727	Abs.	—	K0.0	5.7±2.0	N	2009-MMT	N	
213658737+573848181	-21	0.2	M3.5	0.8±0.7	Y	2010-MMT	Y <sup>5</sup>	Neb.
213659108+573905636	-79	0.4	K5.5	1.8±0.5	Y	2009-MMT	Y <sup>2,5</sup>	
213659472+573134908	-108	—	M1.0	2.0±0.9	Y	2010-MMT	Y <sup>1,2</sup>	Neb.,21365947.5731349
213701319+573418289	-22	—	M3.0	0.6±0.9	Y	2009-MMT	Y <sup>4</sup>	Var., Neb.
"	-2	0.3	M1.0 <sup>b</sup>	1.4±1.0	Y	2010-MMT	Y <sup>4</sup>	Var., Neb.
213701401+572445873	-3	—	M3.0	2.5±1.3	N	2009-MMT	Y <sup>1,4</sup>	11-1499, LiI
213702019+574004207	Abs.	—	K0.5	2.1±0.3	N	2009-MMT	N	
213702260+573901063	Abs.	—	G9.0	6.0±2.1	N	2009-MMT	N	
213702321+573115201	-25:	—	ClassI?	—	P	2010-MMT	P	Neb., Globu,lowSN
213702417+571729455	Abs.	—	E	—	N	2010-MMT	N	
213702967+573746081	Abs.	—	E	—	N	2010-MMT	N	
213703207+572718405	-6	0.3	K5.5	2.5±0.3	N:(24)	2009-MMT	Y <sup>4</sup>	
213704539+573223646	-32	—	M4.0	2.1±0.7	N	2009-MMT	Y <sup>4</sup>	
213706050+573604911	Abs.	—	K0.5	2.3±0.3	N	2009-MMT	N	
213707711+573211012	-35	—	M2.0	1.8±1.5	Y	2010-MMT	Y	Globu
213708137+573616213	-45	0.2	M4.0	1.7±1.0	Y	2010-MMT	Y <sup>5</sup>	
213708281+573023538	-5	0.2	M4.5	1.5±0.8	pN(8)	2010-MMT	Y <sup>4</sup>	Neb.
213708783+572322501	Abs.	pN	K0.0	2.7±0.2	pN(24)	2010-MMT	N	Neb.
213708879+572107012	-55	0.3	M2.0	1.4±1.0	Y	2010-MMT	Y	
213709442+573036722	-32	—	M3.0	1.3±0.9	Y	2009-MMT	Y <sup>4</sup>	
213710231+573030212	Abs.	—	G9.0	4.4±1.4	N	2009-MMT	N	
213710259+572216542	Abs.	—	K1.0	2.4±0.1	N	2009-MMT	N	
213710657+571944106	-17	—	K0.0	4.9±0.3	N	2009-MMT	N	
213710877+573846877	-85	—	M4.5 <sup>b</sup>	1.9±0.7	Y	2009-MMT	Y	
"	-10	—	M2.0	3.0±0.9	Y	2010-MMT	Y	
213711371+571406304	Abs.	—	G9.0	4.9±1.8	N	2009-MMT	N	
213711673+573935409	Abs.	—	G6.0	7.0±1.7	N	2009-MMT	N	
213712353+573331789	-2	0.4	K4.0	1.9±0.6	pN(8)	2009-MMT	Y <sup>4</sup>	NObj.
213712580+574055032	-10	—	M3.5	1.7±0.6	N	2009-MMT	Y <sup>4</sup>	
213713500+573102086	Abs.	—	X	—	N	2009-MMT	N	
213714200+571936677	-5	—	M3.5	0.2±0.7	N	2009-MMT	N	
213714413+573453994	Abs.	N	K1.0	5.3±0.7	N	2010-MMT	N	
213715100+572059280	Abs.	—	K2.0	2.9±0.1	P	2009-MMT	N	
213716349+572640200	-17	0.4	K7.0	6.0±1.0:	Y	2010-MMT	Y <sup>2,4</sup>	Very embedded
213717070+571914883	-2	—	M3.5	0.4±1.0	N	2009-MMT	N	
213720270+571228210	Abs.	—	K7.0	0.8±0.0	N	2009-MMT	N	
213720641+572100571	-4	0.2	M1.0	1.0±0.7	pN(8)	2010-MMT	Y	
213720771+574336243	Abs.	—	G9.0	5.8±0.5	N	2009-MMT	N	
213721087+572812883	Abs.	—	X	—	N	2009-MMT	N	
213721801+572917455	Abs.	—	E	—	N	2010-MMT	N	
213724102+572411541	-107	0.2	K5.5	2.4±0.3	Y	2009-MMT	Y <sup>1,2,5</sup>	oVVI, 21372410+5724115
21372447+5731359	-62	—	M1.0:	3.1±1.7	Y	2009-SAO	Y <sup>1,5</sup>	21372447.5731359
213725743+571257077	-6	—	M1.5	2.6±0.3	N	2010-MMT	P	
213726148+572330562	-28	—	M4.5	1.3±0.7	Y	2009-MMT	Y	
213726272+571258793	-0.5	0.3	M0.5	1.4±0.4	N	2009-MMT	Y	
213726347+573638364	-3	—	M0.5	1.5±0.4	N	2009-MMT	N	
21372643+5731386	-2	—	K2.0	2.4±0.1	P(8)	2009-SAO	P	oVVI
21372685+5732069	-65	—	G5:	0.6±0.6	N	2009-SAO	P	Neb.
213726917+573013266	Abs.	N	G4.0	7.2±2.1	pN	2010-MMT	N	
213727418+573123620	-11	—	M2.5	0.9±0.7	Y	2009-MMT	Y <sup>4,5</sup>	Near 14-160
21372742+5733197	-60	—	K0:	1.0±0.7	N	2009-SAO	pN	2 objects
213727439+572201490	Abs.	—	K1.0	3.1±0.2	N	2009-MMT	N	
213727693+574330146	Abs.	N	G1.0	6.6±1.6	Y	2010-MMT	pN	
213728428+572548289	Abs.	—	G9.0	6.1±2.5	N	2009-MMT	N	
213730069+572431962	-30	—	M3.5	0.5±0.8	N	2009-MMT	X	Nobj., dMe?
21373045+5734263	-3	—	K5:	0.5±0.4	N	2009-SAO	pN	
213730707+572004665	Abs.	—	X	—	N	2009-MMT	N	

Table A.1: Continued.

Spect. ID	H $\alpha$ EW (Å)	Li EW (Å)	Sp. Type	A $_V$ (mag)	Disk?	Campaign	Member?	Comments
213730893+572131278	Abs.	N	G5.0	7.1±2.1	Y	2010-MMT	N	
213731517+573935272	Abs.	—	E	—	Y	2010-MMT	N	
213732341+572503204	-47	0.1	G9.0	1.8±0.5	Y	2010-MMT	Y <sup>4</sup>	UXor?
213732493+574415574	-16	—	M3.0	0.1±0.6	N	2009-MMT	N	
213733557+573550931	-6	0.2	M1.5	1.7±0.7	Y	2010-MMT	Y	
21373404+5735011	-1	—	GK	2.1±0.1	N	2009-SAO	pN	
213734072+572526880	-8	—	M3.5	0.7±0.4	N	2009-MMT	N	
213734113+573431198	-56	—	M0.0	2.1±0.9	Y	2009-MMT	Y <sup>5</sup>	
213734649+571657705	-60	0.2	M1.0	3.1±0.4	Y	2010-MMT	Y <sup>2</sup>	
213735713+573258349	-62	—	M2.0	1.5±1.0	Y	2010-MMT	Y <sup>2,5</sup>	
213735802+571619829	Abs.	N	G8.0	7.9±1.1	N	2010-MMT	N	
213738830+572936901	-7	0.5	K3.5	5.1±0.3	Y	2010-MMT	Y <sup>4</sup>	
213738913+573831249	Abs.	—	G8.0	6.0±0.7	N	2009-MMT	N	
213740217+571903718	-11	—	M1.5	2.1±1.6	N	2010-MMT	P	
213740471+573433203	-7	—	M2.5	2.0±1.0	Y	2010-MMT	Y <sup>5</sup>	Mini-cluster
213740870+571201294	Abs.	—	K0.0	4.6±0.9	N	2009-MMT	N	
213742167+573431486	-60	—	M2.0	1.4±0.8	P	2009-MMT	Y	Neb.
213742758+573325074	-67	—	X	—	Y	2009-MMT	Y <sup>2,4</sup>	UXor?,Mini-cluster
213743142+574105401	Abs.	—	G7.0	4.9±0.2	N	2009-MMT	N	
21374388+5734521	-35	—	M2.0:	2.7±1.7:	P	2009-SAO	P	Neb.
213744131+573331130	-17	0.5	K7.5	2.7±0.7	Y	2009-MMT	Y <sup>4</sup>	Mini-cluster
"	-19	0.4	M1.0 <sup>b</sup>	1.9±0.7	Y	2010-MMT	Y <sup>4</sup>	Mini-cluster
213744268+573651850	Abs.	—	K2.0	3.3±0.3	N	2009-MMT	N	
213744543+572200213	-51	—	M5.0	1.1±1.2	P	2009-MMT	Y	Mini-cluster
213744818+571738025	Abs.	—	X	—	N	2010-MMT	X	
213745147+571942390	-14	0.4	K5.5	1.9±0.2	Y	2009-MMT	Y <sup>1,2</sup>	11-383
213745161+570831180	Abs.	—	X	—	N	2009-MMT	N	
213746157+574331409	Abs.	—	G9.0	5.6±0.3	P	2009-MMT	N	
213746171+571722726	0	—	K0.0	5.5±1.5	N	2009-MMT	N	
213746871+573156208	-42	—	M1.5	2.9±0.8	Y	2009-MMT	Y <sup>5</sup>	
213747928+573114666	Abs.	—	X	—	N	2009-MMT	N	
213747963+573242323	-61	—	M1.0	1.4±0.8	Y	2009-MMT	Y <sup>2,5</sup>	Mini-cluster
213748237+572319411	-8	—	M3.5	0.7±0.8	Y	2010-MMT	Y	
213748821+572717746	Abs.	—	G9.0	5.5±0.9	N	2009-MMT	N	
213748931+572320963	-20	0.2	K5.0	2.7±0.4	Y	2009-MMT	Y <sup>1,2,5</sup>	21374893+5723209
213749041+570808947	Abs.	—	M0.0	0.2±0.6	N	2009-MMT	N	
213749260+573158309	-9	0.2	M0.0	2.5±0.8	N	2010-MMT	Y <sup>4</sup>	
213750222+573009586	-20	0.4	M0.0	3.3±0.0	pN	2009-MMT	Y <sup>4</sup>	
213750297+570909399	-5	—	M1.0	2.1±0.6	N	2009-MMT	P	
213751197+574656428	-6	—	M3.5	2.3±0.5	N	2009-MMT	P	
213751210+572436151	-15	—	K7.5	3.3±0.9	Y	2009-MMT	Y <sup>5</sup>	
213751801+572257095	Abs.	—	K0.0	2.7±0.1	N	2009-MMT	N	
213751808+572559001	Abs.	N	G6.0	4.7±1.8	Y	2010-MMT	N	
213753470+573346291	Abs.	—	K1.0	2.9±0.3	pN(24:)	2009-MMT	pN	oVVI
213755392+570832540	Abs.	—	K1.0	5.2±0.1	N	2009-MMT	N	
213756292+574202942	-2	—	M3.5	0.8±1.3	N	2009-MMT	N	
213756779+573448171	-9	—	M1.5	1.7±1.1	Y	2010-MMT	Y	
213758297+571827161	Abs.	—	M1.5	0.4±0.5	N	2009-MMT	N	
213758352+574224681	Abs.	—	K1.0	3.9±0.4	N	2009-MMT	N	
213759251+570545808	Abs.	—	K1.0	3.1±0.2	N	2009-MMT	N	
213759869+572501968	Abs.	—	K2.5	2.3±0.0	P	2009-MMT	N	
213800487+570954841	Abs.	—	K1.0	2.8±0.4	Y	2009-MMT	N	
213801380+570518164	Abs.	—	K2.5	2.7±0.1	N	2009-MMT	N	
213803117+574644164	Abs.	—	K1.0	3.3±0.1	N	2009-MMT	N	
213803453+570512396	-12	—	M3.0	1.4±0.6	pN	2009-MMT	P	Var.?
213803749+572358069	Abs.	—	K2.0	2.7±0.1	N	2009-MMT	N	
213804820+570754472	-17	—	M1.0	1.9±0.7	N	2010-MMT	P	
213805170+574735827	Abs.	—	K0.0	3.1±0.1	N	2009-MMT	N	
213806612+570424098	Abs.	—	K0.0	2.8±0.1	N	2009-MMT	N	
213808143+573414485	-4	N	M2.0	1.8±0.9	P	2010-MMT	N	
213808157+573917666	Abs.	N	G7.0	5.8±0.9	N	2010-MMT	N	
213808280+573418151	-3	N	G9.0	3.6±0.2	N	2009-MMT	N	
213809221+572038118	-18	—	M4.0	1.3±1.0	N	2009-MMT	P	
213809613+571126151	Abs.	—	G6.0	7.4±2.5	N	2010-MMT	N	
213809997+572352782	-50	—	M2.0	2.2±0.2	Y	2009-MMT	Y <sup>2</sup>	



Table A.1: Continued.

Spect. ID	H $\alpha$ EW (Å)	Li EW (Å)	Sp. Type	A $_V$ (mag)	Disk?	Campaign	Member?	Comments
213810182+572708407	-10	—	M1.5	1.5±0.8	Y	2010-MMT	Y <sup>5</sup>	Var.
213810677+572346025	-3	N	M1.0	1.3±0.7	N	2010-MMT	N	
213810759+574013683	-46	—	M1.5	1.6±0.6	N	2010-MMT	P	Neb.,oVVI
213811281+570619935	Abs.	N	E	—	Y	2010-MMT	N	
213811789+570731057	Abs.	—	K0.0	4.4±0.0	N	2009-MMT	N	
213811817+574738931	Abs.	—	G9.0	3.7±0.0	P	2009-MMT	N	
213812023+572500774	-3	—	M1.0	1.4±0.4	Y	2009-MMT	Y <sup>5</sup>	
213812057+570513385	Abs.	N	K1.0	4.9±1.3	pN	2010-MMT	N	
213812290+571905627	Abs.	—	G8.0	5.9±2.0	N	2009-MMT	N	
213812641+572033696	-159	—	K7.0	2.3±0.4	Y	2009-MMT	Y <sup>2</sup>	
213813973+574913043	Abs.	—	G8.0	2.1±0.1	N	2009-MMT	N	
213815367+574722877	Abs.	—	G9.0	2.8±0.1	N	2009-MMT	N	
213816129+571935798	-13	0.3	M0.0	1.9±0.7	Y	2009-MMT	Y <sup>1</sup>	54-1781
213816170+574104645	-8	0.5	K4.5	2.0±0.5	N	2009-MMT	Y	Near 13-2236
213816198+573956461	-3	—	M3.0	0.5±1.1	N	2009-MMT	N	
213816417+571139019	Abs.	—	K1.0	4.3±0.2	N	2009-MMT	N	
213817880+571136986	Abs.	N	K2.0	3.6±0.4	N	2010-MMT	N	
213819109+570555133	Abs.	—	G9.0	4.9±0.0	N	2009-MMT	N	
213819411+572203907	-14	—	M2.0	2.7±0.7	P(8)	2010-MMT	P	
213819507+572044119	-6	—	M2.0	2.2±0.9	N	2010-MMT	P	
213820201+574757676	Abs.	N	G5.0	5.9±1.1	Y	2010-MMT	N	
213820420+573637691	-26	—	M4.5	1.5±1.1	N	2009-MMT	N	dMe
213820441+572757612	-4	N	M0.5	3.0±0.1	pN(8)	2010-MMT	N	
213820510+571925883	Abs.	—	K0.0	8.2±1.6	N	2009-MMT	N	
213820798+574504614	Abs.	—	M4.0	0.1±0.7	N	2009-MMT	N	
213822171+573454681	Abs.	—	K0.0	2.4±0.1	N	2009-MMT	N	
213822398+573350782	Abs.	—	K1.0	2.3±0.2	N	2009-MMT	N	
213822810+574017294	-18	—	M0.0	2.5±0.9	Y	2009-MMT	Y <sup>2,5</sup>	
213823950+572736175	-18	0.1	M1.0	1.4±0.6	Y	2010-MMT	Y	
213824142+574451513	-5	0.4	K6.0	2.4±0.4	N	2009-MMT	Y <sup>2</sup>	
213824293+570308992	Abs.	—	K0.5	2.6±0.1	N	2009-MMT	N	
213824293+574724141	Abs.	—	K1.5	6.0±2.1	N	2009-MMT	N	
213824650+571320972	Abs.	—	G6.0	5.6±1.9	N	2009-MMT	N	
213824781+571932530	Abs.	—	K1.0	5.3±2.1	N	2009-MMT	N	
213825831+574207487	-2	0.4	K2.0	4.6±0.9	Y	2009-MMT	Y <sup>2</sup>	UXor?
213826477+572017670	Abs.	N	K1.5	6.3±0.1	pN	2009-MMT	N	
"	Abs.	N	K3.0	5.1±1.9	pN	2010-MMT	N	
"	Abs.	N	K3.0	5.9±0.1	pN	2010-MMT	N	
213826573+571649987	Abs.	—	K0.0	4.1±0.1	N	2009-MMT	N	
213826813+573501891	Abs.	—	G9.0	3.7±0.1	N	2009-MMT	N	
213827431+572720767	-36	0.3	K5.0	2.2±0.4	Y	2009-MMT	Y <sup>1,2</sup>	12-2113
213828022+573149808	-5	N	M1.0	1.7±1.2	N	2010-MMT	N	
213828028+574736432	-4	—	M2.5	1.0±0.8	Y	2009-MMT	Y	
213828221+570859896	Abs.	—	K0.0	2.5±0.4	P	2009-MMT	N	
213828887+574732174	Abs.	—	K5.0	6.1±2.0	N	2010-MMT	N	
213829367+573726567	-10	—	M2.0	2.0±1.1	P(8)	2010-MMT	Y	
213829848+570616501	Abs.	—	G9.0	2.7±0.2	N	2009-MMT	N	
213830308+573255218	-31	—	M1.0	1.7±0.9	Y	2010-MMT	Y <sup>2</sup>	
213830349+572618227	-13	0.2	K7.0	2.1±0.6	Y	2009-MMT	Y	IR variable
213831503+571837296	Abs.	—	X	—	X	2010-MMT	X	
213831530+571928643	Abs.	—	K0.0	2.6±0.2	N	2009-MMT	N	
213832121+570637293	-7	—	M4.0	1.9±0.6	N	2009-MMT	X	
213832169+572635943	-43	—	M0.0	2.2±0.7	Y	2009-MMT	Y <sup>1,2</sup>	21383216.5726359
213832251+572253401	0	—	M2.5	0.7±0.8	N	2010-MMT	N	
213832402+574705450	-1	—	M1.0	1.3±0.6	N	2009-MMT	N	
213833130+573145785	Abs.	—	M1.0	2.0±1.2	N	2009-MMT	X	
213834050+573418852	Abs.	—	K0.0	2.2±0.1	N	2009-MMT	N	
213834510+571457281	Abs.	—	G5.0	4.7±1.4	N	2009-MMT	N	
213834689+573544614	Abs.	N	G7.0	6.3±0.1	N	2010-MMT	N	
213835073+571031851	-2	—	M0.5	5.3±1.1	P	2010-MMT	pN	
213835211+573013582	-4	0.4	K6.0	2.5±0.5	N	2009-MMT	Y	
"	-1	0.4	K6.0	2.5±0.5	N	2009-MMT	Y	
213835279+570618712	Abs.	—	G9.0	5.3±1.5	N	2009-MMT	N	
213836234+565852709	-24	—	X	—	N	2009-MMT	N	
213837298+573103776	-4	0.3	K7.0	2.1±0.8	Y	2009-MMT	Y	
213837332+574809899	Abs.	—	G9.0	6.5±2.4	N	2009-MMT	N	

Table A.1: Continued.

Spect. ID	H $\alpha$ EW (Å)	Li EW (Å)	Sp. Type	A $_V$ (mag)	Disk?	Campaign	Member?	Comments
213837841+573230499	Abs.	—	K0.0	2.4±0.1	N	2009-MMT	N	
213838019+572147909	Abs.	N	G7.0	4.8±1.4	pN	2010-MMT	N	
213838232+574826378	Abs.	—	K0.0	3.4±0.1	N	2009-MMT	N	
213838548+573820015	Abs.	—	G3.0	6.3±0.3	N	2009-MMT	N	
213839228+572227624	Abs.	—	G9.0	5.4±1.4	N	2009-MMT	N	
213839571+572916412	-22	—	M1.5	4.7±0.1	Y	2010-MMT	Y	Near HD206267
213839749+572753080	-5	0.2	M2.5	2.2±0.9	Y	2010-MMT	Y	
213840271+573423383	-3	—	M4.0	1.2±1.1	N	2009-MMT	X	
213840422+573535962	Abs.	N	G6.0	6.1±2.0	pN	2010-MMT	N	
213840752+574856934	-47	—	M0.0	3.3±1.2	N	2010-MMT	pN	Nobj.
213842249+573533902	-1	—	M4.0	0.8±0.8	Y	2009-MMT	Y	
213842311+574810036	Abs.	—	K1.0	5.6±0.2	N	2009-MMT	N	
213842640+574603638	Abs.	—	X	—	N	2009-MMT	N	
"	Abs.	N	G4.0	4.9±0.8	N	2010-MMT	N	
213843258+573252183	-1	—	M4.0	0.7±1.5	N	2009-MMT	X	
213843423+571432878	Abs.	—	G7.0	2.2±0.1	P	2009-MMT	N	
213843478+571708183	Abs.	—	G2.0	7.5±1.1	N	2009-MMT	N	
213844343+573626211	-34	—	M1.5	1.0±0.7	Y	2010-MMT	Y	
213845270+571714033	-4	—	M0.5	5.0±0.7	N	2010-MMT	N	
213846019+573020737	-1	N	M0.5	1.3±0.9	N	2010-MMT	N	
213847282+573114405	-29	—	M1.0	1.6±1.1	Y	2009-MMT	Y	Near HD206267
"	Abs.	—	X	—	Y	2010-MMT	Y	Low S/N, Near HD206267
213848223+570753964	Abs.	—	X	—	N	2009-MMT	N	
213848271+570738391	Abs.	—	K0.0	2.8±0.1	P	2009-MMT	N	
213848497+573014186	-10	—	M2.0	2.0±0.8	N	2009-MMT	pN	
"	-2	—	M2.0	2.0±0.8	N	2009-MMT	pN	
213848930+573528505	Abs.	—	K1.0	3.3±0.2	N	2009-MMT	N	
213849438+573043451	Abs.	—	K0.5	2.7±0.2	P	2009-MMT	N	
213849568+572259086	Abs.	N	G6.0	6.2±2.1	N	2010-MMT	N	
213849891+572206173	Abs.	—	G2.0	5.1±1.8	N	2009-MMT	N	
213850077+571523167	-13	—	M2.5	0.9±0.9	N	2009-MMT	pN	
213850571+572628486	Abs.	N	G9.0	6.9±1.6	N	2010-MMT	N	
213850578+573315447	-5	—	G8.0	5.2±1.4	N	2009-MMT	N	
"	Abs.	—	G4.0	6.4±0.8	N	2010-MMT	N	
213852040+571521149	Abs.	—	G5.0	6.4±2.5	N	2010-MMT	N	
213852301+575113260	Abs.	—	G9.0	3.9±0.1	N	2009-MMT	N	
213853970+571650152	Abs.	N	K2.0	4.6±0.5	N	2010-MMT	N	
213854718+571617509	Abs.	—	G6.0	7.3±2.1	N	2009-MMT	N	
213854760+572450268	-5	0.3	M1.0	1.1±0.5	Y	2009-MMT	Y	
213855041+572042307	Abs.	—	G8.0	6.4±0.5	N	2009-MMT	N <sup>1</sup>	21-851
213856153+575244516	-2	—	K7.5	6.0±1.4	pN	2010-MMT	N	
213856538+575002605	Abs.	—	G6.0	6.0±1.0	N	2009-MMT	N	
213858632+575308164	-1	—	X	—	N	2009-MMT	N	
213859147+572045273	-1	—	M1.5	1.6±1.0	N	2010-MMT	P	
213859738+572216816	-10	—	M2.5	2.2±1.1	Y	2010-MMT	Y	
213859937+572108317	Abs.	—	K0.0	2.8±0.3	N	2009-MMT	N	
213900397+575004884	-36	—	M4.0	1.2±0.9	P	2009-MMT	P	
213900562+571742543	Abs.	—	G2.0	6.2±1.7	N	2009-MMT	N	
213901708+574856687	Abs.	—	G9.0	3.0±0.1	N	2009-MMT	N	
213902519+572338005	Abs.	N	G2.0	3.6±0.3	P	2010-MMT	N	
213903212+571555316	-6	0.4	M1.0	0.8±0.5	Y	2009-MMT	Y	Neb.
213903487+574037729	Abs.	—	K0.0	2.9±0.3	N	2009-MMT	N	
213903562+575241481	Abs.	—	G6.0	4.7±0.2	N	2009-MMT	N	
213905519+572349596	-1	0.4	K7.0	1.2±0.2	P(8)	2010-MMT	Y	Mini-cluster
"	0	0.5	K6.0	1.5±0.2	P(8)	2009-MMT	Y	
213905897+572527745	-1	—	M0.5	0.6±0.3	N	2009-MMT	N	
213906172+571316138	Abs.	—	K0.0	2.2±0.2	N	2009-MMT	N	
213906199+571811258	-14	—	M3.5	1.0±0.6	N	2009-MMT	pN	
213907771+572401997	Abs.	N	G4.0	4.5±1.4	N	2010-MMT	N	
213907929+574836087	Abs.	—	G9.0	6.0±1.5	N	2009-MMT	N	
213908479+571436888	Abs.	—	G3.0	6.9±1.0	N	2009-MMT	N	
213909481+574833409	Abs.	—	K2.0	2.5±0.1	N	2009-MMT	N	
213909591+575424972	Abs.	0.3:	K0.0	4.5±1.9	N	2009-MMT	P	
213909728+571803046	-6	—	M1.5	1.8±0.9	pN(8)	2010-MMT	P	
213910429+572235727	-103	—	M0.0	3.2±1.1	Y	2009-MMT	Y	Var., near 21-840
213911452+572425205	-26	0.2	M1.0	2.2±0.7	P	2010-MMT	Y	Var., Mini-cluster

Table A.1: Continued.

Spect. ID	H $\alpha$ EW (Å)	Li EW (Å)	Sp. Type	A $_V$ (mag)	Disk?	Campaign	Member?	Comments
213911500+572655128	-4	—	M2.0	1.2±0.9	N	2010-MMT	pN	
213911720+575314948	Abs.	—	E	—	N	2010-MMT	N	
213911733+573219870	Abs.	—	X	—	N	2009-MMT	N	
213911761+575307477	—	—	K1.0	3.4±0.1	P	2009-MMT	N	
213912509+570810993	-3	—	M3.0	0.6±0.7	N	2009-MMT	N	
213912537+571631434	—	—	M3.0	4.1±1.4	N	2009-MMT	N	
213912667+571522055	0	—	K1.0	2.3±0.3	N	2009-MMT	N	
213913979+573922926	Abs.	—	K0.0	3.0±0.5	N	2009-MMT	N	
213914192+572055421	Abs.	—	K0.0	2.5±0.2	P	2009-MMT	N	
213914453+572304758	-8	—	M3.5	1.4±0.8	P(8)	2009-MMT	P	Nobj.
213914487+574953541	Abs.	—	X	—	N	2009-MMT	N	
213914837+573756779	-13	—	M0.0	3.3±0.8	P(24)	2009-MMT	P	Var.
213914967+571654656	Abs.	—	K0.0	3.0±0.1	N	2009-MMT	N	
213914988+574050473	-25	—	M4.0	3.1±1.1	Y	2009-MMT	Y	
213915002+575023465	-36	—	M4.0	1.7±0.8	N	2009-MMT	P	
21391561+5729186	-1	—	M3.0	11.7±6.6	N	2009-SAO	N	
213915812+574226425	Abs.	—	K4.0	2.4±0.1	N	2009-MMT	N	
213916911+572632770	Abs.	N	G7.0	6.0±1.1	N	2010-MMT	N	
213917062+571643244	-6	0.3	M2.0	1.5±1.0	N	2010-MMT	Y	
213917178+574709597	Abs.	—	K1.0	3.3±0.1	N	2009-MMT	N	
213917371+571605286	-24	—	M3.5	0.9±1.0	N	2009-MMT	P	
213917481+571747432	-33	0.5	K6.0	2.2±0.9	Y	2009-MMT	Y <sup>1</sup>	54-1488
213918291+572818473	-6	—	M2.0	1.0±0.6	N	2009-MMT	P	
213918339+574022609	-4	—	M2.5	1.4±0.7	N	2009-MMT	P	
213918998+573806996	-5	—	M3.0	0.5±0.5	N	2009-MMT	N	
213919348+573914178	Abs.	—	K0.5	2.8±0.4	N	2009-MMT	N	
21391969+5727461	-1	—	G0.0	2.9±0.3	N	2009-SAO	N	
213919719+575331070	-20	—	K3.0	6.7±1.2	N	2009-MMT	N	
213920172+575015967	-22	—	M3.5	0.8±0.7	N	2009-MMT	P	
21392059+5726269	-34	—	LateM:	—	Y	2009-SAO	P	S/N, has 24 $\mu$ m excess
213920591+572308795	Abs.	—	X	—	X	2010-MMT	X	
213920831+571631187	-2	—	M4.0	1.1±1.4	N	2009-MMT	P	
213921298+574857456	-5	—	K2.5	5.0±1.7	N	2009-MMT	N	
21392151+5728398	-5	—	M4.0	3.1±2.0	N	2009-SAO	pN	oVVI
213921607+575153416	Abs.	—	K1.0	3.3±0.0	N	2009-MMT	N	
213923489+573409252	Abs.	—	M1.0	1.7±0.8	N	2009-MMT	N	
213924388+572820999	-8	0.2	K7.5 <sup>b</sup>	2.2±0.5	N	2009-MMT	Y	
"	-23	—	K	—	N	2009-SAO	Y	
213924491+574455317	-90	—	M1.0	3.2±1.0	N	2010-MMT	pN	Nobj., Faint
213924711+571912672	-37	—	M2.5	2.8±1.1	Y	2010-MMT	Y	Var.
213924917+575217654	Abs.	N	K0.0	4.9±1.4	N	2010-MMT	N	
213925130+574942458	Abs.	—	K0.5	3.3±0.0	N	2009-MMT	N	
213925219+574345156	-1	—	K7.0	4.2±1.0	N	2010-MMT	N	
213925363+572830832	Abs.	—	G9.0	3.2±0.4	P	2009-MMT	N	
21392564+5728183	-16	—	K6.0:	2.2±0.1	N	2009-SAO	P	
213925679+575000504	Abs.	N	K0.0	7.3±3.4	pN	2010-MMT	N	
213926421+572538470	-164	—	M1.0	3.2±0.8	Y	2009-MMT	Y	
213926428+573503140	Abs.	—	K0.0	2.9±0.4	N	2009-MMT	N	
21392806+5728420	-12	—	K4.0	3.8±1.4	N	2009-SAO	P	Nobj.
213928151+572521181	-3	0.2	K7.0	2.2±0.3	N	2009-MMT	Y	
213928742+573930163	-7	—	M4.0	2.5±0.9	N	2009-MMT	P	
213928968+574347037	-1	0.3	M3.5	0.2±0.8	N	2009-MMT	P	
213929250+572530299	-14	0.1	M1.0	—	Y	2010-MMT	Y	
213929408+570630605	-24	0.1	K7.0	2.1±0.6	Y	2009-MMT	Y <sup>2</sup>	
213929579+571631626	Abs.	—	K0.0	5.8±0.7	N	2009-MMT	N	
213929648+574809597	-7	—	M3.5	2.1±0.9	N	2009-MMT	P	
213930129+572651433	-4	0.4	M0.5	2.0±0.4	Y	2009-MMT	Y	
21393069+5728116	-5	—	M2.5	0.0±0.8	N	2009-SAO	pN	dMe?
213930870+572227446	-108	—	K7.0	2.3±0.4	Y	2009-MMT	Y <sup>2</sup>	
21393179+5728291	-11	—	M2.0	1.2±0.4	N	2009-SAO	P	
213932189+573539903	-4	—	M4.0	1.4±0.7	N	2010-MMT	pN	
213932752+570700296	-7	—	M3.5	0.0±0.6	N	2009-MMT	N	
213933157+574140639	Abs.	—	G9.0	2.6±0.5	N	2009-MMT	N	
213933219+573300533	-35	—	M3.5	2.0±0.8	Y	2009-MMT	Y	
21393301+5728175	Abs.	—	M1.5	2.3±0.8	Y	2009-SAO	Y	
213933328+571844890	Abs.	—	K0.0	4.9±1.1	N	2009-MMT	N	

Table A.1: Continued.

Spect. ID	H $\alpha$ EW (Å)	Li EW (Å)	Sp. Type	A $_V$ (mag)	Disk?	Campaign	Member?	Comments
213934880+574531915	Abs.	N	G8.0	5.9±1.7	Y	2010-MMT	N	
213934908+571703418	-23	—	M4.0	0.6±0.8	N	2009-MMT	P	
213935018+573353693	-2	—	M3.0	1.5±0.7	N	2009-MMT	P	
213935162+572053128	-25	—	M4.0	1.3±0.9	Y	2009-MMT	Y	
213935320+571928932	-4	—	M2.5	2.8±1.3	pN	2010-MMT	pN	
21393648+5728119	-4	—	G5.0	2.1±0.2	N	2009-SAO	P	
213936638+571153452	Abs.	—	G9.0	2.6±0.2	N	2009-MMT	N	
213937132+572459030	-49	—	M3.0	1.0±0.7	Y	2009-MMT	Y	
213937448+574607113	-30	—	M4.5	1.7±1.0	pN	2009-MMT	P	
213938018+571818056	-9	—	M3.5	0.7±0.6	N	2009-MMT	X	
213938162+572301696	-2	0.8:	M4.5	1.4±1.0	N	2009-MMT	P	
213938169+573218304	0	—	M2.5	1.2±0.6	N	2009-MMT	P	
21393819+5727319	-5	0.4	M1.0	3.3±1.3	N	2009-SAO	Y	
21393921+5727402	-2	—	M0.0	0.1±0.2	N	2009-SAO	X	
213939913+574918687	0	—	M2.0	2.7±0.6	pN	2010-MMT	pN	
21394010+5730113	-24	—	M2.0	1.6±0.3	Y	2009-SAO	Y	
213940600+572108797	-8	—	M1.5	3.0±1.1	N	2010-MMT	P	
213940710+572206160	-6	—	M1.5	0.9±0.5	N	2009-MMT	P	
213940957+574431175	-8	—	M3.5	0.2±0.8	N	2009-MMT	N	
213941211+573749556	-3	—	M4.5	2.1±0.6	N	2009-MMT	P	
213941589+574957427	Abs.	—	K0.5	3.7±0.0	N	2009-MMT	N	
213942083+570508990	Abs.	—	K1.0	3.0±0.1	N	2009-MMT	N	
213942227+571701866	-4	0.5	M0.0	1.3±0.4	N	2009-MMT	Y	
213942289+572902679	-12	—	M2.5	2.1±1.0	Y	2010-MMT	Y	Nobj.
213942378+573348653	-75	0.4	M4.5	1.2±0.7	N	2010-MMT	Y	Strong H $\alpha$ , no disk?
213942399+573431184	-51	—	M3.5	2.0±0.6	Y	2010-MMT	Y	Neb.
21394265+5727008	-1	—	K7.0	1.6±0.0	N	2009-SAO	pN	
213943237+574139252	-2	—	M5.0	1.8±0.7	Y	2009-MMT	Y	
213943422+573705981	0	—	M4.0	1.4±0.7	N	2009-MMT	pN	
213943450+573634560	-5	0.6	M0.0	1.6±0.3	Y	2009-MMT	Y	
213944898+573537212	-4	—	M4.0	0.8±0.7	Y	2009-MMT	Y	
213944912+570731263	Abs.	—	K0.0	2.4±0.2	N	2009-MMT	N	
213945091+571953390	-4	0.4	M3.0	1.3±0.9	pN(6,8)	2010-MMT	Y	
213945201+574912946	-11	0.3	K7.0	2.1±0.3	Y	2009-MMT	Y	
213945297+573304062	Abs.	—	K0.0	2.9±0.4	N	2009-MMT	N	
213945420+571709433	-4	—	G9.0	7.3±2.5	N	2009-MMT	N	
213945709+571855753	Abs.	—	M0.5	1.6±1.0	N	2009-MMT	X	
213945709+572624297	-17	—	M1.0	1.4±0.6	Y	2009-MMT	Y <sup>1</sup>	21-1536
21394574+5727544	Abs.	—	X	—	N	2009-SAO	N	
213945860+573051704	-227	—	K6.0	2.0±0.1	Y	2010-MMT	Y <sup>2</sup>	UXor/IR variable?
213946430+572241563	-2	N	M0.5	1.4±0.5	N	2010-MMT	N	
213946491+573223427	-8	—	M4.5	1.9±0.7	N	2010-MMT	pN	
213946931+574817809	-3	—	G8.0	7.4±2.6	N	2009-MMT	N	
213947013+574403324	-13	—	M2.0	1.9±0.9	Y	2010-MMT	Y	
213947309+571445553	Abs.	—	K0.5	7.3±1.5	N	2009-MMT	N	
213947940+572818541	Abs.	—	G9.0	3.9±0.1	N	2009-MMT	N	
21394794+5728185	Abs.	—	X	—	N	2009-SAO	N	
"	-10	—	X	—	N	2009-SAO	N	
213948050+572049544	-1	0.2	K7.0	1.7±0.5	Y	2009-MMT	Y	Var.
213948819+573344602	Abs.	—	X	—	N	2010-MMT	pN	
213948991+571941648	-1	—	M4.0	1.2±0.8	N	2009-MMT	X	
213949767+574733740	-10	0.2	M2.0	1.8±0.7	Y	2010-MMT	Y	
21394919+5727197	-3	—	K3.0	1.3±0.1	N	2009-SAO	pN	oVVI
213949231+574344716	-41	—	M4.5	2.0±1.0	N	2010-MMT	pN	
213949403+573428327	Abs.	—	G8.0	4.6±2.0	N	2009-MMT	N	
213949540+574330324	-18	—	M3.5	0.7±0.6	Y	2009-MMT	Y	
213950529+574137632	-2	0.3	M0.5	1.1±0.4	P(8)	2009-MMT	Y	
"	-3	0.2	M1.0	0.8±0.4	P(8)	2010-MMT	Y	
21395069+5726410	-12	—	M1.0:	0.0±0.8	N	2009-SAO	N	
213951030+574320313	Abs.	—	E	—	N	2010-MMT	N	
213951058+574614625	-11	—	M2.5	0.7±0.7	N	2009-MMT	N	
213951092+574119848	Abs.	—	M3.0	1.1±0.7	Y(24)	2009-MMT	P	
213951360+573052611	-1	—	M3.5	1.7±0.6	N	2009-MMT	pN	
213951957+571752279	Abs.	—	E	—	pN	2010-MMT	N	
213952060+572506212	-10	—	M2.5	2.3±1.1	Y	2010-MMT	Y	
213952472+571120191	Abs.	—	G9.0	4.1±0.1	N	2009-MMT	N	

Table A.1: Continued.

Spect. ID	H $\alpha$ EW (Å)	Li EW (Å)	Sp. Type	A $_V$ (mag)	Disk?	Campaign	Member?	Comments
213954003+573519730	-2	—	M3.5	0.8±0.8	Y	2009-MMT	P	
213954058+572933454	-30	0.3	K7.5	2.0±0.2	Y	2009-MMT	Y <sup>2</sup>	
213955033+574041533	Abs.	—	K0.5	3.1±0.3	N	2009-MMT	N	
213955699+571638273	-31	—	M0.5	1.4±0.5	Y	2009-MMT	Y <sup>2</sup>	IR variability?
213956180+572416046	-7	—	M4.0	1.3±0.9	pN	2010-MMT	P	Nobj.
213957011+572623514	Abs.	—	G9.0	2.9±0.3	N	2009-MMT	N	
213957340+574454768	Abs.	—	G9.0	3.9±0.1	N	2009-MMT	N	
213957402+574216427	Abs.	—	G9.0	2.9±0.4	P	2009-MMT	N	
213958288+573734930	0	—	M3.5	0.2±0.5	N	2009-MMT	N	
213958480+572552217	Abs.	0.2	G9.0	3.9±1.9	N	2009-MMT	X	
213959078+572643784	-10	—	M3.5	0.5±0.5	Y	2009-MMT	Y	
213959517+573257017	-1	—	M4.0	1.5±0.5	N	2009-MMT	P	
213959902+573538049	Abs.	—	K1.0	5.1±2.3	N	2009-MMT	N	
214000403+572707158	Abs.	—	M4.0	1.9±0.9	N	2009-MMT	X	
214000478+571839617	-5	—	M2.5	1.2±1.0	P	2010-MMT	Y	
214000671+574524541	-2	—	M3.5	2.1±0.8	N	2010-MMT	P	
214000801+571628495	Abs.	—	K0.0	2.8±0.1	N	2009-MMT	N	
214001762+571344963	-4	—	M3.5	0.0±0.4	N	2009-MMT	N	
214003197+573142763	-7	—	G7.0	7.1±1.4	N	2009-MMT	N	
214004008+571852210	-4	—	M2.5	3.1±1.1	N	2009-MMT	pN	
214004159+574358037	-1	—	M4.5	1.0±1.2	N	2009-MMT	P	
214004523+572836367	-33	0.5	K5.5	1.3±0.1	Y	2009-MMT	Y <sup>1, 2</sup>	21400451.5728363
214005072+573217398	Abs.	N	G8.0	3.4±1.4	P	2010-MMT	N	
214005477+573920042	Abs.	—	K0.5	3.9±0.1	N	2009-MMT	N	
214005477+572452410	Abs.	N	G5.0	5.6±1.8	N	2010-MMT	N	
214005669+574417181	-3	—	M3.5	1.5±0.8	pN	2010-MMT	P	
214006191+571230105	Abs.	—	K0.0	3.8±0.0	N	2009-MMT	N	
214006322+571126206	Abs.	—	K0.0	3.0±0.1	N	2009-MMT	N	
214006679+573224772	Abs.	—	K0.0	2.8±0.4	N	2009-MMT	N	
214007558+571937158	Abs.	—	K0.0	3.2±0.1	N	2009-MMT	N	
214008128+571559518	Abs.	N	G6.0	6.1±1.4	N	2010-MMT	N	
214008251+572631425	0	N	M0.5	3.4±0.7	pN	2010-MMT	N	
214009240+574137426	Abs.	—	K0.0	3.0±0.3	N	2009-MMT	N	
214009261+572726452	Abs.	—	K0.0	2.7±0.1	N	2009-MMT	N	
214009618+573854279	Abs.	N	G7.0	5.6±1.3	P	2010-MMT	N	
214010751+573421296	Abs.	—	M4.5	1.5±0.7	N	2009-MMT	N	
214011012+573630756	-38	0.9:	M0.0	2.0±0.8	N	2009-MMT	P	
214011348+574414105	-13	0.3	K5.5	1.9±0.3	P	2009-MMT	Y	Nobj.
214012151+573420637	-5	—	M3.5	1.8±0.7	pN	2010-MMT	P	
214012309+573833048	-11	0.6	K7.5	1.7±0.2	N	2009-MMT	Y	
214013799+572110047	Abs.	N	K1.0	6.0±2.3	N	2010-MMT	N	
214014211+574004976	-1	0.2:	M3.5	0.6±0.5	N	2010-MMT	N	
214014410+572812471	Abs.	—	M2.5	1.3±1.0	N	2009-MMT	pN	
214014458+572205514	Abs.	—	K4.5	3.5±0.9	N	2009-MMT	N	
214015317+571828850	-4	—	M3.5	3.1±0.8	N	2009-MMT	pN	
214015557+573156551	-2	—	M3.5	1.2±0.6	N	2010-MMT	P	
214016573+574043181	-5	—	M2.5	0.5±1.0	pN	2010-MMT	N	
214016690+572229753	-5	—	M3.0	0.4±0.5	N	2009-MMT	N	
"	Abs.	N	M1.0	4.0±0.8	N	2010-MMT	N	
214017542+573124718	-1	0.3	M0.5	1.5±0.2	N	2009-MMT	P	
214017899+571112253	Abs.	—	K0.0	2.8±0.1	N	2009-MMT	N	
214017933+571853789	Abs.	—	K0.0	2.7±0.0	N	2009-MMT	N	
214017981+573254298	Abs.	—	M4.0	1.2±0.6	N	2009-MMT	X	
214018462+573805760	Abs.	—	K1.0	3.2±0.3	N	2009-MMT	N	
214018111+572919447	-5	—	M3.5	1.1±0.7	pN	2010-MMT	P	
214018599+570916966	-3	0.1:	M2.0	1.1±0.8	N	2010-MMT	N	
214019073+572509288	-12	—	M2.5	2.0±1.0	Y	2010-MMT	Y	
214019162+573220460	Abs.	—	G9.0	3.4±0.4	N	2009-MMT	N	
214019849+573922857	-47	0.2	M3.5	1.3±1.0	Y	2010-MMT	Y	
214019897+574013696	Abs.	—	X	—	N	2009-MMT	N	
214020082+574253767	Abs.	—	G9.0	4.2±0.2	N	2009-MMT	N	
214020158+572711662	-14	—	M4.5	1.8±1.4	N	2009-MMT	P	
214020453+573719906	-2	—	M1.5	2.2±0.2	N	2010-MMT	pN	
214021922+572028395	-17	—	M3.5	2.6±0.9	N	2009-MMT	P	
214021922+573005424	-4	0.7	K6.0	1.6±0.3	Y	2009-MMT	Y <sup>1</sup>	21402192.5730054
214021943+572020842	Abs.	—	K0.0	2.5±0.3	N	2009-MMT	N	

Table A.1: Continued.

Spect. ID	H $\alpha$ EW (Å)	Li EW (Å)	Sp. Type	A $_V$ (mag)	Disk?	Campaign	Member?	Comments
214022472+570854169	Abs.	—	K2.0	3.8±0.1	N	2009-MMT	N	
214022698+573540109	-1	—	K0.0	2.9±0.4	N	2009-MMT	N	
214023220+572520343	Abs.	N	M1.5	0.9±0.6	N	2010-MMT	N	
214023790+571738807	-3	—	M2.5	1.5±1.1	N	2010-MMT	P	
214024017+574050899	Abs.	—	K0.0	4.4±0.1	N	2009-MMT	N	
214024168+570821128	Abs.	—	G9.0	1.5±0.3	N	2009-MMT	N	
214024209+573418261	Abs.	—	K1.5	3.0±0.4	N	2009-MMT	N	
214025369+573416284	-72	—	M2.0	1.4±0.3	Y	2009-MMT	Y <sup>2</sup>	
214025658+571327770	-1	—	M0.0	1.0±0.5	N	2009-MMT	N	
214025967+572042499	-9	—	M2.0	1.7±0.7	Y	2010-MMT	Y	
214026221+571230600	-4	—	M1.5	1.2±1.0	N	2009-MMT	N	
214026262+573402317	-4	—	M4.5	1.1±0.7	Y	2010-MMT	Y	
214027457+572600265	Abs.	—	K7.0	5.4±1.6	pN	2010-MMT	pN	
214028542+572414659	-4	—	M4.0	1.1±1.0	N	2009-MMT	P	
214029338+573905279	-3	0.2	M3.5	0.7±0.4	N	2010-MMT	pN	
214029551+572453893	-18	—	M4.0	1.0±0.9	Y	2009-MMT	Y	
214029681+572125016	Abs.	—	K0.0	3.3±0.7	N	2009-MMT	N	
214029977+573719851	Abs.	—	M0.0	2.1±0.8	N	2009-MMT	X	
214030148+573733873	-1	—	K2.5	3.2±0.3	N	2009-MMT	N	
214031700+571351555	Abs.	—	K0.0	2.9±0.1	N	2009-MMT	N	
214033472+573605378	-16	—	M1.0	2.2±0.7	Y	2009-MMT	Y	
214033691+572157206	-2	—	M1.0	1.5±0.8	P	2010-MMT	N	
214034557+572408108	Abs.	—	M1.0	0.7±0.7	N	2009-MMT	N	
214034962+572308795	Abs.	N	G7.0	2.8±0.4	Y	2010-MMT	P	early, no Li but disk?
214035332+573301755	Abs.	—	K0.0	2.9±0.4	N	2009-MMT	N	
214035490+572831395	-2	0.5	K3.0	1.7±0.7	Y	2010-MMT	Y	
214035813+573349875	Abs.	—	G5.0	5.3±1.2	N	2009-MMT	N	
214036692+572843302	Abs.	—	K2.0	5.6±2.1	N	2009-MMT	N	
214037207+572912731	-42	—	M2.5	1.1±0.4	Y	2009-MMT	Y <sup>1</sup>	21403721.5729127
"	-21	0.3	M2.0	1.3±0.5	Y	2010-MMT	Y <sup>1</sup>	21403721.5729127
214038759+572958833	-12	—	M4.0	0.7±0.5	N	2009-MMT	P	
214040558+573418755	Abs.	—	K1.0	3.5±0.4	N	2009-MMT	N	
214042281+573513316	-20	—	M4.0	1.4±0.7	Y	2010-MMT	Y	
214043833+573257141	-2	—	M4.0	0.8±0.7	N	2009-MMT	X	
214047582+571748503	Abs.	—	K1.0	2.6±0.4	N	2009-MMT	N	
214047589+571617220	0	N	K7.0	1.3±1.2	N	2009-MMT	N	
214047589+571617220	Abs.	—	M2.5:	0±1.1	N	2010-MMT	N	Low S/N, JHK error
214048489+573202607	-4	—	M4.5	1.0±0.8	P(8)	2009-MMT	P	
214048997+571705258	Abs.	—	K1.0	4.4±1.4	N	2009-MMT	N	
214049010+573049988	Abs.	—	K1.5	4.0±0.4	N	2009-MMT	N	
214049889+573549818	Abs.	—	K0.0	3.5±0.4	N	2009-MMT	N	
214050411+572155063	Abs.	—	G9.0	2.7±0.2	N	2009-MMT	N	
214052052+571438838	Abs.	—	K3.0	4.8±1.6	N	2009-MMT	N	
214053432+572046495	-9	—	K1.0	5.8±0.6	N	2009-MMT	N	
214055932+571759160	-37	0.2	K4.5	1.6±0.8	Y	2009-MMT	Y <sup>1,2</sup>	Var.?, 53-1561
214057209+572537303	-4	—	M3.0	0.1±0.9	N	2009-MMT	N	
214059633+572210994	-95	0.1:	M0.5	3.0±0.3	Y	2010-MMT	Y	oVVI
214100402+571927517	Abs.	N	G8.0	6.5±1.6	N	2010-MMT	N	
214105277+572627181	Abs.	—	K0.0	2.6±0.7	N	2009-MMT	N	
214106609+572653727	Abs.	—	K1.5	7.0±1.5	N	2010-MMT	N	
214108113+571705903	Abs.	—	K1.0	2.5±0.5	N	2009-MMT	N	
214108552+571847609	Abs.	—	K0.0	2.3±0.6	N	2009-MMT	N	
214110880+572132445	Abs.	—	K5.0	3.4±0.5	N	2009-MMT	N	
214110901+572642342	Abs.	—	K0.0	3.5±0.8	N	2009-MMT	N	
214111182+572611910	Abs.	—	M2.0	4.3±0.8	N	2009-MMT	N	
214111217+572205926	Abs.	—	G9.0	3.6±0.7	N	2009-MMT	N	
214113022+573051128	Abs.	—	G9.0	7.4±1.4	N	2009-MMT	N	
214113661+572449609	Abs.	—	K1.0	6.7±2.0	pN	2010-MMT	N	
214116188+572007480	Abs.	—	K2.5	3.4±0.8	N	2009-MMT	N	
214116538+572548550	Abs.	N	K2.0	5.2±0.6	pN	2010-MMT	N	
214123089+573108225	Abs.	N	K5.0	5.3±2.2	N	2010-MMT	N	
214123913+572613943	-11	—	M3.5	0.1±1.0	N	2009-MMT	N	
214124709+572444280	Abs.	N	K1.0	3.4±0.5	N	2010-MMT	N	
"	Abs.	N	K1.0	6.1±0.6	N	2010-MMT	N	
214126268+572838207	-8	—	G9.0	6.9±1.7	N	2009-MMT	N	
214128527+572716180	Abs.	—	K1.0	2.7±0.7	N	2009-MMT	N	

Table A.1: Continued.

Spect. ID	H $\alpha$ EW ( $\text{\AA}$ )	Li EW ( $\text{\AA}$ )	Sp. Type	A $_V$ (mag)	Disk?	Campaign	Member?	Comments
214129907+572813680	Abs.	N	G5.0	4.4 $\pm$ 0.4	N	2010-MMT	N	
214131981+572909930	Abs.	—	K0.0	3.4 $\pm$ 0.8	N	2009-MMT	N	
214135352+572445970	-1	—	M3.5	4.6 $\pm$ 1.1	N	2009-MMT	N	
214136739+572835955	Abs.	—	K1.0	2.9 $\pm$ 0.7	N	2009-MMT	N	
214136863+572220895	Abs.	—	K2.5	3.1 $\pm$ 0.9	N	2009-MMT	N	
214137721+572410813	0	—	K2.0	2.4 $\pm$ 0.7	N	2009-MMT	N	
214138291+572337085	-83	—	M2.5	1.1 $\pm$ 1.5	Y	2009-MMT	Y <sup>2</sup>	
214147108+572022751	Abs.	—	K1.0	2.8 $\pm$ 0.7	N	2009-MMT	N	
214148062+572609205	-17	—	M2.5	1.9 $\pm$ 1.6	P(8)	2010-MMT	P	
214148412+572659028	Abs.	—	K0.0	5.6 $\pm$ 1.6	N	2009-MMT	N	
214201218+572345558	-1	—	K7.5	1.6 $\pm$ 1.7	N	2009-MMT	pN	oVV1
214202111+572427911	Abs.	—	K0.0	3.1 $\pm$ 0.5	N	2009-MMT	N	

Table A.2: Optical and 2MASS data for confirmed members and probable members. <sup>a</sup> Anomalous optical colors. <sup>b</sup>Near HD206267. <sup>c</sup>Near 21-840, likely contaminated. <sup>d</sup> Near bright star, probably contaminated.

Spect. ID	V (mag)	R <sub>J</sub> (mag)	I <sub>J</sub> (mag)	2MASS ID	J (mag)	H (mag)	K (mag)
213542993+573337049	19.476±0.011	17.613±0.030	15.506±0.002	21354299+5733370	14.302±0.037	13.439±0.033	13.075±0.036
213607980+572637096	—	—	—	21360798+5726371	18.366:	17.484:	14.507±0.088
213618699+573626870	19.516±0.011	17.693±0.030	15.870±0.003	21361870+5736268	14.707±0.046	13.911±0.056	13.600:
213619969+573527805	21.154±0.036	19.230±0.032	16.871±0.004	21361996+5735278	15.721±0.065	15.084±0.089	14.724±0.089
213622159+572327898	19.269±0.013	17.468±0.023	15.416±0.002	21362216+5723278	14.263±0.044	13.496±0.050	13.173±0.039
213622379+573141225	21.277±0.039	19.006±0.031	16.251±0.003	21362238+5731412	14.567±0.036	13.792±0.033	13.404±0.037
213625078+572750265	20.435±0.020	18.558±0.024	16.399±0.004	21362507+5727502	14.952±0.044	14.031±0.048	13.518±0.040
213626897+573304351	20.963±0.035	18.868±0.031	16.709±0.004	21362690+5733043	15.217±0.055	14.158:	13.869:
213633647+573517477	15.826±0.002	14.359±0.030	13.236±0.003	21363365+5735174	12.242±0.024	11.458±0.028	11.254±0.023
213636909+573132683	19.424±0.011	17.422±0.030	15.828±0.003	21363691+5731326	13.754±0.031	12.631±0.037	12.021±0.026
213639147+572953326	18.040±0.007	16.171±0.022	14.129±0.002	21363915+5729533	11.924±0.021	10.422±0.028	9.392±0.021
213641152+573702713	20.024±0.014	18.192±0.030	16.175±0.003	21364115+5737027	14.880±0.044	14.132±0.052	13.866±0.056
213641358+572204113	20.596±0.021	18.769±0.024	16.515±0.004	21364135+5722041	15.220±0.067	14.613±0.076	14.053±0.059
213642470+572523186	19.997±0.016	18.137±0.023	15.958±0.004	21364247+5725231	14.806±0.043	14.089±0.047	13.758±0.049
213648190+573402084	19.159±0.011	17.403±0.030	15.819±0.003	21364819+5734020	14.796±0.043	13.989±0.053	13.785±0.047
213653210+572052112	20.084±0.016	18.404±0.023	16.521±0.004	21365320+5720521	15.459±0.056	14.806±0.064	14.437±0.073
213655201+573030103	21.367±0.046	19.216±0.032	17.013±0.005	21365520+5730301	14.714±0.078	12.665±0.063	11.382±0.034
213655283+572551668	17.220±0.004	15.757±0.022	14.678±0.002	21365527+5725516	13.592±0.030	12.812:	12.613:
213658737+573848181	19.123±0.010	17.391±0.030	15.381±0.002	21365874+5738481	14.140±0.029	13.342±0.037	12.968±0.032
213659108+573905636	17.490±0.004	16.107±0.005	14.660±0.002	21365911+5739056	13.573±0.024	12.650±0.029	12.263±0.026
213659472+573134908	19.956±0.015	18.215±0.017	16.104±0.003	21365947+5731349	14.520±0.034	13.403±0.038	12.765±0.028
213701319+573418289	19.441±0.010	17.857±0.013	15.870±0.003	21370132+5734182	14.721±0.036	13.756±0.034	13.370±0.039
213701401+572445873	19.152±0.014	17.160±0.023	14.429±0.002	21370140+5724458	13.305±0.040	12.459±0.055	12.206±0.055
213702321+573115201	—	—	—	21370232+5731152	16.946:	15.588:	13.254±0.045
213703207+572718405	18.705±0.010	17.095±0.022	15.581±0.003	21370320+5727184	14.414±0.035	13.692±0.044	13.362±0.042
213704539+573223646	21.500±0.053	19.411±0.034	16.972±0.006	21370454+5732236	15.495±0.062	14.588±0.073	14.351±0.091
213707711+573211012	20.218±0.017	18.530±0.021	16.002±0.003	21370771+5732110	14.606±0.035	13.785±0.039	13.522±0.047
213708137+573616213	20.489±0.020	18.546±0.021	16.058±0.003	21370814+5736162	14.576±0.038	13.654±0.038	13.268±0.036
213708281+573023538	19.975±0.016	18.008±0.015	15.580±0.004	21370828+5730235	14.036±0.034	13.263±0.029	12.896±0.029
213708783+572322501	15.399±0.009	14.041±0.012	12.978±0.002	21370878+5723225	12.042±0.023	11.256±0.028	11.064±0.020
213708879+572107012	19.933±0.014	18.258±0.015	16.144±0.006	21370888+5721070	14.671±0.040	13.817±0.051	13.443±0.048
213709442+573036722	19.299±0.011	17.541±0.013	15.383±0.004	21370944+5730367	13.884±0.030	13.036±0.034	12.648±0.033
213710877+573846877	21.755±0.062	19.651±0.033	17.158±0.005	21371088+5738468	15.754±0.092	14.952:	14.647:
213712353+573331789	16.260±0.004	14.965±0.004	13.549±0.003	21371234+5733317	12.570±0.029	11.773±0.032	11.567±0.026
213712580+574055032	21.462±0.040	19.503±0.032	17.278±0.005	21371257+5740550	15.887±0.094	15.268±0.114	14.952±0.144
213716349+572640200	—	—	—	21371635+5726402	14.103±0.027	12.953±0.032	12.315±0.025
213720641+572100571	19.017±0.010	17.498±0.013	15.789±0.004	21372064+5721005	14.763±0.046	14.019±0.046	13.723±0.063
213724102+572411541	18.369±0.010	16.794±0.013	15.347±0.005	21372410+5724115	14.198±0.066	13.293±0.077	12.821±0.047
21372447+5731359	21.028±0.045	19.166±0.043	16.357±0.007	21372447+5731359	14.543±0.032	13.790±0.046	13.278±0.038
213725743+571257077	20.385±0.024	18.345±0.034	16.383±0.011	21372574+5712570	15.292±0.064	14.638±0.093	14.375±0.095
213726148+572330562	21.582±0.048	19.634±0.021	17.292±0.015	21372615+5723305	16.070±0.099	15.343±0.140	14.786±0.136
213726272+571258793	18.626±0.007	17.010±0.020	15.411±0.006	21372627+5712587	14.479±0.053	13.653±0.058	13.415±0.056
21372643+5731386	17.512±0.004	16.161±0.012	15.059±0.005	21372643+5731386	13.882±0.029	13.108±0.037	12.942±0.033



Table A.2: Continued.

Spect. ID	V (mag)	R <sub>J</sub> (mag)	I <sub>J</sub> (mag)	2MASS ID	J (mag)	H (mag)	K (mag)
21372685+5732069	16.596±0.003	15.583±0.011	14.792±0.003	21372685+5732069	14.256±0.032	13.794±0.043	13.684±0.052
213727418+573123620	19.091±0.008	17.445±0.010	15.587±0.004	21372742+5731236	14.375±0.037	13.338±0.040	12.978±0.033
213732341+572503204	17.155±0.009	—	15.232±0.004	21373234+5725032	14.131±0.052	13.371±0.055	12.868:
213733557+573550931	20.341±0.024	18.594±0.023	16.665±0.008	21373355+5735509	15.388±0.062	14.610±0.066	14.356±0.112
213734113+573431198	19.777±0.013	18.148±0.016	16.172±0.005	21373411+5734311	15.002±0.041	13.984±0.043	13.487±0.045
213734649+571657705	—	—	—	21373465+5716577	14.755±0.043	13.770±0.048	13.356±0.045
213735713+573258349	20.135±0.021	18.437±0.027	16.274±0.008	21373571+5732583	14.861±0.044	14.018±0.049	13.616±0.063
213738830+572936901	—	—	—	21373883+5729369	13.119±0.025	12.144±0.028	11.611±0.023
213740217+571903718	20.969±0.028	19.273±0.019	16.736±0.009	21374021+5719037	15.258±0.059	14.581±0.075	14.346±0.091
213740471+573433203	20.556±0.028	18.674±0.025	16.346±0.006	21374047+5734332	14.987±0.049	14.088±0.057	13.771±0.065
213742167+573431486	20.493±0.027	18.786±0.027	16.769±0.009	21374216+5734314	15.466±0.059	14.511±0.057	14.050±0.062
213742758+573325074	17.485±0.004	16.287±0.014	15.128±0.004	21374275+5733250	12.561±0.023	11.308±0.026	10.388±0.021
21374388+5734521	21.723±0.084	19.853±0.079	17.006±0.012	21374388+5734521	15.294±0.061	14.633±0.064	14.238±0.092
213744131+573331130	19.114±0.011	17.363±0.011	15.404±0.004	21374412+5733311	14.210±0.042	13.317±0.045	12.836:
213744543+572200213	21.802±0.051	19.928±0.024	17.312±0.015	21374453+5722002	15.942±0.095	15.346±0.130	15.056±0.184
213945091+571953390	20.361±0.014	18.597±0.008	16.383±0.004	21394508+5719533	15.264±0.043	14.560±0.057	14.414±0.090
213745147+571942390	17.571±0.009	16.121±0.012	14.818±0.003	21374514+5719423	13.903±0.025	12.971±0.033	12.582±0.026
213746871+573156208	20.814±0.039	18.774±0.031	16.445±0.008	21374687+5731562	14.850±0.050	13.953±0.040	13.635±0.049
213747963+573242323	18.975±0.009	17.352±0.010	15.500±0.004	21374795+5732423	14.154±0.043	13.141±0.033	12.767±0.035
213748237+572319411	19.722±0.012	18.037±0.014	16.017±0.015	21374824+5723194	14.725±0.048	13.918±0.055	13.618±0.053
213748931+572320963	18.885±0.010	17.296±0.013	15.714±0.015	21374893+5723209	14.657±0.055	13.682±0.063	13.252±0.049
213749260+573158309	20.182±0.023	18.414±0.022	16.367±0.007	21374926+5731583	15.185±0.048	14.394±0.065	14.153±0.072
213750222+573009586	19.843±0.029	17.746±0.012	15.936±0.006	21375022+5730095	14.639±0.047	13.775±0.049	13.384±0.043
213750297+570909399	19.775±0.013	17.951±0.023	15.982±0.006	21375029+5709093	14.950±0.043	14.034±0.037	13.568±0.041
213751197+574656428	21.460±0.042	19.324±0.019	17.044±0.006	21375119+5746564	15.869±0.094	14.965±0.083	14.658±0.101
213751210+572436151	20.962±0.027	19.089±0.017	16.883±0.011	21375121+5724361	15.481±0.073	14.680±0.096	14.238±0.066
213756779+573448171	20.740±0.033	19.066±0.047	16.858±0.014	21375677+5734481	15.599±0.080	14.798±0.085	14.492±0.091
213803453+570512396	19.017±0.010	16.958±0.020	15.563±0.006	21380344+5705123	14.817±0.088	13.988±0.120	13.874±0.100
213804820+570754472	20.165±0.020	18.410±0.030	16.427±0.009	21380482+5707544	15.360±0.067	14.919±0.085	14.394±0.086
213809221+572038118	21.362±0.036	19.499±0.019	17.114±0.016	21380922+5720381	15.939±0.088	15.139±0.095	14.732±0.099
213809997+572352782	19.967±0.017	17.957±0.014	16.095±0.015	21381000+5723527	14.869±0.067	14.091±0.061	13.704±0.065
213810182+572708407	20.076±0.018	18.387±0.017	16.431±0.009	21381018+5727084	15.048±0.078	13.826:	13.633:
213810759+574013683	20.516±0.029	18.769±0.036	16.860±0.013	21381075+5740136	15.569±0.067	14.938±0.088	14.661±0.103
213812023+572500774	19.195±0.021	17.517±0.013	15.862±0.015	21381202+5725007	14.527±0.047	13.582±0.045	13.316±0.048
213812641+572033696	18.866±0.010	17.225±0.013	15.611±0.004	21381264+5720336	14.527±0.051	13.639±0.038	13.174±0.033
213816129+571935798	18.567±0.009	16.922±0.012	15.120±0.003	21381612+5719357	13.991±0.032	13.092±0.032	12.792±0.030
213816170+574104645	16.547±0.003	15.199±0.004	13.776±0.002	21381617+5741046	12.907±0.026	12.123±0.033	11.804±0.021
213819411+572203907	21.469±0.052	19.412±0.026	17.097±0.013	21381941+5722039	15.863±0.102	15.084±0.130	14.868±0.131
213819507+572044119	21.038±0.032	19.142±0.019	16.865±0.011	21381951+5720441	15.562±0.069	14.846±0.084	14.528±0.096
213822810+574017294	19.953±0.016	18.205±0.020	16.119±0.006	21382281+5740172	14.826±0.036	13.778±0.043	13.349±0.030
213823950+572736175	19.525±0.011	17.872±0.014	16.104±0.006	21382395+5727361	14.931±0.063	14.033±0.050	13.597±0.056
213824142+574451513	18.063±0.011	16.322±0.009	15.158±0.003	21382414+5744515	14.007±0.030	13.261±0.036	12.956±0.026
213825831+574207487	16.939±0.006	15.046±0.004	13.953±0.004	21382583+5742074	11.982±0.038	11.197±0.043	10.953±0.032
213827431+572720767	17.019±0.009	15.545±0.012	14.097±0.015	21382743+5727207	12.856±0.030	11.986±0.035	11.506±0.024

Table A.2: Continued.

Spect. ID	V (mag)	R <sub>J</sub> (mag)	I <sub>J</sub> (mag)	2MASS ID	J (mag)	H (mag)	K (mag)
213828028+574736432	20.127±0.015	18.469±0.014	16.498±0.004	21382803+5747364	15.454±0.071	14.640±0.067	14.270±0.074
213829367+573726567	21.059±0.046	19.251±0.068	16.940±0.013	21382936+5737265	15.497±0.073	14.768±0.088	14.389±0.097
213830308+573255218	19.912±0.017	18.244±0.021	16.226±0.006	21383031+5732552	14.962±0.048	14.091±0.052	13.608±0.043
213830349+572618227	18.857±0.010	17.286±0.013	15.597±0.015	21383035+5726182	14.827±0.050	13.864±0.049	13.455±0.038
213832169+572635943	19.911±0.015	18.202±0.016	16.306±0.015	21383216+5726359	14.811±0.045	13.860±0.044	13.175±0.034
213835211+573013582	17.922±0.004	16.309±0.006	14.667±0.004	21383520+5730135	13.072:	12.918±0.037	12.637±0.071
213837298+573103776	18.800±0.007	17.284±0.010	15.457±0.004	21383730+5731037	14.286±0.034	13.506±0.036	13.161±0.039
213839571+572916412	21.762±0.535: <sup>b</sup>	19.124±0.029	16.770±0.024	21383956+5729164	15.219±0.067	14.319±0.057	14.153±0.068
213839749+572753080	20.859±0.030	18.921±0.018	16.587±0.010	21383975+5727530	14.151±0.051	13.319±0.048	13.038±0.044
213842249+573533902	19.845±0.015	18.083±0.018	15.937±0.005	21384224+5735339	14.660±0.039	13.865±0.047	13.570±0.040
213844343+573626211	19.633±0.013	18.075±0.020	16.290±0.009	21384434+5736262	14.927±0.050	14.193±0.061	13.833±0.070
213847282+573114405	19.503±0.012	17.870±0.019	15.784±0.007	21384727+5731144	14.524±0.047	13.769±0.046	13.282±0.039
213854760+572450268	17.781±0.007	16.193±0.006	14.568±0.003	21385476+5724502	13.043:	12.545±0.048	12.237±0.034
213859147+572045273	20.600±0.017	18.921±0.008	16.841±0.005	21385915+5720452	15.543±0.075	15.134±0.107	15.000±0.151
213859738+572216816	21.200±0.028	19.311±0.011	16.850±0.005	21385973+5722168	15.587±0.078	14.799±0.082	14.335±0.084
213900397+575004884	20.865±0.025	19.008±0.025	16.720±0.004	21390040+5750048	15.470±0.070	14.605±0.076	14.297±0.086
213903212+571555316	18.384±0.007	16.875±0.006	15.326±0.003	21390320+5715553	14.283±0.029	13.499±0.041	13.178±0.033
213905519+572349596	16.762±0.007	15.353±0.006	14.116±0.003	21390552+5723496	13.190±0.026	12.453±0.031	12.225±0.026
213909728+571803046	20.644±0.017	18.900±0.008	16.767±0.004	21390973+5718030	15.792±0.084	14.889±0.085	14.657±0.105
213910429+572235727	20.798±0.019	18.927±0.009	16.537±0.004	21391042+5722357	15.253±0.065:	14.360±0.063:	13.902±0.066: <sup>c</sup>
213911452+572425205	20.317±0.014	18.490±0.008	16.455±0.004	21391145+5724252	15.612±0.094	14.476±0.087	13.749±0.057
213914453+572304758	19.831±0.011	17.984±0.007	15.771±0.004	21391444+5723047	14.462±0.043	13.657±0.042	13.233:
213914837+573756779	20.487±0.033	18.538±0.039	16.308±0.008	21391483+5737567	14.973±0.052	14.213±0.083	13.860±0.068
213914988+574050473	20.952±0.041	18.294±0.036	16.546±0.009	21391498+5740504	15.045±0.053	14.267±0.065	13.836±0.061
213915002+575023465	20.978±0.027	19.006±0.027	16.624±0.004	21391500+5750234	15.272±0.070	14.486±0.074	14.189±0.080
213917062+571643244	20.128±0.011	18.434±0.007	16.312±0.004	21391705+5716432	15.190±0.056	14.503±0.078	14.191±0.064
213917371+571605286	20.628±0.017	18.941±0.008	16.737±0.004	21391737+5716052	15.637±0.080	14.842±0.092	14.462±0.093
213917481+571747432	18.369±0.008	16.914±0.011	15.119±0.003	21391748+5717474	13.774±0.047	13.013±0.046	12.799±0.044
213918291+572818473	19.450±0.017	17.804±0.007	16.043±0.004	21391828+5728184	14.858±0.077	14.052±0.083	13.721±0.068
213918339+574022609	20.295±0.022	18.522±0.037	16.492±0.008	21391834+5740226	15.225±0.061	14.538±0.063	14.235±0.100
213920172+575015967	20.327±0.019	18.604±0.021	16.606±0.004	21392016+5750159	15.625±0.073	15.000±0.088	14.777±0.121
21392059+5726269	21.506±0.037	19.645±0.033	17.146±0.013	21392059+5726269	15.573±0.088	14.883±0.105	14.527±0.098
213920831+571631187	21.279±0.030	19.539±0.026	16.978±0.005	21392082+5716311	15.603±0.079	15.160±0.104	14.814±0.125
21392151+5728398	20.290±0.032	18.846±0.040	18.107±0.021	21392151+5728398	15.297:	15.496±0.155	14.984±0.162
213924388+572820999	19.157±0.008	17.484±0.012	15.745±0.004	21392438+5728210	14.511±0.053	13.607±0.052	13.308±0.048
213924711+571912672	21.793±0.055	19.737±0.022	17.093±0.008	21392471+5719126	15.757±0.099	14.941±0.107	14.655±0.108
21392564+5728183	19.084±0.008	17.479±0.006	16.141±0.004	21392564+5728183	15.258±0.061	14.437±0.061	14.181±0.070
213926421+572538470	21.826±0.045	19.771±0.014	17.408±0.007	21392641+5725384	15.665±0.073	14.536±0.077	13.781±0.058
21392806+5728420	20.978±0.061: <sup>d</sup>	19.358±0.041: <sup>d</sup>	17.002±0.017: <sup>d</sup>	21392806+5728420	15.230±0.113: <sup>d</sup>	14.584±0.107: <sup>d</sup>	14.111±0.095: <sup>d</sup>
213928151+572521181	18.930±0.008	17.276±0.011	15.751±0.008	21392815+5725211	14.454±0.041	13.553±0.038	13.253±0.037
213928742+573930163	21.950±0.095	19.790±0.043	17.143±0.013	21392873+5739301	15.705±0.073	15.173±0.112	14.677±0.107
213928968+574347037	18.936±0.014	17.369±0.018	15.446±0.004	21392897+5743470	14.462±0.061	13.502±0.055	13.361±0.061
213929250+572530299	20.034±0.011	—	—	21392925+5725303	14.921±0.054	13.970±0.056	13.437±0.040
213929408+570630605	18.930±0.009	17.352±0.007	15.688±0.007	21392941+5706306	14.502±0.033	13.725±0.038	13.326±0.033

Table A.2: Continued.

Spect. ID	V (mag)	R <sub>J</sub> (mag)	I <sub>J</sub> (mag)	2MASS ID	J (mag)	H (mag)	K (mag)
213929648+574809597	21.984±0.064	19.971±0.033	17.526±0.008	21392964+5748095	16.118±0.115	15.338±0.124	15.262±0.182
213930129+572651433	18.435±0.007	16.681±0.006	14.926±0.003	21393012+5726514	13.783±0.028	12.839±0.032	12.509±0.028
21393069+5728116	19.458±0.009	18.111±0.013	17.051±0.006	21393069+5728116	16.110±0.098	15.930±0.198	15.357±0.214
213930870+572227446	19.014±0.008	17.366±0.006	15.722±0.004	21393086+5722274	14.469±0.045	13.533±0.046	12.861±0.033
21393179+5728291	18.150±0.007	16.424±0.006	14.715±0.003	21393179+5728291	13.606±0.039	12.770±0.042	12.414±0.033
213933219+573300533	21.342±0.049	19.321±0.040	16.928±0.009	21393321+5733005	15.577±0.058	14.750±0.070	14.281±0.081
21393301+5728175	19.982±0.011	18.111±0.007	15.926±0.004	21393301+5728175	14.588±0.044	13.911±0.055	13.452±0.051
213934908+571703418	20.639±0.018	18.929±0.009	16.831±0.005	21393491+5717034	15.735±0.092	14.919±0.095	14.812±0.134
213935018+573353693	20.635±0.045	18.784±0.040	16.652±0.010	21393502+5733536	15.309±0.084	14.599±0.101	14.404±0.101
213935162+572053128	20.848±0.019	18.985±0.009	16.662±0.004	21393516+5720531	15.453±0.050	14.620±0.070	13.994±0.061
21393648+5728119	16.701±0.007	15.508±0.011	14.634±0.003	21393648+5728119	13.977±0.041	13.396±0.050	13.172±0.045
213937132+572459030	20.017±0.011	18.283±0.007	16.271±0.004	21393713+5724590	15.163±0.050	14.417±0.066	13.866±0.062
213937448+574607113	20.760±0.024	18.753±0.023	16.162±0.004	21393744+5746071	14.736±0.036	13.986±0.036	13.566±0.051
213938162+572301696	20.804±0.020	18.885±0.008	16.369±0.004	21393816+5723016	15.006±0.058	14.215±0.068	13.834±0.063
213938169+573218304	19.875±0.018	18.127±0.035	16.206±0.006	21393817+5732183	15.063±0.050	14.274±0.053	14.106±0.065
21393819+5727319	20.430±0.015	18.421±0.014	15.769±0.003	21393819+5727319	14.331±0.026	13.628±0.042	13.166±0.034
21394010+5730113	19.814±0.018	—	—	21394010+5730113	14.906±0.041	14.114±0.054	13.768±0.056
213940600+572108797	21.430±0.032	19.425±0.012	16.922±0.005	21394059+5721087	15.680±0.065	14.839±0.063	14.571±0.102
213940710+572206160	19.248±0.009	17.649±0.006	16.025±0.004	21394070+5722061	15.231±0.070	14.474±0.079	14.341±0.090
213941211+573749556	21.838±0.081	19.667±0.042	17.196±0.013	21394120+5737495	16.050±0.083	15.303±0.118	14.791±0.115
213942227+571701866	18.129±0.007	16.604±0.006	15.130±0.003	21394222+5717018	14.195±0.037	13.368±0.045	13.145±0.040
213942289+572902679	21.324±0.035	19.427±0.013	17.049±0.006	21394229+5729026	15.558±0.081	14.887±0.082	14.555±0.122
213942378+573348653	21.376±0.060	19.444±0.041	17.176±0.014	21394237+5733486	15.830±0.079	15.102±0.101	14.761±0.119
213942399+573431184	21.277±0.056	19.227±0.041	16.959±0.011	21394240+5734311	15.695±0.063	14.832±0.083	14.681±0.116
213943237+574139252	21.104±0.051	18.971±0.040	16.445±0.008	21394324+5741392	15.094±0.062	14.271±0.085	13.980±0.073
213943450+573634560	18.518±0.013	16.903±0.032	15.394±0.004	21394345+5736345	14.472±0.039	13.601±0.044	13.271±0.030
213944898+573537212	19.517±0.016	17.730±0.034	15.656±0.004	21394489+5735372	14.425±0.054	13.666±0.037	13.400±0.056
213945091+571953390	20.361±0.014	18.597±0.008	16.383±0.004	21394508+5719533	15.264±0.043	14.560±0.057	14.414±0.090
213945201+574912946	18.260±0.012	16.627±0.017	15.128±0.003	21394519+5749129	14.037±0.032	13.120±0.042	12.887±0.037
213945709+572624297	19.026±0.008	17.380±0.006	15.620±0.003	21394570+5726242	14.561±0.040	13.756±0.044	13.224±0.042
213945860+573051704	18.846±0.013	17.307±0.033	16.011±0.006	21394586+5730517	14.906±0.043	13.890±0.043	13.147±0.035
213947013+574403324	21.006±0.029	19.181±0.029	17.003±0.005	21394701+5744033	15.594±0.075	14.821±0.076	14.429±0.087
213948050+572049544	18.489±0.007	17.004±0.011	15.502±0.003	21394805+5720495	15.405±0.060	14.367±0.049	13.765±0.047
213949767+574733740	19.980±0.016	18.147±0.019	16.064±0.004	21394977+5747337	15.021±0.053	14.058±0.050	13.670±0.053
21394919+5727197	16.727±0.007	15.543±0.006	14.734±0.003	21394919+5727197	14.207±0.036	13.698±0.043	13.553±0.050
213949540+574330324	19.570±0.016	17.850±0.019	15.900±0.005	21394954+5743303	14.657±0.038	13.719±0.039	13.460±0.032
213950529+574137632	18.615±0.013	17.082±0.033	15.571±0.005	21395052+5741376	14.560±0.053	13.813±0.050	13.488±0.050
213951092+574119848	19.591±0.016	17.830±0.034	15.825±0.005	21395109+5741198	14.841±0.053	13.992±0.060	13.433±0.051
213952060+572506212	21.365±0.032	19.435±0.012	16.943±0.005	21395205+5725062	15.605±0.073	14.882±0.087	14.589±0.114
213954003+573519730	19.959±0.018	18.242±0.035	16.185±0.006	21395400+5735197	15.072±0.049	14.243±0.052	13.840±0.056
213954058+572933454	18.891±0.008	17.234±0.006	15.727±0.004	21395406+5729334	14.725±0.043	13.870±0.042	13.283±0.048
213955699+571638273	19.060±0.013	17.460±0.006	15.834±0.004	21395569+5716382	14.780±0.050	13.945±0.052	13.726±0.055
213956180+572416046	20.840±0.021	18.975±0.009	16.656±0.004	21395617+5724160	15.402±0.070	14.538±0.086	14.379±0.112
213959078+572643784	19.287±0.009	17.595±0.006	15.770±0.003	21395908+5726437	14.804±0.040	13.948±0.049	13.615±0.052

Table A.2: Continued.

Spect. ID	V (mag)	R <sub>J</sub> (mag)	I <sub>J</sub> (mag)	2MASS ID	J (mag)	H (mag)	K (mag)
213959517+573257017	20.911±0.038	18.926±0.040	16.752±0.009	21395951+5732570	15.293±0.075	14.820±0.225	14.432±0.095
214000478+571839617	20.133±0.012	18.453±0.007	16.303±0.004	21400047+5718396	15.261±0.058	14.701±0.085	14.355±0.102
214000671+574524541	21.188±0.033	19.148±0.029	16.755±0.005	21400066+5745245	15.397±0.050	14.649±0.069	14.430±0.087
214004008+571852210	20.549±0.016	18.023±0.007	16.535±0.004	21400400+5718522	15.834±0.089	15.099±0.093	14.904±0.141
214004159+574358037	20.794±0.025	19.009±0.026	16.532±0.004	21400415+5743580	15.214±0.048	14.398±0.051	14.250±0.086
214004523+572836367	16.304±0.007	14.982±0.011	13.893±0.003	21400451+5728363	13.011±0.032	12.210±0.036	11.810±0.029
214005669+574417181	20.957±0.026	19.085±0.029	16.830±0.005	21400566+5744171	15.608±0.070	14.809±0.071	14.402±0.085
214011012+573630756	19.445±0.033	17.813±0.034	15.957±0.005	21401100+5736307	14.866±0.047	14.005±0.053	13.877±0.067
214011348+574414105	17.699±0.010	16.247±0.017	14.929±0.004	21401134+5744141	13.155:	12.683±0.051	12.110:
214012151+573420637	20.995±0.040	19.019±0.039	16.747±0.009	21401214+5734206	15.578±0.059	14.707±0.083	14.473±0.089
214012309+573833048	18.302±0.012	16.690±0.032	15.289±0.004	21401231+5738330	14.311±0.034	13.353±0.033	12.994±0.032
214015557+573156551	20.242±0.021	18.401±0.035	16.327±0.007	21401555+5731565	15.096±0.039	14.425±0.061	14.125±0.071
214017542+573124718	18.677±0.013	17.006±0.032	15.512±0.004	21401754+5731247	14.348±0.030	13.672±0.044	13.319±0.043
214018111+572919447	20.261±0.013	18.480±0.007	16.380±0.004	21401811+5729194	15.114±0.058	14.393±0.064	13.932±0.060
214019073+572509288	20.926±0.023	19.059±0.011	16.747±0.005	21401907+5725092	15.444±0.066	14.585±0.063	14.497±0.096
214019849+573922857	20.274±0.022	18.486±0.036	16.198±0.006	21401984+5739228	14.814±0.032	14.038±0.048	13.722±0.050
214020158+572711662	21.836±0.047	19.878±0.016	17.075±0.006	21402015+5727116	15.618±0.072	15.035±0.098	14.604±0.106
214021922+572028395	21.615±0.040	19.463±0.014	16.846±0.005	21402192+5720283	15.721±0.249	14.911±0.086	14.442±0.095
214021922+573005424	16.984±0.012	15.446±0.032	14.485±0.004	21402192+5730054	13.608±0.039	12.754±0.038	12.538±0.032
214023790+571738807	21.062±0.023	19.330±0.011	17.044±0.005	21402379+5717388	15.677±0.070	15.181±0.093	14.723±0.112
214025369+573416284	19.578±0.017	17.782±0.034	16.077±0.006	21402536+5734162	14.905±0.032	14.028±0.044	13.608±0.049
214025967+572042499	20.569±0.017	18.760±0.008	16.723±0.005	21402597+5720425	15.434±0.054	14.708±0.067	14.407±0.101
214026262+573402317	20.189±0.023	1.292±0.036	16.072±0.006	21402625+5734023	14.886±0.045	14.031±0.047	13.923±0.067
214028542+572414659	21.206±0.028	19.405±0.012	17.103±0.013	21402854+5724146	15.817±0.095	14.925±0.093	14.652±0.117
214029551+572453893	20.586±0.017	18.801±0.008	16.528±0.004	21402955+5724538	15.315±0.060	14.540±0.064	14.272±0.079
214033472+573605378	20.048±0.021	18.233±0.035	16.208±0.007	21403347+5736053	15.062±0.051	14.159±0.070	13.628±0.056
214033691+572157206	20.196±0.012	18.561±0.008	16.635±0.004	21403369+5721572	15.496±0.066	14.842±0.086	14.397±0.089
214034962+572308795	15.579±0.007	14.231±0.006	13.329±0.007	21403496+5723088	12.135±0.047	11.297±0.047	11.086±0.051
214035490+572831395	—	—	—	21403549+5728314	12.479±0.027	11.739±0.032	11.554±0.023
214037207+572912731	19.472±0.015	17.721±0.007	15.914±0.005	21403721+5729127	14.640±0.053	13.815±0.053	13.512±0.061
214038759+572958833	19.850±0.017	18.066±0.034	16.109±0.006	21403876+5729588	14.973±0.061	14.007±0.056	13.850±0.068
214042281+573513316	21.014±0.039	19.092±0.039	16.869±0.010	21404228+5735133	15.647±0.073	14.734±0.080	14.427±0.094
214048489+573202607	20.620±0.027	18.747±0.039	16.465±0.008	21404848+5732026	15.046±0.043	14.375±0.054	14.135±0.076
214055932+571759160	17.453±0.004	16.248±0.009	14.781±0.004	21405592+5717591	13.814±0.027	12.830±0.035	12.245±0.024
214059633+572210994	20.344±0.025	18.195±0.012	16.557±0.009	21405963+5722110	14.897±0.062	13.973±0.055	13.195:
214138291+572337085	19.679±0.020	18.121±0.025	15.759±0.005	21413828+5723370	14.520±0.030	13.703±0.037	13.325±0.032
214148062+572609205	21.332±0.037	19.578±0.027	16.944±0.009	21414806+5726092	15.641±0.062	14.938±0.081	14.522±0.086
214201218+572345558	17.833±0.004	16.531±0.009	14.312±0.003	21420121+5723455	13.434±0.032	12.864±0.036	12.602±0.035

Table A.3: Spitzer IRAC and MIPS data for confirmed members and probable members. Under 'SED' we specify the SED type (ND = no disk; ClassI= Class I object; Full= typical full disk; TD = transition disk; PTD = pre-transition disk; Dep.= dust-depleted disk; Unc. = Uncertain SED type). Objects listed as "marginal detection" at  $24\mu\text{m}$  have probably excesses but their photometry is compromised by low S/N or different sources of contamination.

Spect. ID	IRAC-1 ( $\mu\text{Jy}$ )	IRAC-2 ( $\mu\text{Jy}$ )	IRAC-3 ( $\mu\text{Jy}$ )	IRAC-4 ( $\mu\text{Jy}$ )	MIPS-1 ( $\mu\text{Jy}$ )	SED	Comments
213542993+573337049	2683±72	1982±57	1808±222	1211±86	881±157	Dep.	
213607980+572637096	19571±94	39189±78	103489±512	—	1159200±6406	ClassI	
213618699+573626870	1251±53	835±53	708±197	146±43	—	ND	
213619969+573527805	522±3	343±3	257±15	163±48	—	ND	
213622159+572327898	2220±53	1434±58	1244±273	—	—	Neb. contamination	
213622379+573141225	1669±43	1066±55	1305±196	1984±230	—	ND	
213625078+572750265	3060±58	3013±61	3021±224	4872±26	9196±103	Full	
213626897+573304351	1392±54	750±54	—	—	—	ND	Neb.
213633647+573517477	10624±79	6568±51	4339±221	2982±72	1800±310	TD/Dep.	Var.?
213636909+573132683	10712±33	10062±77	10814±257	15797±95	13900±3802	Full	
213639147+572953326	156347±511	—	155812±641	—	150577±2912	Full	
213641152+573702713	1045±50	717±54	488±220	235±36	—	ND	
213641358+572204113	876±41	589±53	272±178	—	—	ND	
213642470+572523186	1513±56	1220±55	1093±201	1046±86	1525±100	Full	
213648190+573402084	1203±32	686±42	314±155	1809±67	—	ND	
213653210+572052112	732±50	395±52	673±208	—	—	ND:	$24\mu\text{m}$ marginal
213655201+573030103	38820±158	41537±165	41378±345	—	43405±11034	ClassI	
213655283+572551668	3304±56	1803±43	1195±252	1045±53	2166±101	TD	
213658737+573848181	2764±60	2294±54	2463±205	1866±86	16507±456	PTD	
213659108+573905636	6278±62	6339±53	7337±209	10397±91	47929±108	Full	
213659472+573134908	5918±18	5496±50	5118±213	8387±48	—	Full	
213701319+573418289	1616±53	1282±54	1091±210	887±79	6561±106	TD	
213701401+572445873	5219±61	3358±61	3050±272	1278±73	—	ND:	$24\mu\text{m}$ marginal
213702321+573115201	14245±32	23317±90	26415±245	25066±82	79770±11021:	ClassI	$24\mu\text{m}$ contaminated, excess real
213703207+572718405	1470±53	1021±53	645±16	324±85	1137±287:	ND	$24\mu\text{m}$ may be from cloud
213704539+573223646	701±4	1050±5	—	—	—	ND	
213707711+573211012	1900±54	1611±57	1745±239	1477±106	<2500	Full	
213708137+573616213	2479±42	2266±57	2046±154	2359±93	3592±103	Full	
213708281+573023538	2376±30	1676±48	1498±123	2815±213:	—	ND:	$8\mu\text{m}$ could be contaminated
213708879+572107012	1638±56	1424±41	1298±212	923±63	2228±254	PTD	
213709442+573036722	4224±38	3431±60	3825±166	4464±87	20288±990	Full	
213710877+573846877	667±5	534±3	408±15	404±38	560±104	Full/Dep.	$24\mu\text{m}$ marginal
213712353+573331789	6674±66	4196±50	2673±222	2019±64	—	ND	
213712580+574055032	425±3	4373±11	155±14	—	—	ND	
213716349+572640200	8717±74	9228±77	8503±245	8576±109	46368±982	Full	
213720641+572100571	1195±48	685±52	565±15	383±52	—	ND	
213724102+572411541	5408±63	5263±65	5267±217	7527±98	20691±107	Full	
21372447+5731359	2615±50	2160±58	2285±198	2499±88	4596±271	Full	
213725743+571257077	983±4	692±4	441±15	259±36	—	ND	
213726148+572330562	509±3	—	304±15	382±62	2029±104	TD	
213726272+571258793	1650±51	1045±54	902±222	144±72	—	ND	
21372643+5731386	2243±54	1447±55	1079±199	998±85	—	TD	
21372685+5732069	1030±40	574±53	802±161	184±84	—	ND	
213727418+573123620	3761±59	3184±59	2518±201	2934±91	—:	Full	Detected at $24\mu\text{m}$ , contaminated by nearby strong source
213732341+572503204	4430±62	4052±61	3510±204	4564±97	16350±104	Full	
213733557+573550931	972±5	793±3	694±16	620±12	544±215	Dep.	$24\mu\text{m}$ marginal but detected
213734113+573431198	2360±53	2158±57	1902±255	1552±73	3507±391	Full	

Table A.3: Continued.

Spect. ID	IRAC-1 ( $\mu$ Jy)	IRAC-2 ( $\mu$ Jy)	IRAC-3 ( $\mu$ Jy)	IRAC-4 ( $\mu$ Jy)	MIPS-1 ( $\mu$ Jy)	SED	Comments
213734649+571657705	2510±59	2415±60	1911±221	1649±96	6819±98	PTD	
213735713+573258349	1454±32	1409±40	1058±143	1364±63	12338±750	TD	
213738830+572936901	12477±83	11942±83	10094±245	10801±112	29362±106	Full	
213740217+571903718	1025±50	718±45	493±224	276±36	—	ND	
213740471+573433203	1502±52	1440±55	1765±247	3793±84	39580±984	TD	
213742167+573431486	981±50	764±53	485±222	499±74	<2100	TD	Potential 24 $\mu$ m excess, Nobj.
213742758+573325074	57090±185	44097±113	50220±344	64140±162	71760±925	Unc.	
21374388+5734521	927±51	920±54	1245±235	536±77	—	Unc./Dep.	
213744131+573331130	6609±61	6725±20	6739±229	7452±30	28334±705	Full	
213744543+572200213	608±3	1026±4	919±170	513±86	—	Unc.	Anomalous SED shape
213745147+571942390	7693±70	7686±66	7621±237	9257±89	11219±341	Full	
213746871+573156208	2124±52	1784±57	1944±249	1421±73	9424±102	PTD	
213747963+573242323	4209±58	3693±60	2966±221	4167±83	21461±106	PTD	
213748237+572319411	1433±41	1070±39	797±153	923±58	<4900	TD	
213748931+572320963	3178±46	2952±48	2146±157	2740±65	4917±99	Full	
213749260+573158309	1113±50	697±55	462±15	134±39	—	ND	
213750222+573009586	1447±46	1097±40	595±208	528±64	—	ND	
213750297+570909399	1170±51	847±53	704±222	357±78	1910±100	TD:/ND:	Nebulosity, but 24 $\mu$ m excess probably real
213751197+574656428	691±8	990±4	286±18	270±68	—	ND	
213751210+572436151	1261±51	1210±54	1360±240	1580±77	1243±100	Full	
213756779+573448171	660±4	464±3	284±14	294±37	1168±302	TD	
213803453+570512396	1967±53	1004±54	1024±297	668±80	—	ND	
213804820+570754472	703±4	483±4	334±16	167±68	—	ND	
213809221+572038118	315±48	377±53	—	—	—	ND	
213809997+572352782	2256±55	2015±57	2051±205	2792±87	2476±98	Full	
213810182+572708407	2276±40	2006±5	1617±184	1650±11	9319±360:	PTD:	24 $\mu$ m contaminated by nearby star
213810759+574013683	580±3	405±3	—	212±44	—	ND	
213812023+572500774	2429±41	1770±57	1699±149	1879±88	3551±99	Full	
213812641+572033696	2929±56	2468±58	1994±247	3013±81	10120±101	PTD	
213816129+571935798	3543±44	2884±58	2517±192	1994±78	3406±101	Full	
213816170+574104645	6346±54	4193±45	2884±182	1494±66	—	ND	
213819411+572203907	537±3	373±3	249±15	233±53	<900	TD/Dep.	
213819507+572044119	626±4	436±3	288±16	—	—	ND	
213822810+574017294	3313±42	2917±36	2149±182	1911±47	1675±98	Full	
213823950+572736175	1423±53	1208±53	1190±235	1188±45	2522±99	Full	
213824142+574451513	2134±55	1421±56	1056±228	483±83	—	ND	
213825831+574207487	16758±91	11809±81	9318±237	7860±94	14366±100	TD	
213827431+572720767	19438±104	19177±102	20070±269	24421±142	—	Full	
213828028+574736432	930±41	562±55	619±213	581±68	557±131:	Dep.	24 $\mu$ m marginal
213829367+573726567	766±5	500±4	352±14	317±46	—	TD	
213830308+573255218	1528±4	1174±5	760±11	450±41	4352±101	TD	
213830349+572618227	2951±55	2568±57	2445±207	2777±82	3335±99	Full	IR Variable
213832169+572635943	3303±57	3122±58	2391±208	2374±82	4205±99	Full	
213835211+573013582	4813±47	2978±34	2079±189	1182±9	—	ND	
213837298+573103776	2260±53	1919±59	1198±240	861±71	1909±99	TD	
213839571+572916412	1132±5	950±4	836±14	1059±12	791±204	TD/Dep.	
213839749+572753080	2106±6	2078±7	1513±13	1123±17	690±207:	Dep.:	24 $\mu$ m may be contaminated by nearby star
213842249+573533902	1709±57	1566±57	1422±218	1580±93	3033±101	Full	
213844343+573626211	1677±5	1449±4	1200±12	1247±12	150±100	Dep.	24 $\mu$ m detected, sky problem

Table A.3: Continued.

Spect. ID	IRAC-1 ( $\mu$ Jy)	IRAC-2 ( $\mu$ Jy)	IRAC-3 ( $\mu$ Jy)	IRAC-4 ( $\mu$ Jy)	MIPS-1 ( $\mu$ Jy)	SED	Comments
213847282+573114405	2412±9	2119±6	1924±19	2018±14	1484±101	Full	
213854760+572450268	5246±63	3532±62	3021±227	2034±89	2939±98	Dep./TD	
213859147+572045273	493±3	332±2	235±15	113±54	—	ND	
213859738+572216816	1034±5	960±5	850±15	929±17	1291±99	Full	
213900397+575004884	898±50	824±40	405±240	931±51	OUT	TD:	
213903212+571555316	1988±56	1381±49	1105±17	1289±75	5096±100	TD	
213905519+572349596	4363±15	2823±10	1970±18	1512±17	—	TD	
213909728+571803046	546±3	361±3	202±14	177±55	—	ND	
213910429+572235727	2485±58	2190±59	1654±205	1671±88	3765±100	Full	24 $\mu$ m contaminated by 21-840
213911452+572425205	2109±6	1731±7	1578±197	3587±20	35788±593:	Full/PTD	24 $\mu$ m contaminated, Mini-cluster
213914453+572304758	1964±43	1418±41	753±181	1057±60	—	TD	Near cloud, prob. 24 $\mu$ m excess
213914837+573756779	1195±53	1162±50	906±177	429±85	330±103	TD	
213914988+574050473	1155±50	985±54	323±218	673±73	2311±98	TD	
213915002+575023465	906±50	929±4	440±215	284±80	OUT	ND	
213917062+571643244	783±4	533±3	330±15	—	—	ND	
213917371+571605286	558±3	2033±8	233±15	—	—	ND	
213917481+571747432	3820±58	3051±59	2715±217	2934±82	3482±98	Full/PTD	
213918291+572818473	1254±54	950±44	799±214	386±70	—	ND	
213918339+574022609	821±49	503±38	344±15	247±51	—	ND	
213920172+575015967	611±3	—	361±15	64±41:	—	ND	Very faint
21392059+5726269	811±41	734±54	1011±153	631±80	1817±184	TD	Contaminated by nebula, excess 24 $\mu$ m real
213920831+571631187	537±3	410±3	258±15	112±55	—	ND	
213924388+572820999	1878±58	1337±57	1456±216	429±90	—	ND	
213924711+571912672	983±53	812±52	—	863±50	1591±98	Full	
21392564+5728183	814±55	659±49	—	696±50	—	ND	
213926421+572538470	2588±56	2702±58	2141±200	2088±84	4969±99	Full	
21392806+5728420	6380±11	4766±9	—	—	—	ND	Nobj.
213928151+572521181	1582±53	1055±53	992±205	475±81	—	ND	
213928742+573930163	552±3	1093±5	563±221	136±76	—	ND	
213928968+574347037	1619±42	1168±39	1035±173	405±62	—	ND	
213929250+572530299	1641±7	1542±6	1457±16	2431±19	4925±100	PTD	
213929408+570630605	1926±52	—	1310±240	—	13059±101	TD	
213929648+574809597	452±3	443±3	202±14	161±42	—	ND	
213930129+572651433	3843±52	3154±59	2410±177	2178±91	2483±98	Dep.	
213930870+572227446	4559±60	3980±61	3316±246	2030±78	2933±101	Full	
21393179+5728291	3710±53	2557±58	1948±267	782±68	—	ND	
213933219+573300533	752±46	508±53	766±184	305±82	2619±98	TD	
21393301+5728175	2194±50	1791±56	1878±267	1829±72	4827±99	Full	
213934908+571703418	567±3	757±3	251±15	41±39	—	ND	
213935018+573353693	955±44	835±54	603±145	389±88	—	ND	
213935162+572053128	1357±51	1407±54	553±215	778±71	1847±98	Full	
21393648+5728119	1979±47	1126±54	1047±198	665±68	—	ND	
213937132+572459030	1495±54	1412±44	1421±212	1239±64	2069±101	Full	
213937448+574607113	1604±53	1237±53	1238±190	750±78	OUT	ND	
213938162+572301696	993±51	642±53	499±233	192±79	—	ND	
213938169+573218304	722±52	535±51	391±14	118±50	—	ND	
21393819+5727319	2225±50	1307±56	1085±232	640±68	—	ND	
21394010+5730113	1339±52	1098±55	500±227	821±78	736±97	TD/Dep.	
213940600+572108797	633±4	417±3	332±15	—	—	ND	

Table A.3: Continued.

Spect. ID	IRAC-1 ( $\mu$ Jy)	IRAC-2 ( $\mu$ Jy)	IRAC-3 ( $\mu$ Jy)	IRAC-4 ( $\mu$ Jy)	MIPS-1 ( $\mu$ Jy)	SED	Comments
213940710+572206160	729±43	471±51	344±12	—	—	ND	
213941211+573749556	538±4	641±4	423±206	187±55	—	ND	
213942227+571701866	2266±48	1399±56	1144±147	290±87	—	ND	
213942289+572902679	1062±5	850±4	746±15	671±40	604±139	Dep.	
213942378+573348653	653±2	451±3	330±10	162±45	—	ND	
213942399+573431184	727±3	553±4	626±12	593±52	<400	Dep.	
213943237+574139252	1382±39	1081±47	1365±185	1234±64	1115±148	Full	
213943450+573634560	2382±54	2076±52	1560±227	1676±72	1908±97	Full	
213944898+573537212	2217±53	1648±55	1298±241	791±75	463±109	Dep.	
213945091+571953390	1219±5	742±3	719±16	462±54	—	ND:/Dep.:	
213945201+574912946	2889±71	2577±107	2110±231	2026±135	OUT	PTD	
213945709+572624297	3100±55	2533±62	2670±247	2699±77	6886±102	Full	
213945860+573051704	3948±13	4397±15	3339±21	3026±21	9548±99	Full	IR Variable?
213947013+574403324	883±4	784±4	687±15	705±34	OUT	Full	
213948050+572049544	2989±10	2431±9	2548±221	2519±85	3839±97	Full	
213949767+574733740	1214±5	899±5	732±16	723±43	OUT	TD	
213949540+574330324	2072±52	1850±42	1402±224	1463±55	OUT	Full	
213950529+574137632	1745±52	1061±55	843±16	729±35	OUT	TD	
213951092+574119848	2057±47	1718±57	967±204	1029±71	1200:,EDGE	Dep.	Potential excess at 8 and 24 $\mu$ m
213952060+572506212	815±4	685±4	551±16	621±41	740±218	Dep.	
213954003+573519730	1367±40	978±54	868±169	1284±81	2021±97	TD	
213954058+572933454	3238±45	2691±59	1947±167	1513±87	10540±99	PTD	
213955699+571638273	1249±47	826±52	842±219	614±69	4358±98	TD	
213956180+572416046	1646±4	—	—	732±69	—	ND:/TD:	Nobj., 24 $\mu$ m excess likely
213959078+572643784	1606±53	1317±47	1206±220	1149±67	1417±99	Full	
213959517+573257017	727±49	453±42	383±15	99±51	—	ND	
214000478+571839617	738±3	494±4	391±11	308±41	<700	Dep./TD	
214000671+574524541	749±4	531±4	320±15	—	—	ND	
214004159+574358037	796±52	583±54	492±15	363±89	—	ND	
214004523+572836367	11998±83	11542±82	11385±231	14312±121	17948±102	Full	
214005669+574417181	599±4	437±4	277±15	229±48:	OUT	ND:/TD:	Unclear whether there is a disk
214011012+573630756	884±37	719±42	825±159	334±60	—	ND	
214011348+574414105	5512±67	3913±71	3125±223	3247±112	OUT	Full	Nobj.
214012151+573420637	628±4	442±3	312±15	201±32	—	ND	
214012309+573833048	2736±55	1984±56	1425±238	1326±77	—	ND	
214015557+573156551	904±3	607±4	563±11	161±38	—	ND	
214017542+573124718	1854±52	965±54	941±199	344±78	—	ND	
214018111+572919447	895±4	626±3	397±15	306±36	—	ND	
214019073+572509288	1133±6	934±5	768±15	864±38	1461±98	Full	
214019849+573922857	1800±7	1517±6	1350±18	1285±18	OUT	Full	
214020158+572711662	659±3	901±4	465±183	263±61	—	ND	
214021922+572028395	852±45	624±53	381±13	248±69	—	ND	
214021922+573005424	3801±57	2877±58	2671±218	2482±82	2056±155	Dep.	
214023790+571738807	461±3	337±4	202±15	144±42	—	ND	
214025369+573416284	2067±42	1635±52	1702±210	1179±17	6393±144	PTD	
214025967+572042499	797±4	539±4	361±14	309±35	2272±96	TD	
214026262+573402317	1311±4	871±4	936±195	829±64	—	Dep./TD	
214028542+572414659	567±3	—	240±15	182±62	—	ND	
214029551+572453893	757±3	—	402±189	435±69	1742±97	TD	



Table A.3: Continued.

Spect. ID	IRAC-1 ( $\mu\text{Jy}$ )	IRAC-2 ( $\mu\text{Jy}$ )	IRAC-3 ( $\mu\text{Jy}$ )	IRAC-4 ( $\mu\text{Jy}$ )	MIPS-1 ( $\mu\text{Jy}$ )	SED	Comments
214033472+573605378	3154±57	3022±45	2914±226	2568±63	OUT	Full	
214034962+572308795	19315±96	13768±34	9903±245	8153±38	26806±98	PTD	
214035490+572831395	8319±26	5621±17	4812±23	7078±30	31567±103	TD	
214037207+572912731	2172±8	2087±8	2203±20	2726±21	3506±98	Full	
214038759+572958833	1136±54	636±55	369±216	246±89	—	ND	
214042281+573513316	903±4	821±4	827±16	823±38	OUT	Full	
214048489+573202607	782±49	477±43	409±15	334±56	—	ND/TD	Unclear whether there is a disk
214055932+571759160	9208±67	—	6370±201	—	10585±99	Full	
214059633+572210994	2873±10	3033±10	2926±20	3951±23	6773±99	Full	
214138291+572337085	2694±56	—	2355±239	—	3269±145	Full	
214148062+572609205	566±3	401±3	292±15	274±48:	OUT	ND:/TD:	Unclear whether there is a disk

Table A.4: WISE data for confirmed members and probable members. Only good quality data in agreement with the Spitzer fluxes are taken into account (see text). Uncertain data are marked with ':'. Data that were not used in the SEDs (due to uncertainty or evident contamination) are marked with <sup>a</sup>.

Spect. ID	WISE-1 (mJy)	WISE-2 (mJy)	WISE-3 (mJy)	WISE-4 (mJy)
213633647+573517477	11.54±0.26	5.85±0.11	17.35±0.15	3.56±1.13 <sup>a</sup>
213639147+572953326	148.01±3.54	164.49±3.03	1699.31±4.54	343.75±12.03 <sup>a</sup>
213642470+572523186	1.63±0.04	1.27±0.03	8.44±0.09	2.38±0.99 <sup>a</sup>
213655283+572551668	3.68±0.08	1.80±0.04	5.26±0.10	2.56: <sup>a</sup>
213659108+573905636	6.55±0.15	6.66±0.12	156.60±0.30	54.89±1.77 <sup>a</sup>
213701319+573418289	1.66±0.06	1.25±0.04	27.49±0.13	10.13±1.65 <sup>a</sup>
213708137+573616213	2.36±0.06	2.14±0.05	28.03±0.19	9.78±1.04 <sup>a</sup>
213708879+572107012	1.75±0.04	1.41±0.04	5.01±0.10	2.06:
213716349+572640200	6.98±0.15 <sup>a</sup>	7.69±0.15 <sup>a</sup>	111.07±0.23	46.63±1.63
21372447+5731359	2.64±0.07	2.48±0.06	43.61±0.15	7.93±0.93 <sup>a</sup>
213726148+572330562	0.39±0.01	0.28±0.01	10.82±0.10	3.12: <sup>a</sup>
213732341+572503204	4.03±0.09	3.44±0.07	50.07±0.17	18.94±1.06 <sup>a</sup>
213734649+571657705	2.33±0.06	2.06±0.05	22.18±0.14	11.55±0.77 <sup>a</sup>
213738830+572936901	13.20±0.29	12.68±0.24	143.22±0.33	30.64±1.21
213740471+573433203	1.66±0.04	1.72±0.03	72.11±0.23	48.74±1.80
213742167+573431486	0.86±0.02 <sup>a</sup>	0.82±0.02 <sup>a</sup>	9.69±0.12	9.14±0.96 <sup>a</sup>
213742758+573325074	59.06±1.14 <sup>a</sup>	61.98±1.03 <sup>a</sup>	857.42±1.03	155.84±3.59 <sup>a</sup>
21374388+5734521	1.00±0.04	0.96±0.03	3.20±0.13	3.93±1.06 <sup>a</sup>
213744543+572200213	0.44±0.02	0.41±0.02	3.40±0.15	2.20±0.65
213746871+573156208	1.80±0.05	1.66±0.04	19.09±0.17	11.19±1.01 <sup>a</sup>
213747963+573242323	3.98±0.10	3.22±0.07	56.75±0.24	24.11±1.40 <sup>a</sup>
213751210+572436151	1.28±0.03	1.24±0.03	16.08±0.16	7.45±0.71 <sup>a</sup>
213756779+573448171	0.69±0.02	0.51±0.02	2.67: <sup>a</sup>	3.28 <sup>a</sup>
213809997+572352782	2.13±0.05	2.13±0.05	27.75±0.16	2.52±0.77
213812023+572500774	2.09±0.05 <sup>a</sup>	1.52±0.04 <sup>a</sup>	19.68±0.13	3.97±0.87
213812641+572033696	2.49±0.06 <sup>a</sup>	2.03±0.05 <sup>a</sup>	37.05±0.18	8.97±0.72
213816129+571935798	3.10±0.07 <sup>a</sup>	2.44±0.06 <sup>a</sup>	18.93±0.15	3.79±0.65
213822810+574017294	2.56±0.06 <sup>a</sup>	2.12±0.05 <sup>a</sup>	15.30±0.19	5.81±0.75 <sup>a</sup>
213823950+572736175	1.61±0.04	1.31±0.04	14.94±0.11	1.85±0.69
213825831+574207487	17.74±0.39	10.91±0.20	86.69±0.25	16.95±1.08 <sup>a</sup>
213828028+574736432	0.86±0.02	0.66±0.02	4.21:	1.61±0.70 <sup>a</sup>
213829367+573726567	0.79±0.02	0.51±0.02	6.47±0.12	4.08±0.69
213830308+573255218	1.43±0.04	1.09±0.03	2.70±0.10	2.48±0.76
213830349+572618227	2.32±0.06	1.86±0.05	27.56±0.12	5.41±0.82 <sup>a</sup>
213832169+572635943	4.87±0.10 <sup>a</sup>	4.07±0.08 <sup>a</sup>	15.76±0.11	3.55±0.69
213842249+573533902	1.50±0.04	1.32±0.03	16.17±0.14	3.75±0.66
213847282+573114405	2.36±0.05	2.07±0.04	12.69±0.17	2.76: <sup>a</sup>
213854760+572450268	5.93±0.13	3.69±0.08	20.03±0.12	1.90±0.79
213903212+571555316	1.76±0.04	1.17±0.03	33.11±0.19	7.77±0.81 <sup>a</sup>
213905519+572349596	4.79±0.10	2.64±0.06	25.11±0.12	16.52±0.90
213911452+572425205	2.27±0.05	1.70±0.04	63.56±0.19	13.01±1.46 <sup>a</sup>
213914837+573756779	1.40±0.03	0.91±0.03	4.08±0.12	2.01: <sup>a</sup>
213917481+571747432	4.16±0.10	3.42±0.08	18.59±0.16	3.62: <sup>a</sup>
21392059+5726269	0.77±0.02	0.60±0.02	5.75±0.11	1.68:
213926421+572538470	2.54±0.06	2.56±0.05	15.82±0.11	3.41±0.83
213929250+572530299	1.40±0.03	1.20±0.03	27.34±0.15	3.49: <sup>a</sup>
213929408+570630605	2.00±0.05	1.38±0.03	29.08±0.14	6.84±1.27 <sup>a</sup>
213930129+572651433	3.84±0.08	2.81±0.06	20.43±0.12	4.83±0.83 <sup>a</sup>
213930870+572227446	5.18±0.11	4.20±0.09	15.50±0.11	2.08: <sup>a</sup>
213937132+572459030	1.28±0.03	1.12±0.03	11.79±0.12	2.61±0.85
213943237+574139252	1.39±0.05	1.10±0.03	11.12±0.10	2.28±0.76 <sup>a</sup>
213945201+574912946	3.20±0.07	2.45±0.06	26.27±0.13	6.39±0.75
213945709+572624297	3.04±0.07	2.42±0.05	36.68±0.14	6.94±0.96
213945860+573051704	10.06±0.21 <sup>a</sup>	10.95±0.20 <sup>a</sup>	97.54±0.23 <sup>a</sup>	19.42±0.95 <sup>a</sup>
213949540+574330324	1.83±0.05	1.50±0.04	11.05±0.11	1.76: <sup>a</sup>
213949767+574733740	1.22±0.03	0.82±0.02	9.91±0.11	2.77±0.86
213954058+572933454	3.49±0.12	2.79±0.09	19.95±0.13	9.23±1.26
213959078+572643784	1.48±0.04	1.25±0.04	13.25±0.11	1.86: <sup>a</sup>
214000478+571839617	0.70±0.02	0.42±0.02	2.53: <sup>a</sup>	1.81: <sup>a</sup>

Table A.4: Continued.

Spect. ID	WISE-1 (mJy)	WISE-2 (mJy)	WISE-3 (mJy)	WISE-4 (mJy)
214011348+574414105	8.13±0.18	5.47±0.11	35.93±0.18 <sup>a</sup>	6.71±0.94 <sup>a</sup>
214019073+572509288	0.89±0.03 <sup>a</sup>	0.76±0.03 <sup>a</sup>	8.31±0.10	2.92: <sup>a</sup>
214021922+573005424	4.12±0.09	2.73±0.06	20.02±0.17	1.95±0.87
214025369+573416284	2.01±0.05	1.64±0.05	14.49±0.14	4.30±0.91
214025967+572042499	0.70±0.02	0.44±0.02	8.31±0.10	2.57±0.77
214026262+573402317	1.11±0.03	0.76±0.02	3.88±0.11	1.93±0.86
214034962+572308795	23.43±0.50	14.18±0.27	69.25±0.23	23.67±1.11
214035490+572831395	9.15±0.19	5.02±0.10	134.65±0.26	32.08±1.48
214037207+572912731	2.40±0.06 <sup>a</sup>	2.21±0.05 <sup>a</sup>	21.41±0.13	2.05: <sup>a</sup>
214042281+573513316	0.85±0.02	0.77±0.03	5.74±0.11	3.07: <sup>a</sup>
214055932+571759160	7.84±0.17	7.25±0.14	74.79±0.23	14.60±0.97 <sup>a</sup>
214059633+572210994	2.96±0.07	3.17±0.07	42.14±0.16	7.19±0.80
214138291+572337085	2.57±0.06	2.28±0.05	16.12±0.10	3.99±0.74
214148062+572609205	0.45±0.01 <sup>a</sup>	0.32±0.01 <sup>a</sup>	2.29±0.09	2.12: <sup>a</sup>

Table A.5: Other emission lines observed.

Stars with multiple emission lines and their identifications. The lines have been identified according to Sicilia-Aguilar et al.(2012), the NIST database, Appenzeller et al. (1986), and Hamman & Persson (1992). <sup>a</sup> Probably nebular.

Spect. ID	Line $\lambda$ (Å)	Obs. $\lambda$ (Å)	EW (Å)
213659108+573905636	H $\alpha$ 6562.6	6562.5	-76.5
"	H $\beta$ 4861.3	4860.9	-22.0
"	H $\delta$ 4101.7	4101.6	-7.2
"	H $\gamma$ 4340.5	4340.1	-10.8
"	Ca II 8498.0	8498.2	-4.0
"	Ca II 8542.1	8542.1	-3.7
"	Ca II 8662.1	8662.2	-3.7
213659472+573134908	H $\alpha$ 6562.6	6564.5	-108.3
"	O I 8446.4	8446.0	-4.8
"	Ca II 8498.0	8497.9	-16.8
"	Ca II 8542.1	8541.9	-17.3
"	H I 8598.4	8598.2	-2.0
"	Ca II 8662.1	8662.0	-14.4
"	H I Pa 12 8750.5	8750.3	-1.7
"	H I Pa 11 8862.8	8862.8	-1.7
"	He I 5875.6	5875.6	-2.2
"	He I 6678.2	6677.6	-0.9
"	H $\beta$ 4861.3	4862.3	-7.5
"	He I 4921.9	4923.9	-1.9
"	Fe II 5018.4	5018.3	-1.6
"	Fe II 5169.0	5168.6	-2.2
"	Ca II H 3933.7	3933.8	-4.3
"	Ca II K 3968.5	3968.0	-2.3
"	H $\gamma$ 4340.5	4341.7	-1.8
"	O I 7772/4/5	7773.5	-1.4
213708879+572107012	H $\alpha$ 6562.6	6562.9	-55.4
"	H $\gamma$ 4340.5	4339.6	-5.6
"	H $\delta$ 4101.7	4101.1	-3.1
"	H $\delta$ 4101.7	4101.1	-3.0
"	H $\beta$ 4861.3	4860.9	-13.9
213716349+572640200	H $\alpha$ 6562.6	6562.7	-17.2
"	H $\beta$ 4861.3	4860.8	-4.5
"	H $\gamma$ 4340.5	4339.5	-1.7
"	H $\delta$ 4101.7	4101.4	-0.7
"	Ca II K 3968.5/ H $\epsilon$ 3970.0:	3968.7	-1.0
213734649+571657705	H $\alpha$ 6562.6	6563.0	-59.6
"	He I 6678.2	6677.1	-0.6
"	H8 3889.0	3888.5	-1.7
"	Ca II H 3933.7	3933.5	-15.4
"	Ca II K 3968.5	3968.0	-10.5
"	H $\delta$ 4101.7	4101.5	-4.3

Table A.5: Continued.

Spect. ID	Line $\lambda$ (Å)	Obs. $\lambda$ (Å)	EW (Å)
"	H $\gamma$ 4340.5	4339.9	-7.2
"	O I 8446.4	8445.5	-1.8
"	Ca II 8498.0	8497.9	-13.5
"	Ca II 8542.1	8541.7	-11.9
"	Ca II 8662.1	8661.9	-9.5
"	H I 8598.4	8597.7	-0.6
"	H $\beta$ 4861.3	4860.8	-23.0
"	He I 4921.9	4923.5	-2.5
"	Fe II 5018.4	5018.1	-2.7
"	Fe II 5169.0	5168.6	-3.2
"	Fe II 5234.6	5233.6	-1.1
"	Fe II 5276.0	5275.6	-0.8
"	Fe II 5316.6	5316.6	-1.2
"	H $\gamma$ 4340.5	4339.9	-7.1
"	H $\delta$ 4101.7	4101.5	-4.6
"	Ca II K 3968.5	3968.0	-10.6
"	Ca II H 3933.7	3933.5	-12.8
"	He I 5875.6	5875.5	-1.6
"	Na ID 5890/96	5891.3	-1.4
213735713+573258349	H $\alpha$ 6562.6	6562.7	-62.3
"	Ca II 8498.0	8498.0	-5.2
"	Ca II 8542.1	8541.9	-5.1
"	Ca II 8662.1	8662.2	-3.1
"	He I 5875.6	5876.1	-0.6
"	Na ID 5890/96	5890.1	-0.8
"	H $\beta$ 4861.3	4861.0	-10.4
"	H $\gamma$ 4340.5	4339.9	-1.9
"	Ca II K 3968.5	3968.4	-2.3
"	Ca II H 3933.7	3933.6	-2.3
213744131+573331130	H $\alpha$ 6562.6	6562.5	-19.5
"	[S II] 6730.8	6730.0	-0.9
"	[S II] 6716.4	6714.9	-0.4
"	[O I] 6300.3	6299.4	-1.5
"	[O I] 6363.8	6364.3	-0.2
"	H $\beta$ 4861.3	4861.0	-6.6
"	H $\gamma$ 4340.5	4339.6	-2.3
213810759+574013683	H $\alpha$ 6562.6	6562.8	-46.5
"	[N II] 6583.4	6583.2	-4.8
"	[S II] 6716.4	6715.7	-1.1
"	[S II] 6730.8	6730.3	-0.9
213827431+572720767	H $\alpha$ 6562.6	6561.9	-35.8
"	Fe I 8824.2:	8827.6	-0.9
"	Ca II 8498.0	8496.9	-4.2
"	Ca II 8542.1	8540.8	-3.7
"	Ca II 8662.1	8660.9	-3.5
213830308+573255218	H $\alpha$ 6562.6	6562.9	-31.4
"	H $\beta$ 4861.3	4860.8	-4.7
"	H $\delta$ 4101.7	4101.1	-1.4
"	He $\epsilon$ 3970.0	3970.1	-1.2
213844343+573626211	H $\alpha$ 6562.6	6563.1	-33.7
"	Ca II 8498.0	8497.5	-6.4
"	Ca II 8542.1	8541.9	-6.5
"	Ca II 8662.1	8661.8	-4.2
"	O I 8446.4	8447.0	-1.3
"	Ca II H 3933.7	3933.6	-2.8
"	Ca II K 3968.5	3968.2	-3.1
213911452+572425205	H $\alpha$ 6562.6	6563.0	-26.2
"	H $\beta$ 4861.3	4860.7	-9.2
"	Fe II 4555.9	4555.2	-1.6
"	H $\gamma$ 4340.5	4339.9	-4.6
"	Cr II 4284.2	4283.6	-2.6

Table A.5: Continued.

Spect. ID	Line $\lambda$ (Å)	Obs. $\lambda$ (Å)	EW (Å)
"	H $\delta$ 4101.7	4099.5	-3.4
"	Ca II K 3968.5	3968.9	-1.8
"	H8 3889.0	3888.7	-2.2
"	He I 5875.6	5875.9	-1.1
"	He I 6678.2	6678.1	-0.3
213942378+573348653	H $\alpha$ 6562.6	6562.9	-75.7
"	[S II] 6716.4	6716.3	-1.8
"	[S II] 6730.8	6730.5	-1.1
213950529+574137632	H $\alpha$ 6562.6	6562.5	-3.2
"	He I 6678.2:	6672.0	-1.6
214019849+573922857	H $\alpha$ 6562.6	6562.5	-47.0
"	He I 6678.2	6677.7	-1.1
"	He I 5875.6	5876.3	-2.8
"	H $\beta$ 4861.3	4860.5	-9.7
"	H $\gamma$ 4340.5	4339.3	-7.9
"	He I 4471.6	4472.5	-1.4
"	H $\delta$ 4101.7	4101.0	-5.6
"	H $\epsilon$ 3970.0	3969.3	-3.1
"	H8 3889.0	3888.7	-4.3
"	Fe I 3841.0:	3840.8	-5.5
214037207+572912731	H $\alpha$ 6562.6	6562.8	-21.1
"	H $\beta$ 4861.3	4860.8	-8.3
"	H $\gamma$ 4340.5	4339.9	-7.8
"	H $\delta$ 4101.7	4101.5	-2.9
"	H $\epsilon$ 3970.0	3969.2	-2.7
"	H8 3889.0	3889.1	-2.4
"		3921.3	-0.9
214055932+571759160	H $\alpha$ 6562.6	6563.2	-34.4
"	He I 6678.2	6677.6	-0.7
"	Ca II 8498.0	8497.2	-8.9
"	Ca II 8542.1	8541.2	-7.8
"	Ca II 8662.1	8661.2	-6.9
214059633+572210994	H $\alpha$ 6562.6	6563.0	-95.1
"	He I 6678.2	6677.5	-1.4
"	O I 8446.4	8445.8	-2.5
"	H I 8467.3	8466.7	-1.3
"	Ca II 8498.0	8497.3	-12.3
"	Ca II 8542.1	8541.2	-12.8
"	H I 8598.4	8597.3	-1.6
"	Ca II 8662.1	8661.3	-9.2
"	H I Pa 12 8750.5	8748.8	-2.3
"	H I Pa 11 8862.8	8860.6	-3.0
"	[O I] 6300.3	6300.2	-1.9
"	[O I] 6363.8	6364.3	-0.6
"	He I 5875.6	5875.5	-4.4
"	Na ID 5890/96	5891.2	-2.2
"	Fe II 5169.0	5168.2	-4.1
"	Fe II 5018.4	5017.5	-3.5
"	He I 4921.9	4923.5	-3.3
"	H $\beta$ 4861.3	4860.9	-25.8
"	H $\gamma$ 4340.5	4340.0	-9.5
"	H $\delta$ 4101.7	4101.7	-7.5
"	Ca II K 3968.5	3968.7	-7.3
"	Ca II H 3933.7	3933.3	-7.6
214138291+572337085	H $\alpha$ 6562.6	6561.9	-87.2
"	He I 6678.2	6677.5	-1.1

## Appendix B: SEDs of all the members with IR excesses

The following figures show the SEDs of all the members with IR excesses. Only those with clear excess are displayed; objects with uncertain colors (for instance, due to nebular contamination or contamination by a nearby object) are not displayed, but marked in Table A.3. Objects without an evident IR excess are also not displayed, since they are consistent with bare photospheres. According to the definitions in the main text, the SEDs have been organized by disk types:

- Typical full-disks, with strong IR excesses and evidence of ongoing accretion (see Figures B.1 and B.2).
- Transition disks, candidates to have inner holes or inside-out evolution, with  $[3.6]-[4.5]<0.2$  and strong excesses at  $24\mu\text{m}$  (Figure B.3).
- Pre-transitional disks, candidates to inner gaps (Espaillat et al. 2010), with reduced near-IR excesses, and strong  $8\mu\text{m}$  (and  $24\mu\text{m}$ ) fluxes (Figure B.4).
- Dust-depleted disks, candidates to low small-dust mass given their reduced IR excesses at all wavelengths, specially at  $24\mu\text{m}$ . Note that some of the transition disks have also very low excesses, so they are also candidates for dust depletion (or candidates for homologously depleted disks; Figure B.5).
- Class I objects, consistent with very embedded objects with strong accretion and remnant envelopes (all associated to dense parts in the IC 1396A nebula; Figure B.6).
- Finally, a few objects (usually with very small excesses, uncertain photometry, and/or likely contamination by nearby bright sources; see Figure B.6) cannot be safely classified in any of the previous groups; they are therefore labeled and excluded from most plots and statistical analysis.

Probable members are labeled as 'P', all other SEDs correspond to confirmed members. In addition, information on the spectral type and the  $H\alpha$  emission is also given in the plot, and the data are compared to a MARCS model with the appropriate spectral type (Gustafsson et al. 2008).

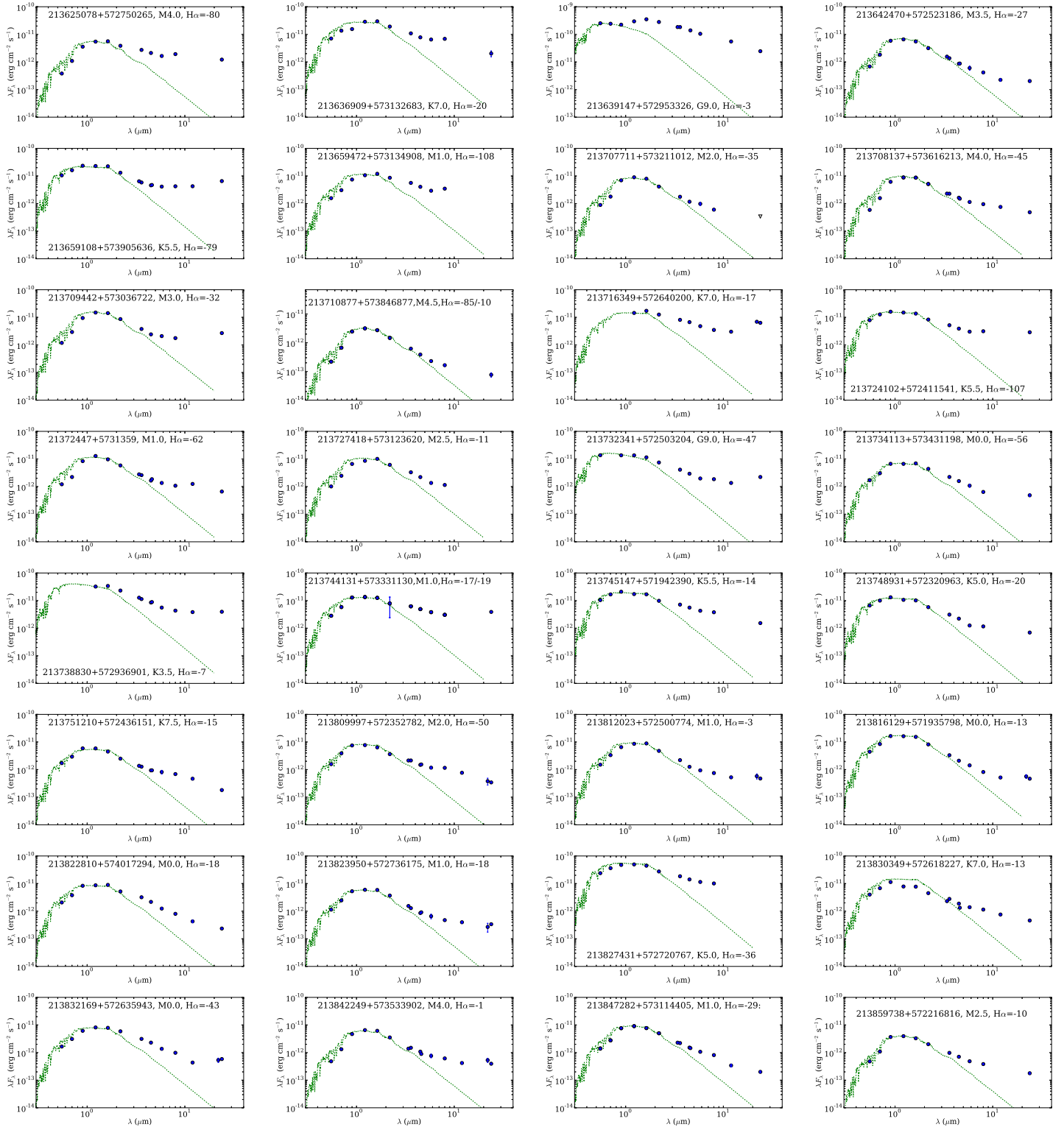


Fig. B.1: SEDs of the members and probably members with IR excess typical of full-disks. Inverted triangles represent upper limits.

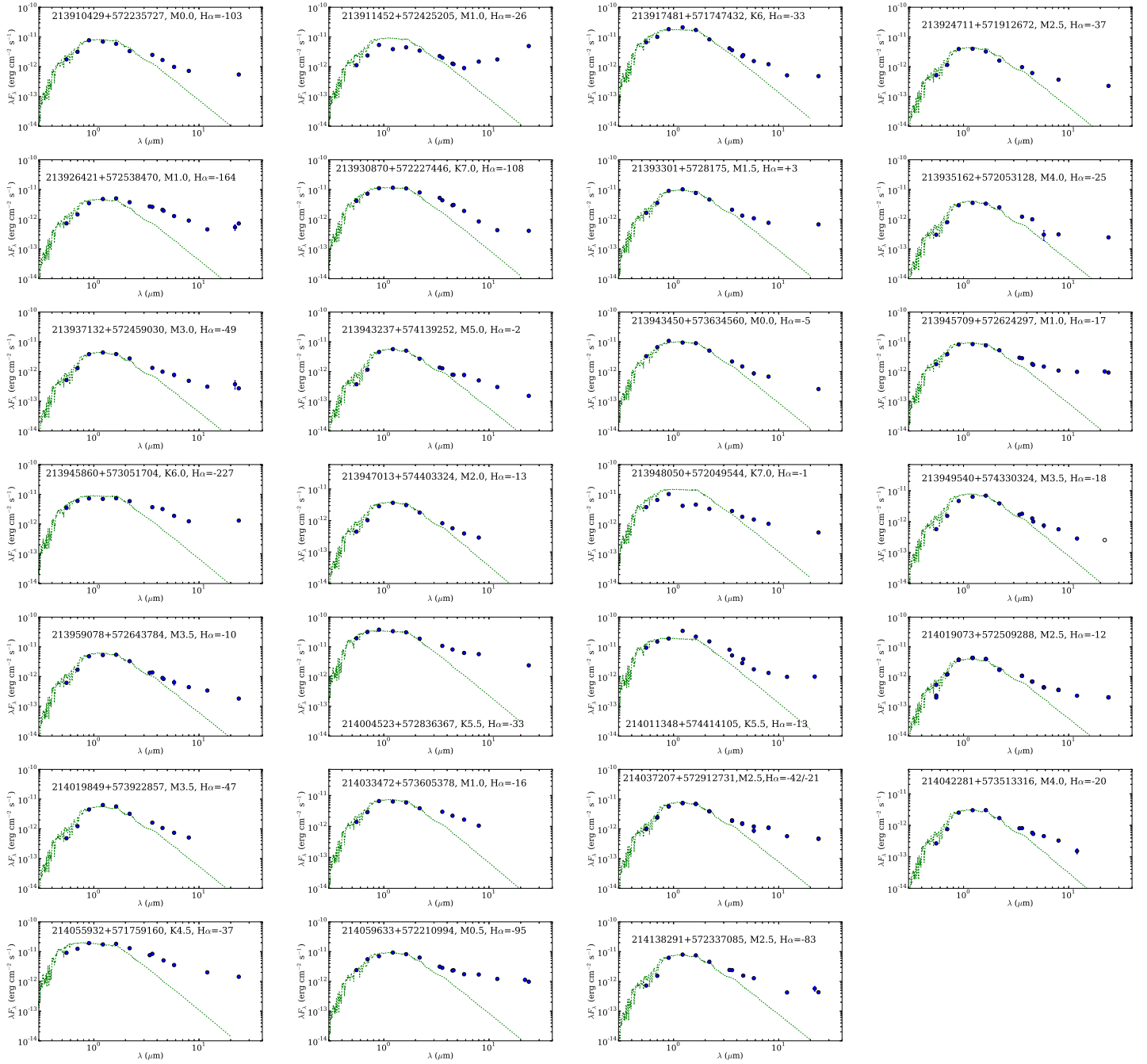


Fig. B.2: SEDs of the members and probably members with IR excess typical of full-disks (continued). 213917481+571747432 has strong  $8\mu\text{m}$ , could be PTD. 213911452+572425205 has  $[3.6]-[4.5]=0.27$  and a strong kink in the SED, it could be a PTD although its  $24\mu\text{m}$  flux is likely contaminated by cloud emission. 214011348+574414105 has  $[3.6]-[4.5]=0.11$  but a SED that suggests strong variability and a flared, massive full-disk.



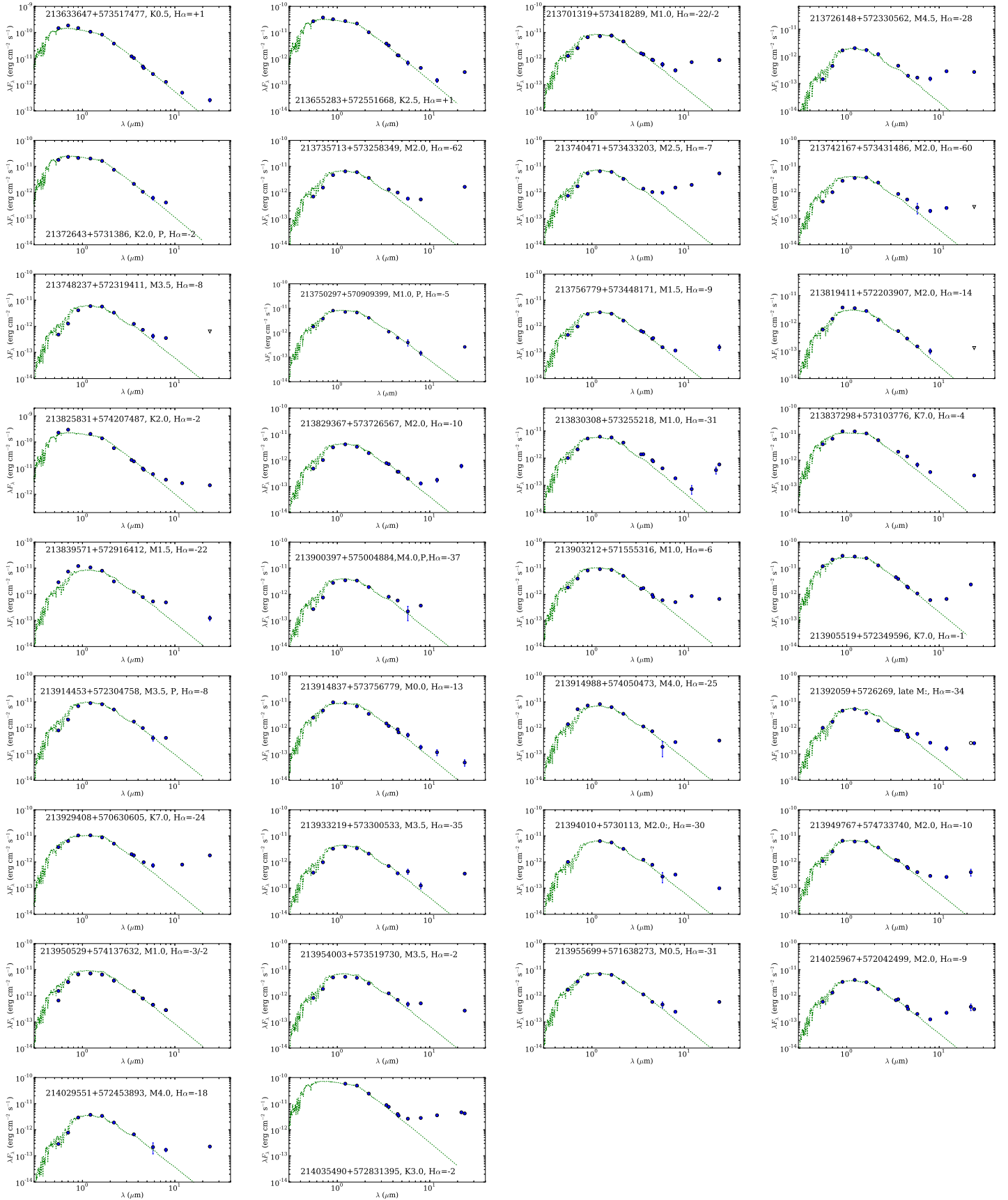


Fig. B.3: SEDs of the members and probably members with IR excess consistent with TD. Objects like 213819411+572203907, 213839571+572916412, 21394010+5730113 may be also dust-depleted. 213750297+570909399 may be partially contaminated by nebular emission but the detection is real. Inverted triangles mark upper limits, and open circles are uncertain values.

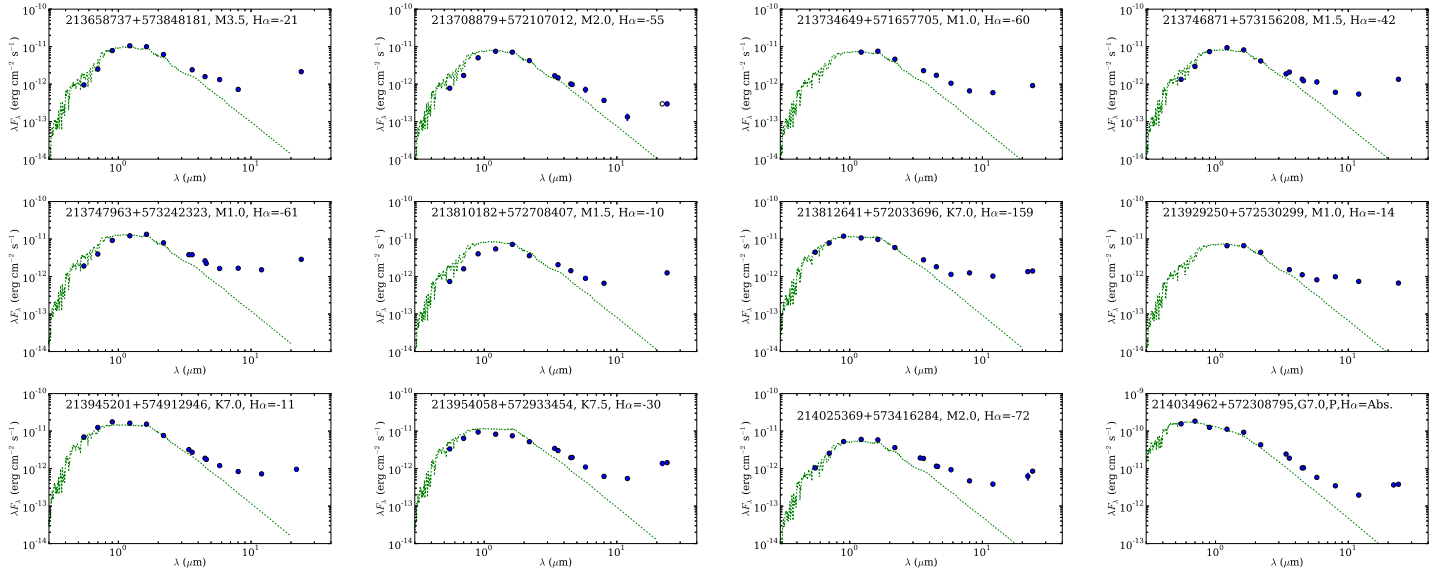


Fig. B.4: SEDs of the members and probably members with IR excess consistent with PTD. Note that the  $24\mu\text{m}$  flux of 213810182+572708407 is contaminated by a nearby star, but the object still presents the kink in the SED typical of PTD.

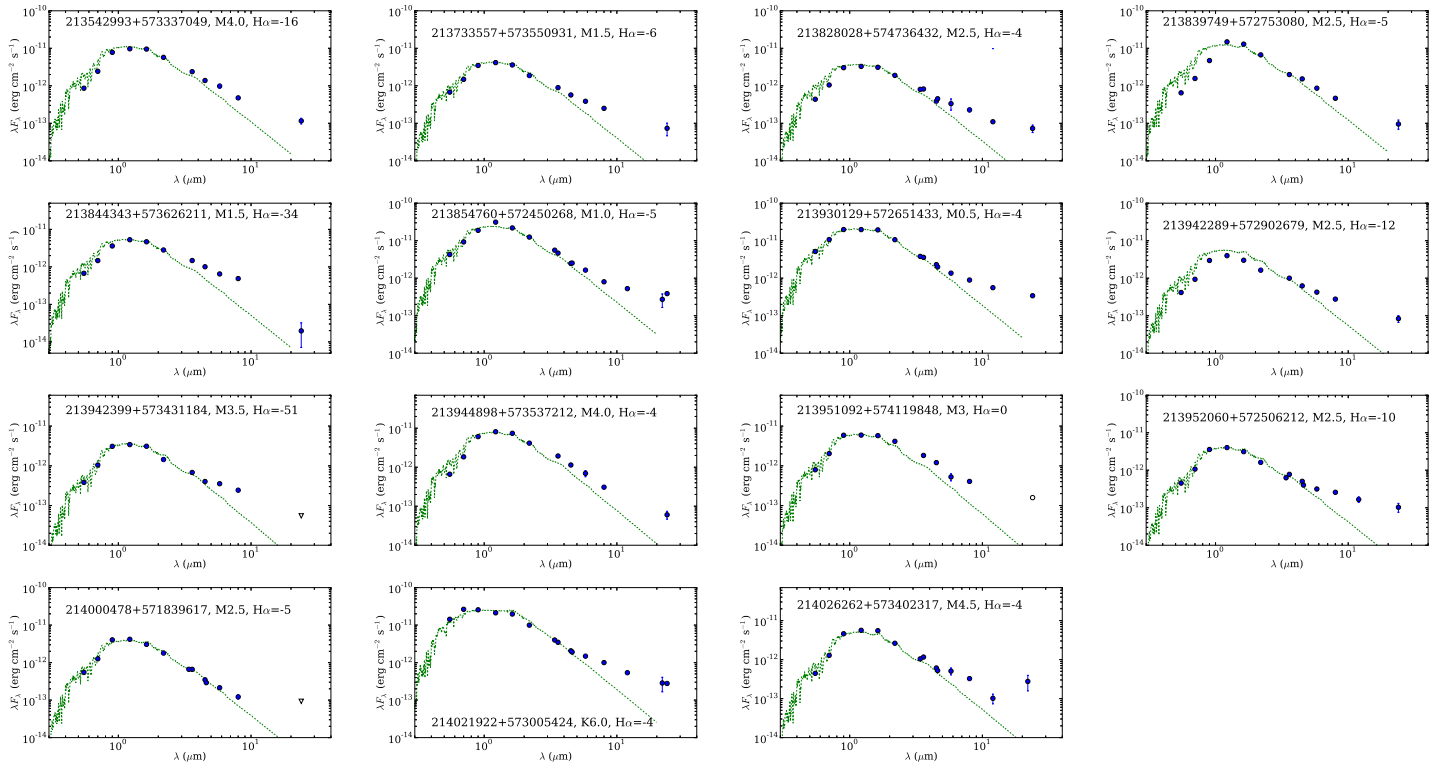


Fig. B.5: SEDs of the members and probably members with low IR excess consistent with dust-depleted disks. This includes objects with disks but no significant  $24\mu\text{m}$  detection, in cloud-free regions. Some objects like 213844343+573626211 could be truncated disks. Objects like 213839749+572753080, 213854760+572450268, 213944898+573537212, 214000478+571839617, 214021922+573005424, and 214026262+573402317 may also have inner holes being thus both transitional and dust-depleted disk candidates. Inverted triangles mark upper limits, and open circles are uncertain values.

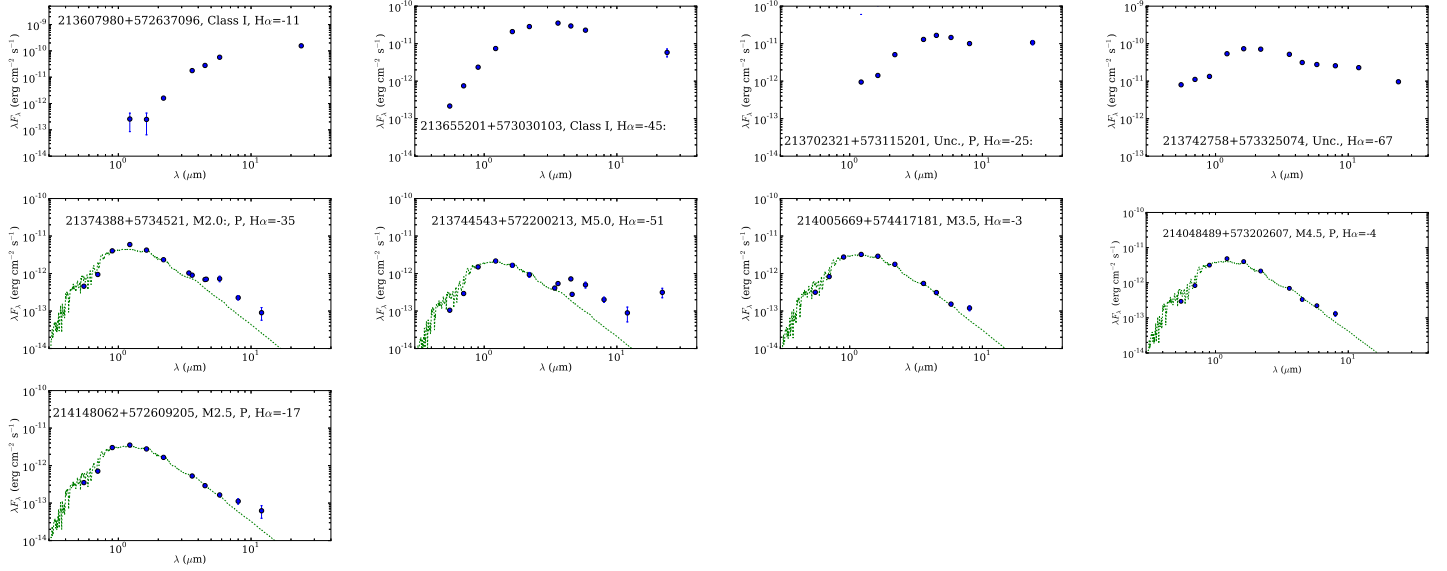


Fig. B.6: SEDs of the members and probably members with IR excess typical of Class I objects, early-type very embedded stars, and uncertain objects within the cloud. 21374388+5734521 is an uncertain case that could be a depleted disk or a combination of two sources. In the case of 214005669+574417181, 214048489+573202607, and 214148062+572609205, the small excess at  $8\mu\text{m}$  with uncertain photometry does not allow us to determine if they are TD or diskless sources. These sources are not included in the statistics of disk types discussed in the text.